UNIVERSITÀ
DEGLI STUDI
DI PADOVA

UNIVERSITÀ DEGLI STUDI DI PADOVA

DIPARTIMENTO DI BIOLOGIA

SCUOLA DI DOTTORATO DI RICERCA IN BIOSCIENZE E BIOTECNOLOGIE

INDIRIZZO: BIOLOGIA CELLULARE

XXVI CICLO

THE NEURO-CARDIAC JUNCTION: THE HOTLINE FOR BIDIRECTIONAL DIALOGUE BETWEEN NEURONS AND CARDIOMYOCYTES

Direttore della scuola: Ch.mo Prof. Giuseppe Zanotti

Coordinatore d'indirizzo: Ch.mo Prof. Paolo Bernardi

Supervisore: Dott. Marco Mongillo

Dottorando: Mauro Franzoso

Index

Abbreviations

6-OH-DOPA	6-hydroxy-dopamine
AMP	Adenosine monophosphate
AMI	Acute myocardial infarction
ANF	Atrial natriuretic factor
AP	Adaptor protein
AR	Adrenergic receptor
AraC	1-β-D-Arabinofuranosylcytosine
BAX	BCL-2 associated X protein
BDNF	Brain derived neurotrophic factor
bHLH	Basic helix loop helix
BMP	Bone morphogenetic protein
BSA	Bovine serum albumin
CaMKII	Ca^{2+}/calmodulin dependent protein kinase II
Ca_v	Voltage gated calcium channel
CF	Cardiac fibroblasts
CL	Clenbuterol
CM	Cardiomyocyte
CREB	Cyclic AMP responsive element bindin
cTnI	Cardiac troponin I
cTnT	Cardiac troponin T
DAG	Diacylglycerol
DAPI	4',6-diamidino-2-phenylindole
DBH	Dopamine β-hydroxylase
DM	Differentiating medium
DTT	Dithiothreitol
ECL	Enhanced chemiluminescence
ECFP	Enhanced cyan fluorescent protein

Edn3	Endothelin-3
EdnrA	Endothelin receptor type A
EDTA	Ethylenediaminetetraacetic acid
EGFP	Enhanced green fluorescent protein
ELISA	Enzyme-linked immunosorbent assay
ERK	Extracellular signal regulated kinase
F.I.	Fluorescence intensity
FBS	Fetal bovine serum
FDM	First day medium
Fmoc	Fluoren-9-ylmethoxycarbonyl
FRET	Fluorescence resonance energy transfer
Gs	G stimulatory
HN	Hippocampal neurons
HPLC	High performance liquid chromatography
HRP	Horseradish peroxidase
HS	Horse serum
IF	Immunofluorescence
IGF1	Insulin-like growth factor 1
IgG	Immunoglobulin g
IP_3	Inositol 1,4,5-triphosphate
I_{to}	Transient outward current
KO	Knock out
K_v	Voltage gated potassium channel
L-DOPA	L-3,4-dihydroxyphenylanine
LB	Luria Bertani
LC3	Light chain 3
MCS	Multiple cloning site
MES	2-(*N*-morpholino)ethanesulfonic acid
MI	Myocardial infarction
mTORC1	Mammalian target of rapamycin complex 1
MURF1	Muscle specific ring finger 1

Musa1	Muscle ubiquitin ligase of the SCF complex in atrophy 1
NCJ	Neuro-cardiac junction
NCS	Newborn calf serum
NCX	Na^{2+}/Ca^{2+} exchanger
NE	Norepinephrine
NGF	Nerve growth factor
NMJ	Neuromuscular junction
NPY	Neuropeptide Y
NT	Neurotrophin
OCT	Optimal cutting temperature compound
ON	Over night
P/S	Penicillin/streptomycin
PBS	Phosphate buffered saline
pCMV	Promoter of cytomegalovirus
PCR	Polymerase chain reaction
PFA	Paraformaldehyde
PH	Phenylephrine
PI3K	Phosphatidylinositol 3-kinase
PIP3	Phosphatidylinositol (3,4,5)-triphosphate
PKA	Protein kinase A
PLCγ	Phospholipase Cγ
PNMT	Phenylethanolamine N-methyl transferase
POH	Prolyl-4-hydroxylase β
PSA-NCAM	Polysialylated neural cell adhesion molecule
PVDF	Polyvinylidene fluoride
RAS	Rat sarcoma
RFP	Red fluorescent protein
ROI	Region of interest
RT	Room temperature
RT-qPCR	Real time quantitative PCR
RyR	Ryanodine receptor

s.e.m.	Standard error of the mean
SB	Sample buffer
SCG	Superior cervical ganglia
SDM	Second day medium
SDS	Sodium dodecyl sulfate
SERCA	Sarco/endoplasmic reticulum Ca^{2+}-ATPase
SGN	Sympathetic ganglia neuron
SN	Sympathetic neurons
ST	Sympathetic terminal
TBS	Tris-buffered saline
TEM	Transmission electron microscopy
TMB	3,3’,5,5’-Tetramethylbenzidine
TOH	Tyrosine hydroxylase
TRITC	Tetramethylrhodamine
TTBS	Tween tris-buffered saline
TX-100	Triton X-100
UM	Undifferentiating medium
UPS	Ubiquitin-proteasome system
VAMP	Vesicle associated membrane protein
YFP	Yellow fluorescent protein
β-MHC	β-myosin heavy chain

Summary

Rationale: The heart is mainly innervated by the sympathetic nervous system that is involved in the fight or flight response. Sympathetic neurons (SNs), whose cell bodies are placed in the stellate and superior cervical ganglia, mediate the main physiological mechanism increasing the frequency and force of cardiac contraction through release of norepinephrine. Recently, we have reported that SNs regulate heart trophism through stimulation of β2 adrenergic receptors and repression of muscle specific ubiquitin ligases (i.e. Murf1 and Atrogin1) but not much is known about the effects of SNs on sarcomeres. Nerve growth factor (NGF) released by the myocardium controls cardiac innervation by SNs after binding to its receptor (TrkA) and is required for neuronal survival. Thus, bidirectional coupling between SGNs and the heart takes place: the heart needs to be coupled to the SNs to receive norepinephrine stimulation for an efficient increase in heart contraction, and conversely, SNs are coupled to the heart for neurotrophic stimulation that is required for neuronal viability. However, whether a cell-cell interaction occurs in the SN-heart coupling is not known. An interaction between the muscle and the neuron that has been well described both in terms of function and structure, is the neuro-muscular junction (NMJ), characterized by membrane thickenings, acetylcholinergic receptor clustering, reduced intermembrane space (70-50 nm) and neurotrophin release by the postsynaptic myocyte (e.g. NT3, NT4). Considering the interaction between the SNs and the heart (neuro-cardiac junction, NCJ), this study aims i) to evaluate the effects of anterograde SN stimulation on sarcomeric structures, ii) to determine whether specific cellular structures are present at the SN/Cardiomyocyte (CM) contact site, iiI) to investigate the role of SGN/CM contact in NGF-mediated signaling.

Results: To analyze changes in sarcomere structure, cultured CMs were treated with adrenergic stimuli (clenbuterol, phenylephrine and norepinephrine) or nutrient/serum deprived by HBSS incubation. Since starvation and sympathetic denervation share common targets (e.g. ubiquitin ligases), we can make a parallelism between the two pro-atrophic stimuli for alterations in the sarcomeres. Incubation with adrenergic agonists did not cause significant changes, whereas starvation caused a 41.86% decrease in sarcomere area, suggesting that sarcomere degradation is faster than its

synthesis. This result was confirmed by experiments of in live imaging performed on CMs transfected with a construct encoding for the z-line localized RFP-zasp.

To understand whether all sarcomeric proteins share the same fate during HBSS treatment, immunofluorescence (IF) and western blot (WB) analyses were performed on different proteins localized in the sarcomeres. While α actinin and cardiac tropoinin (cTn) I showed delocalization and degradation, no significant changes were measured for cTnT upon HBSS treatment, suggesting that sarcomeric proteins are degraded in different ways. To understand which protein degradation system is involved in sarcomere disassembly, we considered the autophagy-lysosome and ubiquitin proteasome systems (UPS). WB and IF analyses supported the activation of both systems in cells treated with HBSS. In live imaging of CMs co-transfected with constructs encoding for RFP-zasp and EGFP-LC3 showed LC3 enrichment near sarcomeres in nutrient/serum deprived cells, suggesting that autophagy may be involved in sarcomere degradation. Moreover, IF staining showed ubiquitin marked sites near the M-line of sarcomeres in cells incubated with HBSS, suggesting that ubiquitin ligases may be involved in sarcomere disassembly. Since Murf1 is a muscle specific ubiquitin ligase, localized in the M-line of sarcomeres and upregulated upon nutrient/serum deprivation, we evaluated its role. Its overexpression caused a 88.57% decrease in the sarcomere area, when compared to controls, whereas its silencing in starved CMs did not prevent sarcomere degradation (446.19 ±35.65 vs 144.91 ±26.25 μm^2 of sarcomeric area in controls and silenced CMs respectively). These results were confirmed by in live imaging on RFP-zasp transfected CMs, and suggest that UPS and in particular Murf1 are involved in HBSS induced sarcomeric disassembly and that Murf1-mediated degradation is not the only process.

Considering the analysis of the neuro-cardiac interaction, IF staining on rat heart cryosections showed dense innervation of the heart by sympathetic neurons that mainly interact with CMs when compared to other cardiac cell types that are well represented in the heart (e.g. cardiac fibroblasts, CFs). Electron microscopy on mouse heart slices and rat SN/CM co-cultures showed a close association between SNs and CMs (intermembrane distance around 70 nm), neurotransmitter vesicle accumulation

and increased membrane protein density. These data support that a direct interaction between the sympathetic neurons and the CMs exists.

To analyze such interaction, SN/CM co-cultures were developed by isolating sympathetic ganglia neurons (SGN) from the superior cervical ganglia and CMs from the hearts of neonatal rats. Both cell types were characterized using IF staining for dopamine β-hydroxylase, a maker for noradrenergic neurons, and for α actinin, a sarcomeric protein. Moreover, IF staining showed an enrichment of cell-to-cell adhesion molecules including β-catenin and cadherin at the contact sites between processes and CMs. Such enrichment developed after 2 weeks of co-culture, suggesting that SGN/CM co-cultures are subjected to time dependent maturation. In spotted co-cultures allowing to identify processes on wither CMs or non CM cardiac cells (mainly fibroblasts), a higher area occupied by processes was measured on CMs when compared to the other cardiac cells after NGF withdrawal (67.11 ±12.36% vs 3.79 ±1.12% of area occupied by processes respectively), supporting the preferential interaction of SGNs with CMs. This idea is further supported by the observation that SGNs develop larger contact sites on CMs than in other cardiac cells (82.88 ±1.3% decrease in contact area on non CM cardiac cells when compared to CMs). Taken together, all these data suggest that SGNs establish a direct and stable interaction with CMs and not other cardiac cells.

Since the myocardium is known to produce NGF that is required for SN viability, the functional role of the NCJ was assessed considering NGF signaling. This neurotrophin is synthesized by CMs, as detected by the western blot analysis. Transfection of CMs with siRNA against NGF caused a 72.91% decrease of the neurotrophin expression, reducing neuronal density in SGN/CM co-cultures (65.72 ±9.33% decrease in mean neuronal density when compared to the scramble siRNA). This effect was abolished by the addition of NGF in the culture medium and supports that SGNs are dependent on CM derived NGF.

NGF binding to its receptor enables TrkA activation, endocytosis and retrograde transport to the neuronal soma. TrkA retrograde movements were assessed by monitoring transport velocity, using imaging in transiently TrkA-DsRed2 transfected SGNs. The speed of retrograde TrkA-DsRed2 movements depended on the presence of

NGF (0.32 ±0.06 vs 0.19 ±0.03µm/s in presence or absence of NGF). In co-cultures, retrograde movements were higher and faster in processes contacting CMs than those contacting other cardiac cells (0.24 ±0.05 vs 0.11 ±0.02µm/s respectively), supporting the idea that TrkA is activated on CMs and not on the other cardiac cells and that SGN survival requires CM derived NGF.

Since SGNs interact with CMs and depend on CM released NGF, we tested the hypothesis that the NCJ is necessary for neuronal survival. IF on mouse heart slices showed TrkA enrichment at SGN/CM contact site, suggesting that NGF signaling may be involved in the NCJ. Moreover, CM-conditioned medium did not prevent neuronal death (58.21 ±10.42% decrease in mean neuronal density when compared to SGN/CM co-cultures), suggesting that NGF in the medium is not sufficient for neuronal survival. Consistently, we measured NGF concentration in CM-conditioned medium and it was a 1000-fold lower than the minimal dose required for neuronal survival (0.13 ±0.08pM). To evaluate whether a single cell-to-single cell NGF signaling occurs between SGNs and CMs, co-cultures were co-transfected with siRNA against NGF and a plasmid encoding for the GFP that allows the identification of NGF silenced CMs. Sympathetic processes on NGF-silenced CMs showed a 19.56 ±4.01% decrease in the neuro-cardiac contact area when compared to those on untransfected CMs of the same co-culture, supporting that direct cell-cell NGF mediated signaling is present. Moreover, co-cultures were transfected with a construct encoding NGF in order to detect NGF accumulation in processes using the IF. Only processes in contact with transfected CM contained NGF puncta, while those in contact with untransfected cells of the same co-culture did not contain NGF (43.43 ±10.77 vs 4.17 ± 4.1% of processes on transfected or un-transfected CMs). Taken together, these data suggest that the establishment of a neuro-cardiac interaction is necessary to allow NGF signaling.

In the end of this work, we interfered with NGF signaling using different strategies. First, we used an anti-NGF antibody to sequester NGF. Second, since from TEM analysis we detected sites of cell-to-cell distance of 10nm, we used the smaller TrkA antagonist c(92-96). Third, we used k252a that has a size comparable to that of c(92-96) and that is membrane permeable. Whereas every approach worked on SGNs alone leading to a significant reduction in neuronal density, only k252a was able to reduce

neuronal density in co-cultures (73.24 ±4.18% decrease in mean neuronal density when compared to the control), suggesting that the NCJ is an isolated microenvironment protected from diffusion. Since k252a led to neuronal loss in co-cultures, we used this inhibitor to estimate NGF concentration at the contact site, incubating SGNs alone with k252a and NGF at increasing concentrations. The estimated concentration was 1.4 ±0.03nM, 3.5 times higher than the minimal dose required for neuronal survival, supporting that the NCJ is characterized by high NGF concentration.

Conclusions: Taken together, our results suggest that sympathetic neurons establish a direct interaction with CMs and that they are dependent on CM derived NGF. Morever, NGF-dependent pro-survival signal to the SGN needs this direct interaction that facilitates NGF activation of TrkA thanks to the development of an isolated microdomain characterized by a high NGF concentration and TrkA enrichment. Finally, sarcomere dismantlement during atrophic remodeling involves the activation of protein degradation systems and in particular of the ubiquitin ligase Murf1, whose regulation by SNs may affect sarcomere structure.

Riassunto

Introduzione: il cuore è innervato principalmente dal sistema nervoso simpatico coinvolto nella risposta 'lotta o fuga'. I neuroni simpatici (NS) sono collocati nei gangli stellato e cervicale superiore e mediano il principale meccanismo fisiologico per aumentare la frequenza e la forza di contrazione cardiaca attraverso il rilascio di noradrenalina. Recentemente abbiamo riportato che i NS regolano il trofismo cardiaco attraverso la stimolazione dei recettori β2 adrenergici e la repressione delle ubiquitina ligasi muscolo specifiche (ovvero MuRF1 e Atrogin1), ma non si conoscono gli effetti dei NS sui sarcomeri. Il fattore di crescita neuronale (NGF) è rilasciato dal miocardio e controlla l'innervazione cardiaca da parte dei NS dopo il legame al suo recettore (TrkA) ed è necessario per la sopravvivenza neuronale. Di conseguenza l'accoppiamento tra neuroni simpatici e il cuore riguarda una comunicazione bidirezionale: il cuore ha bisogno di essere accoppiato ai NS per ricevere lo stimolo noradrenergico per un aumento efficiente della contrazione del cuore, e, viceversa, i NS sono accoppiati al

cuore per ricevere lo stimolo neurotrofico che è necessario per la sopravvivenza dei neuroni. Tuttavia, non si conosce se è presente un'interazione cellula-cellula nell'accoppiamento tra cuore e neuroni. La giunzione neuromuscolare (GNM) costituisce un'interazione tra il muscolo e il neurone, ben descritta sia in termini di funzione che di struttura. E' caratterizzata da ispessimenti della membrana, accumulo dei recettori acetilcolinergici, ridotto spazio intermembrana (70-50 nm) e rilascio di neurotrofine da parte dei miociti (ad esempio NT3, NT4). Considerando l'interazione tra i NS ed il cuore (giunzione neuro cardiaca, GNC), questo studio ha lo scopo di i) valutare gli effetti della stimolazione anterograda dei NS sulle strutture sarcomeriche, ii) determinare se strutture cellulari specifiche sono presenti a livello del sito di contatto tra NS e cardiomiocita, iii) studiare il ruolo del contatto tra cardiomiociti e neuroni nella segnalazione mediata da NGF.

Risultati: Per analizzare i cambiamenti nella struttura del sarcomero, colture di cardiomiociti sono state trattate con stimoli adrenergici (clenbuterolo , fenilefrina e norepinefrina) oppure con HBSS. Poiché la rimozione di nutrienti e la denervazione simpatica agiscono su meccanismi comuni, possiamo fare un parallelismo tra i due stimoli proatrofici sull'alterazione nei sarcomeri. L'incubazione con agonisti adrenergici non ha causato cambiamenti significativi, mentre l'HBSS ha provocato una diminuzione del 41.86% dell'area sarcomerica, suggerendo che la degradazione dei sarcomeri è più veloce rispetto alla loro sintesi. Questo risultato è stato confermato da esperimenti di imaging in tempo reale su CM trasfettati con un costrutto codificante per la RFP-zasp, proteina localizzata nella linea z.

Per capire se le proteine sarcomeriche condividono lo stesso destino durante il trattamento con HBSS, sono state effettuate analisi di immunofluorescenza (IF) e western blot (WB). Mentre α actinina e troponina cardiaca (cTn) I hanno mostrato delocalizzazione e degradazione, non sono stati misurati cambiamenti significativi per cTnT in seguito al trattamento con HBSS, suggerendo che le proteine sarcomeriche sono degradate in modi diversi. Per capire quale meccanismo di degradazione delle proteine è coinvolto nello smantellamento dei sarcomeri, abbiamo considerato il sistema autofagico-lisosomale e ubiquitina-proteasoma. Analisi di WB e IF hanno mostrato l'attivazione di entrambi i sistemi in cellule trattate con HBSS. In esperimenti

di imaging in tempo reale su cardiomiociti co-trasfettati con costrutti codificanti per RFP-zasp e EGFP-LC3 è stato osservato l'arricchimento di LC3 vicino ai sarcomeri in seguito a deprivazione di nutrienti e siero, suggerendo che l'autofagia potrebbe essere coinvolta nella degradazione dei sarcomeri. Inoltre analisi di IF hanno mostrato una marcatura per l'ubiquitina in corrispondenza della linea M dei sarcomeri in cellule incubate con HBSS, suggerendo che le ubiquitina ligasi potrebbero essere coinvolte nello smantellamento dei sarcomeri. Poiché MuRF1 è un'ubiquitina ligasi muscolo specifica localizzata nella linea M dei sarcomeri e sovraespressa in condizioni di digiuno, abbiamo valutato il suo ruolo nella degradazione delle proteine sarcomeriche. La sua sovraespressione ha provocato un calo dell'area sarcomerica dell'88.57% rispetto ai controlli, mentre il suo silenziamento in cardiomiociti incubati con HBSS non ha impedito la degradazione dei sarcomeri (446.19 ±35.65 vs 144.91 ±26.25μm^2 di area sarcomerica nei controlli e nei cardiomiociti silenziati e incubati con HBSS rispettivamente). Questi risultati sono stati confermati da esperimenti di imaging in tempo reale su cardiomiociti trasfettati con RFP-zasp, e suggeriscono che il sistema ubiquitina-proteasoma ed in particolare Murf1 siano coinvolti nella degradazione dei sarcomeri, anche se quello mediato da Murf1 non è l'unico meccanismo.

Considerando l'analisi dell'interazione neuro-cardiaca, le analisi di IF su criosezioni di cuore di ratto hanno mostrato densa innervazione del cuore da parte dei neuroni simpatici che sembrano interagire soprattutto con cardiomiociti rispetto ad altri tipi cellulari che sono ben rappresentati nel cuore (ad esempio fibroblasti cardiaci, FC). L'analisi di microscopia elettronica su criosezioni cardiache di topo e ratto e co-culture di NS e cardiomiociti ha mostrato una stretta associazione tra NS e cardiomiociti (con una distanza intermembrana di circa 70nm), accumulo di vescicole di neurotrasmettitore e l'aumento della densità delle proteine di membrana. Questi dati supportano l'esistenza dell'interazione diretta tra i neuroni simpatici e i cardiomiociti.

Per analizzare tale interazione, sono state sviluppate co-culture di NS e cardiomiociti, isolando i neuroni simpatici gangliari (NSG) dai gangli cervicali superiori e i cardiomiociti dal cuore dei ratti neonati. Entrambi i tipi cellulari sono stati caratterizzati analizzando in IF la dopamina β-idrossilasi, un marcatore per i neuroni noradrenergici, e l'α actinina, una proteina sarcomerica. Inoltre l'arricchimento di

molecole di adesione cellula-cellula, tra cui β catenina e caderina, è stato osservato nei siti di contatto tra processi simpatici e cardiomiociti. Tale arricchimento è stato misurato dopo 2 settimane di co-coltura, suggerendo che co-culture di neuroni e cardiomiociti sono sottoposte a maturazione in funzione del tempo. In co-colture a spot, che consentono di identificare processi in contatto con cardiomiociti o altre cellule cardiache (principalmente fibroblasti), una superficie superiore era occupata dai processi simpatici su cardiomiociti rispetto alle altre cellule cardiache dopo la rimozioni dell'NGF (67.11 ±12.36% vs 3.79 ±1.12% della superficie occupata da processi rispettivamente), sostenendo la presenza di un'interazione preferenziale tra neuroni e cardiomiociti. Questo concetto è ulteriormente supportato dall'osservazione che i neuroni simpatici sviluppano contatti più grandi sui cardiomiociti che su altre cellule cardiache (82.88 ±1.3% di diminuzione della superficie di contatto su altre cellule cardiache rispetto ai cardiomiociti). Nell'insieme, questi dati suggeriscono che i NS stabiliscono un'interazione diretta e stabile con i cardiomiociti e non altre cellule cardiache.

Poiché si conosce che il miocardio produce NGF che è necessario per la vitalità dei NS, il ruolo funzionale della GNC è stato valutato considerando il signaling mediato dall'NGF. Questa neurotrofina è sintetizzata dai cardiomiociti, come rilevato dalle analisi di western blot. La trasfezione di siRNA contro l'NGF nei cardiomiociti ha causato una diminuzione del 72.91% nell'espressione della neurotrofina e ridotto la densità neuronale in co-culture di neuroni e cardiomiociti (65.72 ±9.33% di diminuzione della densità neuronale rispetto alla trasfezione con il siRNA di controllo). Questo effetto è stato abolito dall'aggiunta di NGF nel mezzo di coltura e supporta che i neuroni dipendono dall'NGF prodotto dai cardiomiociti.

Il legame dell'NGF al suo recettore TrkA consente la sua attivazione, endocitosi e trasporto retrogrado al soma neuronale. Sono stati valutati i movimenti retrogradi del TrkA, monitorando la velocità di trasporto utilizzando tecniche di imaging in tempo reale in co-culture con NS trasfettati con il costrutto TrkA-DsRed2. La velocità dei movimenti retrogradi del TrkA-DsRed2 nei neuroni dipende dalla presenza di NGF (0.32 ±0.06 vs 0.19 ± 0.03µm/s in presenza o assenza di NGF). In co-culture, i movimenti retrogradi erano più alti e più veloce nei processi in contatto con

cardiomiociti rispetto ad altre cellule cardiache (0.24 ±0.05 vs 0.11 ±0.02µm/s rispettivamente), sostenendo l'idea che il TrkA è attivato sui cardiomiociti e non sulle altre cellule cardiache e che i neuroni dipendono da NGF derivato da cardiomiociti.

Poiché i NS interagiscono con i cardiomiociti e sono dipendenti dall'NGF che questi rilasciano, abbiamo testato l'ipotesi secondo cui la GNC sia necessaria per la sopravvivenza neuronale. Analisi di IF su criosezioni di cuore murino hanno mostrato accumulo di TrkA nel sito di contatto tra il cardiomiocita e il NS, suggerendo che il signaling mediato dall'NGF potrebbe essere coinvolto nella GNC. Inoltre, terreno condizionato da cardiomiociti non ha impedito la morte neuronale (58.21 ±10.42% di diminuzione della densità neuronale rispetto alla co-cultura), suggerendo che l'NGF nel mezzo non sia sufficiente per la sopravvivenza neuronale. Coerentemente abbiamo misurato la concentrazione di NGF nel terreno condizionato da cardiomiociti ed è risultata 1000 volte inferiore rispetto alla dose minima necessaria per la sopravvivenza neuronale (0.13 ±0.08pM). Per valutare se il signaling mediato dall'NGF avviene da una singola cellula all'altra, co-culture sono state co-trasfettate con siRNA contro l'NGF e un plasmide codificante per la GFP che permette l'identificazione dei cardiomiociti silenziati per la neurotrofina. I processi simpatici su cardiomiociti silenziati hanno mostrato una riduzione del 19.56 ±4,01% della zona di contatto neuro-cardiaca rispetto ai cardiomiociti non trasfettati della stessa co-coltura, a sostegno del fatto che il singaling dell'NGF sia localizzato nel sito di contatto tra una cellula e l'altra. Inoltre, le co-colture sono state trasfettate con un costrutto codificante per l'NGF per rilevare l'accumulo della neurotrofina nei processi utilizzando tecniche di IF. Solo i processi in contatto con i cardiomiociti trasfettati contenevano accumuli di NGF, mentre quelli a contatto con cardiomiociti non trasfettati non possedevano NGF (43.43 ±4.17 vs 10.77 ±4.1% dei processi in contatto con cardiomiociti trasfettati e non rispettivamente). Nel loro insieme, questi dati suggeriscono che la presenza dell'interazione neuro-cardiaca sia necessaria per consentire la segnalazione dell' NGF.

Alla fine di questo lavoro abbiamo interferito con il signaling dell'NGF utilizzando diverse strategie. In primo luogo abbiamo utilizzato un anticorpo anti-NGF per sequestrare la neurotrofina dal terreno. In secondo luogo, poiché nelle analisi di microscopia elettronica abbiamo rilevato siti di distanza cellula-cellula di 10nm,

abbiamo usato un antagonista del TrkA più piccolo dell'anticorpo, il c(92-96). In terzo luogo abbiamo utilizzato il k252a che ha una dimensione paragonabile a quella del c(92-96) e che è permeabile alle membrane. Considerando che ogni approccio ha funzionato sui NS, causando una significativa riduzione della densità neuronale, solo il k252a è stato in grado di ridurre la densità neuronale in co-colture (73.24 ±4.18% di diminuzione della densità neuronale media rispetto al controllo), suggerendo che la GNC è un microambiente isolato protetto dalla diffusione. Poiché il k252a ha causato la riduzione neuronale in co-colture, abbiamo usato questo inibitore per stimare la concentrazione di NGF nel sito di contatto, incubando i neuroni da soli con k252a e NGF in concentrazioni crescenti. La concentrazione stimata è stata di 1.4 ±0.03nM, 3.5 volte superiore alla dose minima necessaria per la sopravvivenza neuronale, supportando che la GNC è caratterizzata da un'alta concentrazione di NGF.

Conclusioni: Nell'insieme, i nostri risultati suggeriscono che i neuroni simpatici stabiliscono un'interazione diretta con i cardiomiociti e che dipendono dall'NGF derivato dai cardiomiociti. Inoltre, il signaling mediato dall'NGF necessita di questa interazione diretta che facilita l'attivazione del TrkA grazie allo sviluppo di un microdominio isolato e caratterizzato da una elevata concentrazione di NGF e dall'arricchimento del TrkA. Infine, lo smantellamento dei sarcomeri comporta l'attivazione dei sistemi di degradazione delle proteine e, in particolare, dell'ubiquitina ligasi MuRF1, la cui modulazione da parte dei NS può modificare la struttura del sarcomero.

1. Abstract

The sympathetic nervous system stimulates the myocardium with norepinephrine tuning cardiac rate, contractile force and trophism. The sarcomeric structure is influenced by the hypertrophic and atrophic remodeling. However, the mechanism whereby adrenergic signaling regulates sarcomere dynamics is still unclear. Moreover, the heart regulates sympathetic neuron (SN) innervation through the release of a small amount of nerve growth factor (NGF), allowing neuronal survival, differentiation and axonal sprouting. However, whether a direct interaction based on a specific structure is established, and what is the functional effect of such interaction on NGF signaling is yet unclear.

The first part of this PhD work was focused on sarcomere dynamics. Incubation with adrenergic agonists did not significantly increase the area occupied by sarcomeres. On the contrary, we detected sarcomeric disassembly and differential degradation of sarcomeric proteins (e.g. α actinin and cardiac troponin I) in nutrient/serum deprived cardiomyocytes, a condition that upregulates autophagy and many muscle specific ubiquitin ligases (e.g. Murf1), similarly to sympathetic denervation. These results, together with almost complete sarcomere loss upon Murf1 overexpression, suggest that sarcomere disassembly may be faster than its synthesis, and may involve Murf1 activation.

In the second part of this PhD work, we investigated NGF signaling. We provided electron microscopy and immunofluorescence evidence of the neuro-cardiac interaction in mouse and rat heart cryosections. Moreover, we evaluated the role of the neuro-cardiac interaction in NGF mediated pro-survival effects on neurons. We obtained that SNs are dependent on NGF derived from CMs and not other cardiac cells. Moreover, our data support that the neuro-cardiac interaction is an isolated microenvironment that allows NGF signaling thanks to TrkA clustering and high NGF concentrations. Without this contact site, NGF would diffuse and SNs die. These results are relevant considering that alterations of NGF signaling in diseased hearts (e.g. in diabetes) may cause aberrant innervation patterns and lethal arrhythmias.

2. Introduction

2.1. Anatomy of heart innervation

The heart is innervated by three branches of the autonomic nervous system that originate from the neural crest cells of the neuroepithelium in the developing embryo: the sensory, the parasympathetic and the sympathetic nerves (figure 1, panel a). The first system has a role in pain perception in situations of pathological damage of the heart whereas the other two are mainly involved in tuning heart contraction.

2.1.1. Sensory neurons

The cardiac sensory nervous system relays pain perception and is involved in the initiation of the protective cardiovascular response during myocardial ischemia. Afferent sensory axons innervating the heart project to the upper thoracic horn via the dorsal root ganglia (Kimura K, 2012).

2.1.2. Parasympathetic nervous system

The parasympathetic neurons extend from cardiac ganglia placed at the base of both atria. They are responsible for 'rest and digest' activities that typically occur when the body is at relaxation (e.g. after eating), thanks to the release of its neurotransmitter acetylcholine. The parasympathetic nervous system decreases cardiac contractility and rate. The parasympathetic neurons innervate the myocardium at low extent in mice and rats and, consistently, in the rat left ventricle there are far less choline transporter-positive neurons than tyrosine hydroxylase positive (sympathetic) fibers. Moreover, the neurons distribute uniformly throughout the myocardium and no differences of innervation between the subepicardial and the subendocardial region (Kanazawa H, 2010) were detected.

2.1.3. Sympathetic nervous system

The sympathetic nervous system is involved in the 'fight or flight' response, a complex physiologic regulatory mechanism including the enhancement of cardiac contractility and beating rate. Two main neurotransmitters are produced and released by

sympathetic neurons: neuropeptide Y (NPY), mainly involved in vasoconstriction, and norepinephrine (NE), a catecholamine. The synthesis of NE requires three reaction steps that are catalyzed by three enzymes. First, tyrosine is converted in L-3,4-dihydroxyphenylanine (L-DOPA) by tyrosine hydroxylase (TOH), one of the enzymes that can be used as a sympathetic neuronal marker. Second, the product of the first reaction is decarboxylated by an aromatic amino acid decarboxylase to produce dopamine that is finally hydroxylated to NE by dopamine β-hydroxylase (DBH, see figure1, panel b). DBH is used as a sympathetic marker and allows distinguishing between dopaminergic neurons (TOH^+, DBH^-) and sympathetic neurons (TOH^+, DBH^+). Sympathetic cardiac nerves originate from postganglionic neurons located in cervical and upper thoracic (stellate) ganglia, which are part of the sympathetic chain ganglia that run bilaterally and ventrolaterally to the spinal column. These ganglia are innervated by preganglionic cholinergic neurons located in the intermediolateral column of the thoracic and lumbar spinal cord (Vincentz JW, 2012). During fetal development, sympathetic neurons extend their axons from the ganglia, reaching the carotid artery. Following the great arteries, sympathetic axons join the cardiac plexus, located dorsal and caudal to the heart. Finally, these neurons project from the region between the aorta and the pulmonary trunk, and reach the heart following the coronary arteries. Sympathetic innervation of the heart begins during the first days of postnatal development, when the axons project from the subepicardial region of the myocardium to the subendocardium. When the innervation process is completed, sympathetic axons, that are characterized by a 'pearl and necklace' structure with 'varicosities' corresponding to the neurotransmitter releasing sites, exhibit a higher density in the subepicardial area when compared to the subendocardial one (Vincentz JW, 2012). Even if heart innervation by the sympathetic neurons is well described from a morphological point of view, it is not known whether the neurons establish a direct cell-cell interaction with the myocardial cellular targets, and whether such interaction requires the development of a specific structure.

Like the other neurons that innervate the myocardium, SNs are derived from neural crest cells. During development, SN progenitors differentiate in SNs, upregulating the three enzymes that are required for NE synthesis (TOH, DBH and PNMT). This process is driven by local, paracrine stimulation occurring in a region proximal to the aorta: smooth muscle cells of the dorsal aorta are known to release bone morphogenetic proteins (BMP), specifically BMP2, BMP4 and BMP7, that are sufficient for the upregulation of SN markers. In particular, BMPs activate several transcription factors, among which the paired like homeodomain Phox2b together with the bHLH Hand2 and the Zn-finger Gata3 are thought to be crucial for sympathetic program activation (Vincentz JW, 2012). Evidence suggests that Phox2b is the most important transcription factor, since catastrophic autonomic neuronal death is observed in mice without Phox2b (Pattyn A, 1999).

2.2. Effects of sympathetic neurons on the heart

Through the release of NE, sympathetic neurons exert different effects on the cardiomyocytes, and their action encompasses a time range from immediate (seconds) to long term (days). These actions include:

- positive chronotropic effect, that means an increase in the frequency of heart contraction;
- positive dromotropic effect, the increase in the conduction velocity;
- positive inotropic effect, the increase in contractility;
- positive lusitropic effect, the increase in relaxation (Kimura K I. M., 2012);
- the increase in cardiomyocyte size (Zaglia T, 2013).

2.2.1. PKA-mediated post-translational modifications

Cardiomyocyte contraction is triggered by membrane depolarization and driven by the activation of Ca^{2+} induced Ca^{2+} release. At resting conditions, CM membrane potential is -90mV. Membrane depolarization to about -50mV activates opening of voltage dependent Na^{2+} channels (Jaggar JH, 1998). The subsequent Na^{2+} influx in the cell amplifies membrane depolarization, triggering the opening of voltage dependent L-type Ca^{2+} channels that occurs when the membrane potential is higher than -40mV

(Lipscombe D, 2002). The increase in cytoplasmic Ca^{2+} concentration leads to opening of ryanodine receptors (RyR) located at the level of sarcoplasmic reticulum membrane, in the so-called 'Ca^{2+} induced Ca^{2+} release' process (Bers DM, 2004). High Ca^{2+} concentrations activate contraction as Ca^{2+} binds to the thin filament protein Troponin C, switching its conformation and causing troponin I/tropomyosin displacement that allows myosin-actin interaction (Bers DM, 2000).

The relaxation phase starts upon inactivation of RyR and L-type Ca^{2+} channels, mediated by high Ca^{2+} concentrations, and is completed by the decrease in cytosolic [Ca^{2+}] to low values operated by the action of the sarco/endoplasmic reticulum Ca^{2+}-ATPase (SERCA), which pumps Ca^{2+} in the sarcoplasmic reticulum, and of the Na^{2+}/Ca^{2+} exchanger, which extrudes Ca^{2+} from the cell (Bers DM, 2002).

The mechanism, through which SNs acutely modulate CM contraction, is mediated by NE binding to β-adrenergic receptor that leads to adenylyl cyclase activation by Gs protein, cAMP increase and the subsequent activation of PKA (Brodde OE, 1984). Activated PKA phosphorylates several targets that are involved in the regulation of Ca^{2+} homeostasis and myofibril contraction (figure 1, panel c). The main targets include:

- L-type Ca^{2+} channel: PKA-phosphorylation of the channel increases its open probability and Ca^{2+} conductance, contributing to the positive inotropic effect (Qu Y, 2005);
- RyR: in its unphosphorylated form, the channel is associated to the enzyme calstabin2 that reduces Ca^{2+} sensitivity of RyR. Calstabin2 affinity for RyR is lowered after channel phosphorylation by PKA, increasing heart contraction (Marx SO, 2000);
- phospholamban: it is an intermembrane protein interacting with SERCA pumps in its dephosphorylated form, and inhibits the pump activity; after phosphorylation by PKA, phospholamban inhibitory effect is relieved, thus increasing Ca^{2+} influx in the sarcoplasmic reticulum and heart relaxation (Li L, 2000);

- troponin I: it is known to interact with troponin C and its PKA-phosphorylation lowers the affinity of troponin C for Ca^{2+}, facilitating release of Ca^{2+} from the myofilaments and accelerating cardiac relaxation (Li L, 2000).

PKA is not the only kinase activated downstream of β-AR responsible for the acute effects of NE stimulation. Increased cytosolic Ca^{2+} binds to calmodulin and activates CaMKII. This serine/threonine protein kinase also phosphorylates L-type Ca^{2+} channels (Maier LS, 2007), RyR (Guo T, 2006) and phospholamban (Wang W, 2004), with similar effects to those described for the PKA.

These posttranslational modifications are enacted acutely and result in a positive inotropic, chronotropic, dromotropic and lusitropic way, thus increasing heart contraction, relaxation and conduction velocity.

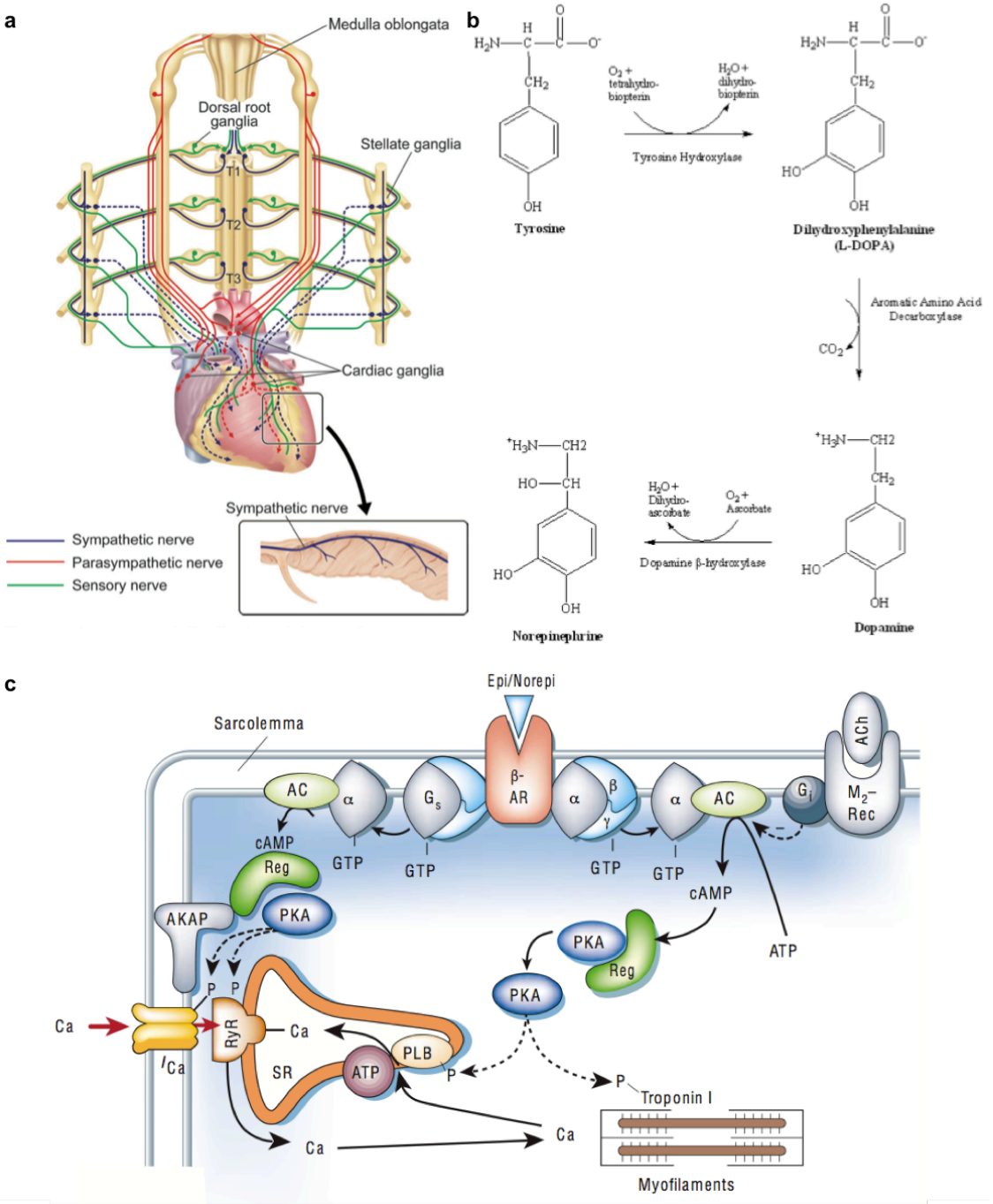

Figure 1 (**a**) Schematic view of heart innervation by sensory, parasympathetic and sympathetic neurons. From (Kimura K I. M., 2012). (**b**) Reactions and enzymes involved in norepinephrine synthesis. From (http://usefulchem.wikispaces.com). (**c**) Posttranslational modifications that occur upon NE binding to β-adrenergic receptors. From (Bers DM, 2002).

2.2.2. Effects on channel transcription

In addition to the post-translational modifications described above, SNs can modulate heart electrophysiological properties both acutely and by influencing channel

expression. In this regard, it is known that sympathetic innervation and endogenous NE and NY are involved in transcriptional regulation of channels activated during transient outward currents (I_{to}), which are involved in the repolarizing phase of cardiac action potential (Qu J, 2004). In particular, it has been demonstrated that catecholamine depletion in the myocardium by reserpine treatment reduced Kv4.2 and Kv4.3 messenger RNA levels and I_{to} density in adult rats. Such effect was reversed by 10 hours incubation of adult CMs with NE at high concentrations or NE/NPY mix. Nevertheless, a reduction in plasma epinephrine levels in adrenalectomized rats similar to that induced by reserpine was without effects, suggesting a specific regulation of channel expression by SNs (Bru-Mercier G, 2003).

Not only K^+ channels are transcriptionally modulated by SNs. T-type Ca^{2+} channels are thought to be involved in the pacemaker activity of the heart and $Ca_v3.1$ is one of the 3 subunits that constitute these channels. It has been shown that $Ca_v3.1$ mRNA increases during perinatal development, correlating with the well-known time course of heart innervation (Qu J, 2004).

2.2.3. Effects on CM growth

Cardiac growth occurs through cardiomyocyte replication during fetal development. After birth, cardiomyocytes become terminally differentiated and lose their ability to divide, unlike other myocardial cell types (e.g. cardiac fibroblasts). During postnatal development, cardiac size increases thanks to hypertrophy of individual CMs (figure 2, panel a). Such physiologic postnatal hypertrophy results generally in a two- or more-fold increase in heart mass and is triggered by the mechanical stretch caused by greater hemodynamic demand and by increased circulatory concentration of growth hormone and insulin-like growth factor 1 (IGF1). Moreover, after developmental growth, the heart maintains plastic potential and is able to modify its size through a physiological hypertrophic growth. Physiological hypertrophy is a form of cardiac growth that takes place in particular conditions (e.g. exercise and pregnancy) and is characterized by a 10-20% increase in cardiac mass, with general beneficial effects. Such hypertrophic remodeling differs from the so-called pathological hypertrophy, i.e. that occurring in response to pressure or volume overload, and does not share its

peculiar features, such as the switch from oxidative to glycolytic metabolism, activation of fetal gene program (e.g. ANF, β-MHC) and interstitial or replacement fibrosis. Moreover, physiologic hypertrophy is reversible, whereas pathologic hypertrophy is only reversible in the initial phases. For example, in women cardiac size normalizes 8 month after labor (Maillet M, 2013).

During hypertrophic growth, the balance between protein synthesis and degradation is altered. In particular, the main operators of physiologic hypertrophy are insulin, IGF1 and stretch activating mechanosensing signaling systems. All these stimuli converge in the PI3K signaling pathway, thus leading to PIP3 production, Akt, PKA and mTORC1 activation (Maillet M, 2013). Active mTORC1 promotes protein synthesis and sustains cardiac hypertrophy, and its pharmacological inhibition by rapamycin reverses cardiac hypertrophy induced by AKT overexpression (Shiojima I, 2005).

On the other hand, when cellular proteostasis is unbalanced in favor of degradation (e.g. fasting), CM atrophy occurs. Two main mechanisms mediate protein degradation (figure 2, panel b): the autophagy-lysosome system and the ubiquitin-proteasome system (UPS).

The first system allows the removal of organelles, big protein complexes and aggregates, upon their segregation within membrane-boud vesicles that fuse with lysosomes during the final stages of maturation. In the autofago/lysosome, lytic enzymes proteolyze the content. One of the markers of autophagy activation is the C-terminal lipidation of LC3-I that is converted into LC3-II when it associates with the autophagosome membrane. Whereas the basal levels of autophagy are low, the process can be significantly upregulated by a variety of different stressors, including ischemia/reperfusion injury, cardiac hypertrophy, heart failure and nutrient deprivation (Portbury AL, 2011).

The UPS relies on recognition of the target protein to be degraded by ubiquitin ligases, and after polyubiquitination the protein is sent to the 26S proteasome that degrades it. Ubiquitination is a multi step process operated by three families of ubiquitin ligases, among which E3 ligases are responsible for target specificity. There are two main muscle-specific E3 ubiquitin ligases: Atrogin1 (MaFbx) that is strongly induced in fasting conditions, and MURF1, a myofibrillar associated protein that localizes in the

M-line where interacts with titin (Powell SR, 2006). The expression of these two ubiquitin-ligases is regulated by FOXO transcription factors that are the intersection point between pro-atrophic and pro-hypetrophic pathways. Indeed, FOXO phosphorylation by AKT inhibits its transport in the nucleus and consequently decreases ubiquitin ligase transcription (figure 3, panel a).

In addition to the degradation systems described above, a third mechanism may be involved in sarcomere degradation. Calpains are Ca^{2+} dependent, non-lysosomal cysteine proteases, whose proteolitic action can facilitate access of E3-ubiquitin ligases to sarcomeric substrates. Interestingly, calpain 1 and 2 are found in the myocardium and have been linked to degradation of sarcomeric proteins, such as troponins, tropomyosin and titin (Portbury AL, 2011).

The idea that SNs can control heart size arises from several pieces of evidence. Interestingly, cardiac specific NGF overexpression leads to heart hyperinnervation and hypertrophy (Kiriazis H, 2005). Moreover, animals treated with β2-agonists showed cardiac hypertrophy (Ryall JG, 2006) and, conversely, animals treated with β-blockers (Nayler WG, 1980) or KO for β-adrenergic receptors (Lee S, 2010) showed decreased heart-to-body weight ratio. Recently, we have provided evidence that SNs regulate cardiac trophism through NE release. In particular, we have shown that cardiac sympathetic denervation causes a decrease in CM size that is mediated by the activation of the ubiquitin-proteasome and the autophagy-lysosome system through the FOXO dependent pathway (Zaglia T, 2013). Considering UPS, Atrogin1 and Murf1 upregulation was detected in denervated hearts.

Although atrophic and hypertrophic cardiac remodeling are well-studied processes, not much is known about sarcomere dynamics during these processes. The understanding of sarcomere assembly and degradation is of crucial interest, since changes in the sarcomeric structure and organization occur in cardiac remodeling associated to pathologic hypertrophy and heart failure. Moreover, given that myofibrils occupy roughly half of the CM volume (Bers DM, 2001), it is reasonable to expect that atrophic and hypertrophic changes may dramatically involve myofibrils.

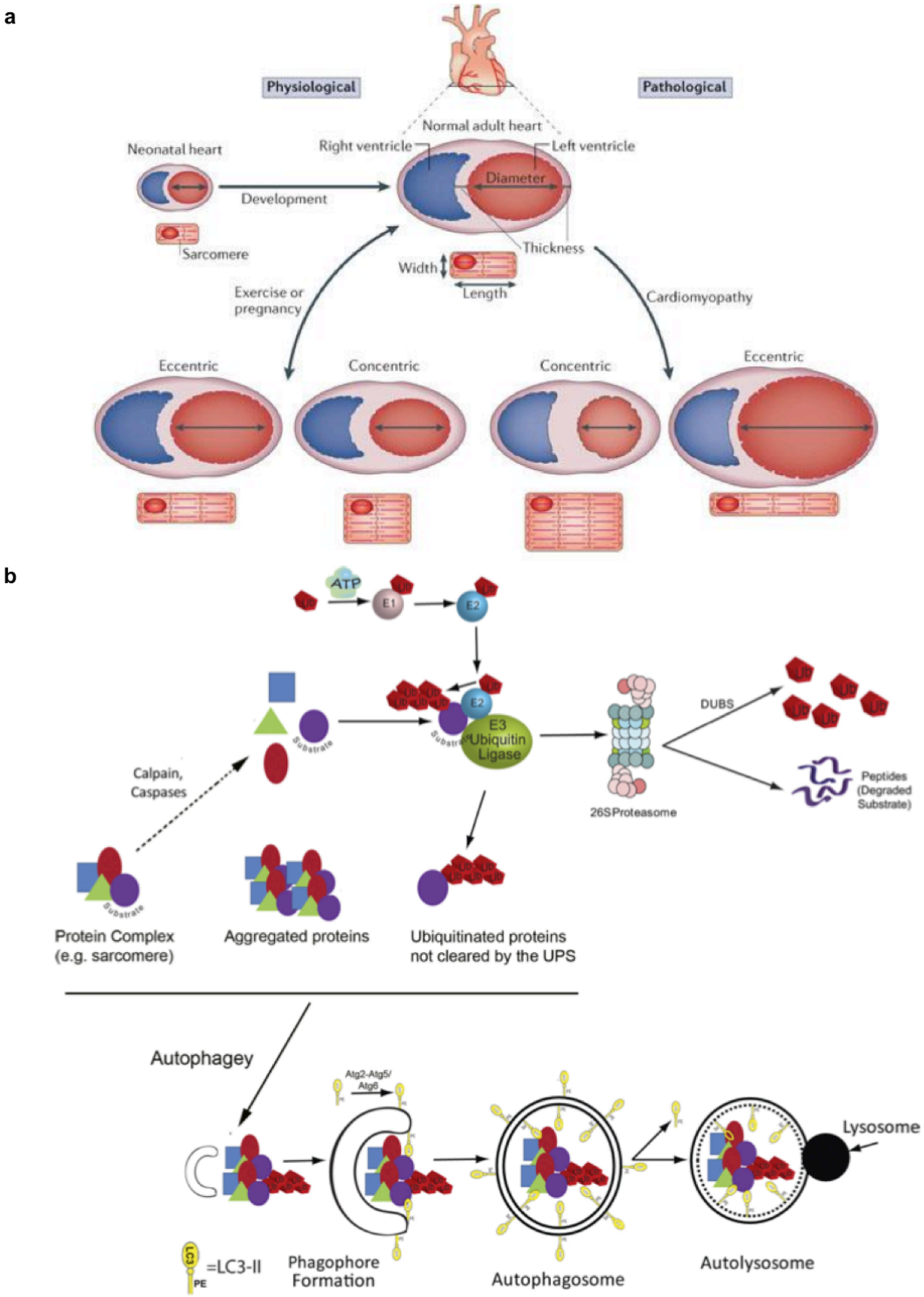

Figure 2 (**a**) Scheme of cardiac hypertrophic remodeling. From (Maillet M, 2013). (**b**) Different mechanisms of protein degradation. From (Portbury AL, 2011).

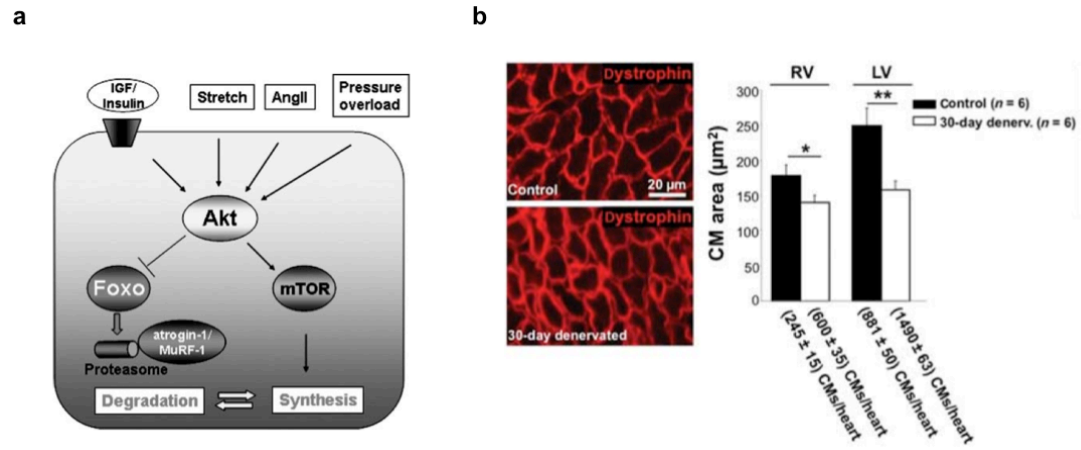

Figure 3 (**a**) Akt inhibits Foxo and activates mTor, thus increasing protein synthesis. From (Powell SR, 2006). (**b**) Figure from (Zaglia T, 2013), that shows cardiomyocyte atrophy upon heart denervation.

Sarcomere structure

Myofibrils are made by a repeated stretch of sarcomeres, the cardiomyocyte contractile units identified as the region between two subsequent Z-disks (figure 4, panel a and b). Anchored to the Z-disks, actin filaments are formed by polymerization of 43kDa G-actin monomers that extend in both directions from the Z-line interacting with the regulating protein troponin and tropomyosin to give rise to the thin filaments of the I-band (figure 4, panel c). Myosin molecules constitute thick filaments of the A-band that are held in place by the so-called M-band, the central line of the sarcomere, and that interdigitate with actin filaments (Boateng SY, 2008). Three functional subdomains characterize myosin: the motor domain, which binds to actin filaments and possesses ATPase activity, the neck, whose conformation change is central to sarcomeric shortening during contraction, and the tail that anchors and positions the motor domain so that it can interact with actin (Sellers JR, 2000). The interaction between myosin heads and actin filaments is crucial for sarcomere contraction and is mediated by the complex formed by four proteins:

- tropomyosin, which in its low Ca^{2+} configuration prevents myosin binding to actin filaments;
- troponin C, which responds to Ca^{2+};
- troponin I, which holds actin-tropomyosin complex in place and inhibits myosin binding;
- troponin T, which binds to tropomyosin.

After membrane depolarization and cytoplasmic Ca^{2+} increase, Ca^{2+} binds to troponin C, which binds tightly to inhibitory troponin I. The latter moves and weakens the interaction between troponin T and tropomyosin that relocates along the filaments allowing myosin to interact with actin. This process mediates the sliding of thick filaments on actin filaments in an ATP dependent manner and muscle contraction (White SP, 1987).

Several structural proteins are located in correspondence to the Z-disk, (figure 4, panel d), such as:

- α actinin, which forms a crosslink between actin filaments of opposite polarity originating from contacting sarcomeres (Luther PK, 2009);
- zasp, an adaptor protein that lacks enzymatic activity and that binds to α actinin2, stabilizing the Z-lines (Zhou Q, 1999);
- desmin, a 53 kDa intermediate filament protein that maintains muscle cytoarchitecture by forming a three dimensional cytoskeleton around the Z-disk and by connecting myofibrils to the cytoskeleton of the subsarcolemmal region (Paulin D, 2004).

The stability of sarcomere structure is guaranteed by titin, a 3MDa protein that runs from Z-disk to M-band with mechanical functions. Titin is the main determinant of myocardial passive tension thanks to its elasticity (Linke WA, 2008).

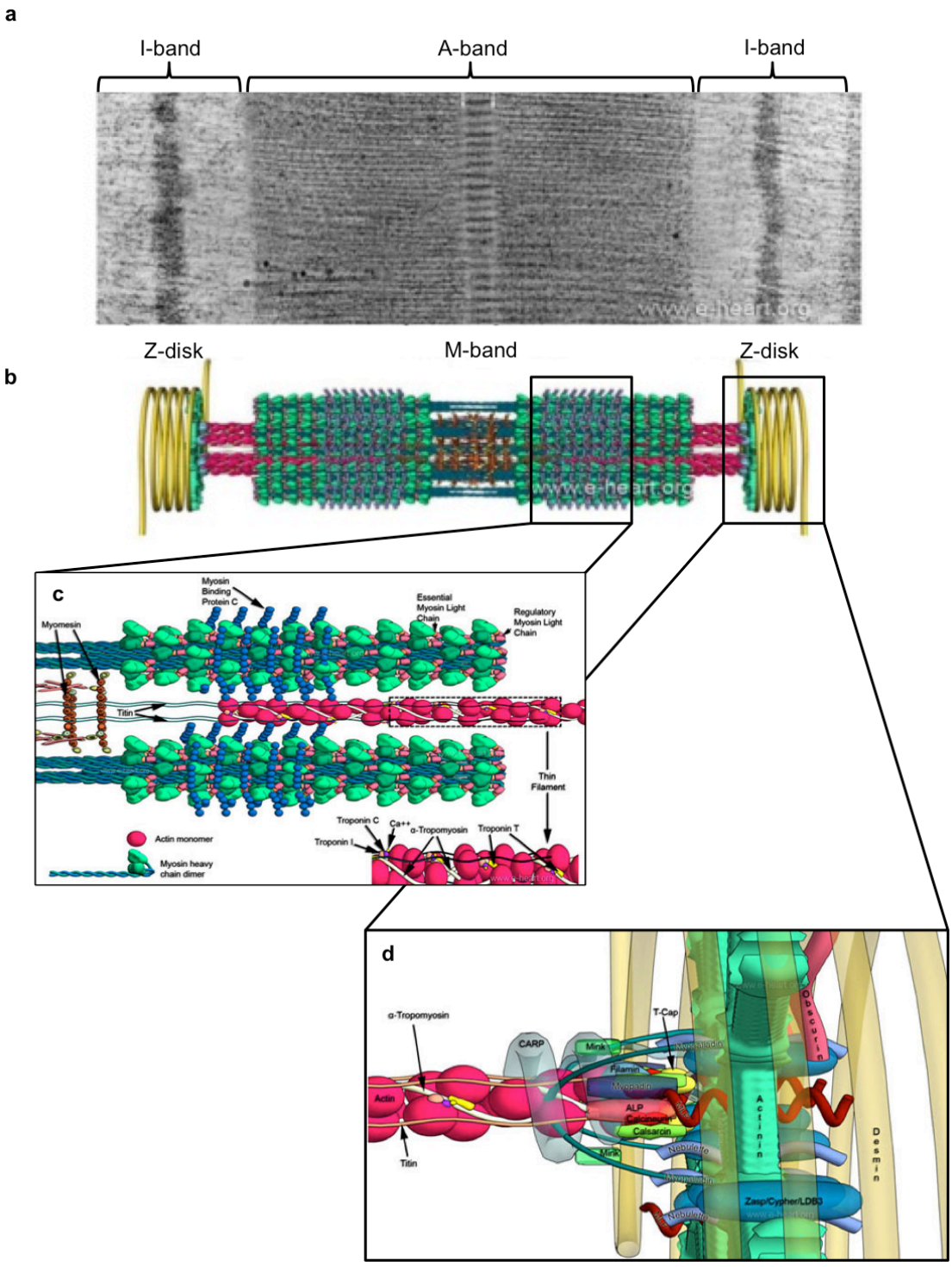

Figure 4 (**a**) Electron microscopy on sarcomeres. From (http://www.e-heart.org). (**b**) Schematic representation of a sarcomere, from (http://www.e-heart.org). (**c**) Interaction between myosin and actin filaments. From (http://www.e-heart.org). (**d**) Z-disk structure. From (http://www.e-heart.org).

2.3. Neurotrophins

Neurotrophins are a family of secreted proteins required for survival, differentiation and development of different subtypes of neurons. They include nerve growth factor (NGF), brain derived neurotrophic factor (BDNF), neurotrophin 3 (NT3) and neurotrophin 4/5 (NT4/5). The first neurotrophin discovered is NGF, which was described by Rita Levi Montalcini in the early 1950s as a soluble factor inducing sympathetic neuron hypertrophy and fiber outgrowth after mouse sarcoma tumor implantation close to the spinal cord in the developing chicken embryo (Levi Montalcini R, 1953). Consistent with the discovery of NGF effects on sympathetic neurons, it is now clear that NGF, NT3 and BDNF play an important role in the regulation of survival and differentiation of the peripheral neurons. In particular, NT3 is the first neurotrophin expressed by the peripheral nervous system during embryogenesis. During perinatal development, both sensory and sympathetic neurons depend on NT3 for their survival and differentiation and become dependent on NGF at later stages of postnatal development. BDNF also acts as a target derived survival factor for a subtype of dorsal root ganglia neurons and other sensory neurons. Despite the pro-survival effects of neurotrophins on peripheral neurons, neither of the neurotrophins seems to be crucial for survival of central neurons (Lessmann V, 2003). This can be explained by an overlapping role of neurotrophins on neurons that depend on the trophic input of more neurotrophins. For example, the effects of BDNF and NT3 on hippocampal neuronal survival are brought to light only when interference with both neurotrophin is achieved (Minichiello L, 1996).

Since NGF is the most important neurotrophin that determines differentiation, target organ innervation and survival of the sympathetic nervous system, the study of its role in the interaction between the heart and sympathetic neurons is of great interest and may provide new insights in disease conditions characterized by altered innervation.

2.3.1. NGF synthesis

NGF is synthesized from two transcripts that originate from alternative splicing (Bierl MA, 2005) and differ for an exon. As many other neurotrophins, NGF is expressed as a pre-pro-protein giving rise to 2 pre-proisoforms: a 34KDa (variant A) and a 27kDa

(variant B) isoforms. Once the protein translocates to the endoplasmic reticulum, the pre-peptide is cleaved to produce the 32kDa and 25kDa species of NGF, namely variant A and B respectively. In the endoplasmic reticulum, the pro-neurotrophin can spontaneously produce non-covalently linked dimers between the same or different variants. The pro-NGF is transported to the Golgi apparatus, where it is cleaved by the pro-protein convertases (e.g. furin) to produce the mature 13kDa NGF protein that is released as a homodimeric protein. In addition to pro-domain cleavage, NGF processing includes N-linked glycosylation of pro-domain residues and sulfatation of these N-linked oligosaccharides. The glycosylation has been described to be required for efficient neurotrophin expression, exit from the endoplasmic reticulum and escape from intracellular degradation (Seidah NG, 1996). In figure 5, panel a, a schematic representation of the variant B NGF sequence is reported.

Since its discovery, NGF function was described first in controlling organ innervation by sympathetic and sensory neurons. Its mRNA and protein can be found in innervated organs (e.g. submandibular glands, heart, lung, liver, kidney, spleen), where it is produced in low amounts. Its release is crucial for organ innervation, so that the degree of sympathetic innervation of an organ correlates with the amount of NGF it produces (Korsching S, 1983). In the central nervous system of rodents, NGF was found predominantly in the hippocampal and neocortical targets of cholinergic neurons projecting from the basal forebrain, and in some thalamic nuclei in the cerebellum and in the hypothalamus, during development. In the adult, NGF expression in all brain areas decreases especially when compared to those of NT3 and BDNF (Lessmann V, 2003). Because of the low NGF expression, it is difficult to detect endogenous NGF localization in tissues and many investigators have used overexpression strategies to address NGF biology in neurons or cell lines. NGF overexpression in hippocampal neurons showed a diffused localization when the neurotrophin levels were low; when NGF was overexpressed at higher levels, its pattern was vesicular, suggesting that NGF localization changes with the expression levels, and that diffused localization is consistent with low NGF expression (Mowla SJ, 1999). Since a diffused pattern is associated with constitutive secretory pathway, it seems more likely that NGF is constitutively released, even if it cannot be excluded that NGF is also processed

intracellularly from the regulated pathway. Overexpression of the neurotrophin in cell lines showed different secretion patterns depending on the characteristics of the cell line.

2.3.2. NGF signaling pathways

NGF binds to two distinct classes of receptors: the generic low affinity p75 neurotrophin receptor ($p75^{NTR}$) and the specific high affinity tyrosine kinase receptor TrkA. The first receptor belongs to the tumor necrosis factor receptor family, and binds to all neurotrophins with nanomolar affinity. It is a transmembrane glycoprotein with a cytoplasmic portion that contains a death domain analogous to that described in many other apoptosis-inducing receptors (e.g. Fas). Its ectodomain comprises four cysteine reach repeats that are all required for an efficient NGF binding. The biological function of the $p75^{NTR}$ depends on the neurotrophin that it binds as well as on the presence of the TrkA receptor at the surface of the cell (Wiesmann C d. V., 2001). For instance, TrkA affinity to NGF is increased by the presence of $p75^{NTR}$, thus enhancing the pro-survival neurotrophin effect in SNs. On the other hand, $p75^{NTR}$ stimulation by NGF in cells expressing $p75^{NTR}$ but not TrkA leads to neuronal apoptosis (Frade JM, 1996).

TrkA receptors bind NGF with picomolar affinity. Being a tyrosine kinase receptor, TrkA undergoes dimerization and subsequent tyrosine phosphorylation on several residues in the cytoplasmic domain (e.g. Tyr674, Tyr675) upon NGF binding. These events are followed by activation of downstream TrkA-mediated signaling pathways, which include ERK1/ERK2, that act on the transcription factors CREB and MEF2; PI3K, that phosphorylates AKT; PLCγ, that produces DAG and IP_3, triggering Ca^{2+} release from the intracellular stores (Harrington AW G. D., 2013). These pathways upregulate prosurvival genes and are responsible for inhibition of apoptosis (Pazyra-Murphy MF, 2009) by preventing activation of the pro-apoptotic transcription factor c-jun and of pro-caspase 3 (Mok SA, 2009) and BAX translocation to the mitochondria (Putcha GV, 1999).

Moreover, TrkA activation involves the production and retrograde transport of an endosome-based signaling platform that is described by the so-called signaling endosome hypothesis (Harrington AW G. D., 2013). The mechanism of endocytosis

upon NGF binding can be classified as clathrin-dependent or clathrin-independent (figure 5, panel b). The first form of endocytosis is characterized by the development of complexes that include TrkA, clathrin and AP2 (Howe CL, 2001), while the second process involves the production of macropinocytotic structures that require the presence of the NGF-regulated GTPase Pincher (Shao Y, 2002). The early stages of TrkA endocytosis involve the activation of PLCγ and in particular PI3K, since PI3K inhibition through LY294002 at distant axons affected retrograde [^{125}I]NGF transport (Kuruvilla R, 2000). PI3K activation leads to the recruitment of AP2, the RAS related protein RAB5 and dynamin, which is involved in scission of the endocytic vesicle from the cellular membrane (Harrington AW G. D., 2013). Moreover, long-distance movements of the endosome require disassembly of the actin cytoskeleton that is achieved after activation of Rac1-cofilin pathway, thanks to the stability of NGF-TrkA complex in the acid pH of early endosomes. In comparison to NGF, NT3 can bind to the TrkA and it activates the initial stages of endocytosis, but its labile interaction is interrupted during pH acidification in the endosome and thus NT3 cannot activate the subsequent steps (Harrington AW S. H., 2011). Finally, activated endosomes are transported back to the soma through dynein driven transport along the microtubules. In these endosomes, TrkA is maintained in a phosphorylated state (Riccio A, 1997) and PLCγ, PI3K and Erk signaling persist during endosome transport.

2.3.3. NGF structure

Human NGF crystal structure has been solved in complex with human TrkA (Wiesmann C U. M., 1999). The NGF monomer is characterized by a pair of 2 stranded twisted β sheets with a reverse loop (L3) and a cysteine knot-motif, characterized by 3 disulfide bonds on one end, and 3 β hairpin loops (L1, L2, L4) on the other (figure 5, panel c). In the dimer, the central β sheets of the two monomers pack against each other and interaction between residues of these two β sheets are responsible for the stabilization of the dimeric structure (Wiesmann C d. V., 2001).

Like the other neurotrophin receptors, TrkA is a transmembrane protein characterized by an extracellular domain that comprises a leucine-rich domain between two cysteine-rich clusters, followed by two immunoglobulin (Ig)-like domains. These two

domains are thought to be involved in NGF binding. In particular, TrkA Ig-like domain 5 by itself binds NGF with a similar affinity to the TrkA and consists of a β sandwich characterized by two four-stranded sheets. One comprises strands A, B, E and D, the other strands C, C', F and G (Wiesmann C U. M., 1999).

The crystallographic structure of NGF in complex with domain 5 of TrkA shows 2 patches of interaction, as represented in figure 5, panel c. One patch is considered specific for NGF binding to its receptor, the other one is considered conserved since it is maintained throughout all neurotrophins. Since neurotrophins share a 50% of sequence identity, the presence of both patches allows TrkA binding to many neurotrophins but SN survival only upon NGF binding. For example, in SNs from the superior cervical ganglia, NT3 is able to interact with NGF receptor and to trigger its phosphorylation but not its retrograde transport and SN survival (Harrington AW S. H., 2011).

The conserved patch is the larger one and involves residues from the AB, C'D and EF loops, the C-terminus of TrkA, the β hairpin loop L1 and residues of the four β strands of NGF. Arg103 is the highly conserved among neurotrophins and its side chain protrudes from NGF to stack against the phenyl group of Phe327 on TrkA, forming a hydrogen bond with the carboxyl group of Asn349.

The specific patch is characterized by interactions between the N-terminal residues 2-13 of NGF and the ABED sheet of TrkA, and shows small conservation among neurotrophins and receptors. In this interaction patch, residues 6-9 of NGF develop a helical conformation; His4 and Ile6 are the most important residues involved in the ligand-receptor interaction. Ile6 is located in a hydrophobic pocket at the surface of the TrkA with Pro5 and Phe7 contributing to the hydrophobic interactions. His4 and Glu11 increase the strength of the interaction by establishing hydrogen bounds with Ser304 and Arg347 of the 5^{th} domain of TrkA (Wiesmann C U. M., 1999).

2.3.4. NGF effects on sympathetic neurons

As described above, NGF is produced only in low amount by the target organs, is required for sympathetic neuronal survival and axonal outgrowth. These observations are supported by the almost complete loss of sympathetic innervation in $NGF^{-/-}$

(Crowley C, 1994) or TrkA$^{-/-}$ (Smeyne RJ, 1994) mice, and are the basis of the neurotrophic factor theory: according to this working hypothesis, the neurons and their ramifications are abundant during the development phase of peripheral innervation, and only the ones that efficiently reach the target organ receive adequate NGF amounts to survive, while the ones that fail in establishing contact with the target cells undergo apoptosis. In this manner, the amount of innervation that the organ receives is appropriate for its size and demand (Harrington AW G. D., 2013). This theory is supported by the observation that perinatal treatment of mice with anti-NGF antibodies causes death of the majority of sympathetic neurons, whereas NGF administration when innervation has completed does not result in neuronal loss (Davies AM, 2009).

Consistent with the concept that neurons receive the required NGF from the peripheral target organs, it has been demonstrated that NGF withdrawal from the ST caused accumulation of phosphorylated c-jun in the cell body that could no be rescued by direct NGF administration at the soma (Mok SA, 2009). These data support that signaling at the axonal terminal is required for neuronal survival. However, it remains to be studied whether NGF signaling requires the establishment of a contact site between the sympathetic neuron and the heart or whether its release in the interstitial space is sufficient to allow prosurvival neurotrophin signaling.

Interestingly, NGF upregulates TrkA expression, influencing neuronal selection in the phase of target organ innervation. This implicates that neurons, which are in close contact with the target organs would express more copies of TrkA, and as a consequence would have a reduced NGF requirement for survival. Conversely, neurons that are not well placed would express lower levels of TrkA and have a higher requirement of NGF that, when insufficient would result in neuronal death (Deppmann CD, 2008).

There may be another mechanism, through which NGF regulates neuronal selection. It is known that NGF signaling upregulates BDNF and NT4 in SNs. Since SNs do not express the BDNF/NT4 receptor (the TrkB), these neurotrophins act as an agonist of the p75^{NTR}, causing neuronal death. This evidence has led to the idea that SNs that establish an efficient interaction with the target organ express BDNF and NT4 leading

to death of neurons that fail to innervate the target organ in a paracrine manner, while being protected thanks to TrkA upregulation and NGF signaling (Deppmann CD, 2008).
In addition to promoting neuronal survival, other effects of NGF on SGNs were supported by experiments performed on *NGF*$^{-/-}$ and *Bax*$^{-/-}$ mice (Glebova NO, 2004). As described above, Bax is part of the apoptotic machinery activated upon NGF withdrawal, and its deletion prevents sympathetic neuronal loss in NGF KO mice. Interestingly, despite neurons grow normally along vessels and reach the target organ in *NGF*$^{-/-}$ and *Bax*$^{-/-}$ mice, sympathetic innervation is absent in the heart and heterogeneously altered in the other organs. This work not only showed that NGF requirement by SNs varies among different organs and that initial sympathetic outgrowth does not depend on NGF, but also suggest that NGF regulates heart innervation independently of its pro-survival activity.

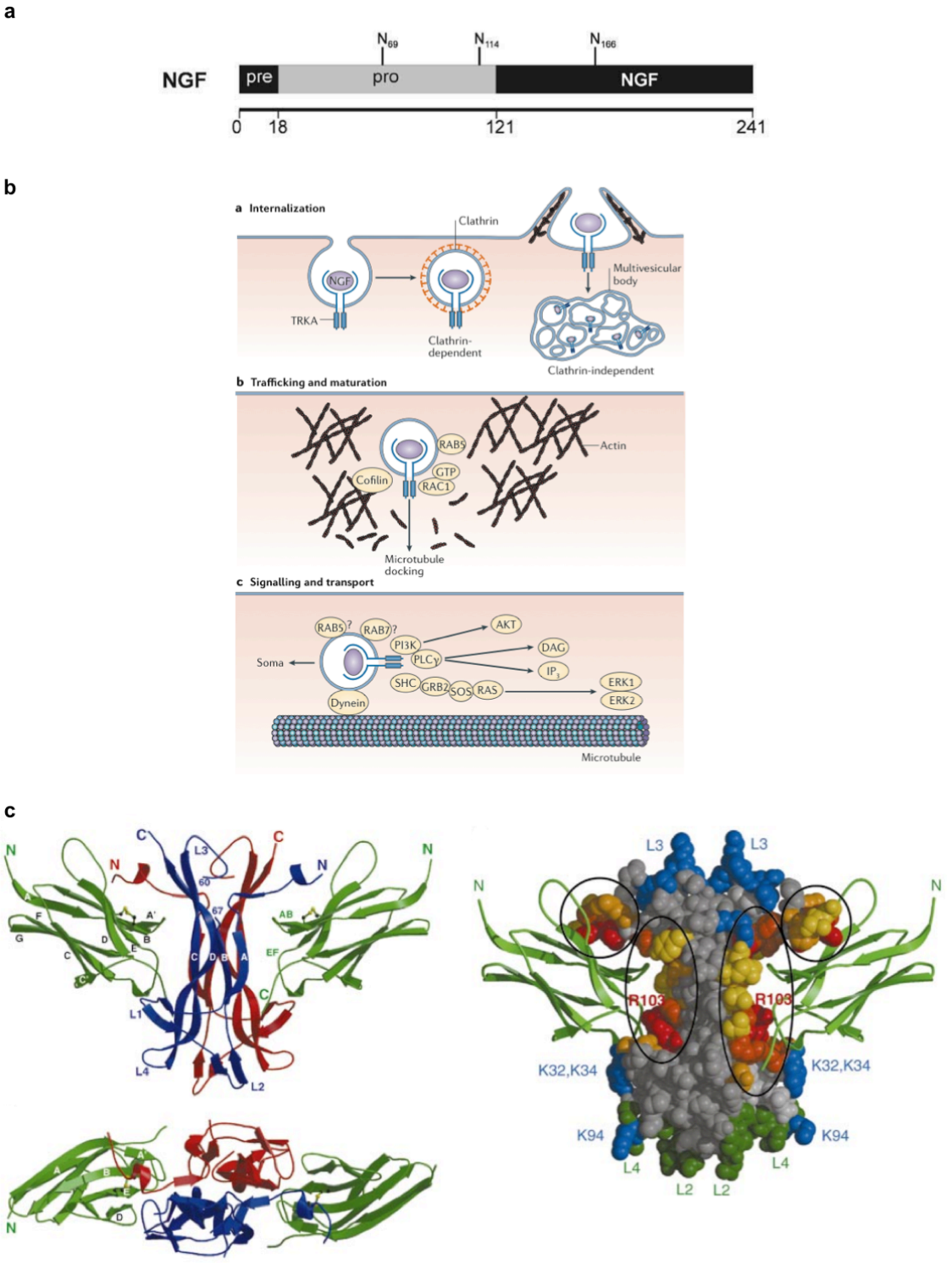

Figure 5 (**a**) Schematic representation of pre-proNGF. From (Lessmann V, 2003). (**b**) Mechanism of TrkA activation, endocytosis and retrograde transport. From (Harrington AW G. D., 2013). (**c**) NGF structure in complex with domain 5 of TrkA. From (Wiesmann C d. V., 2001).

2.3.5. Other neurotrophins acting on SNs

In addition to NGF, a number of other neurotrophin-like factors have roles in SGN growth and survival.

- Artemin is expressed by smooth muscle cells and its receptors Ret and GFRα3 are expressed by SGNs. Moreover, artemin is known to promote axonal growth along the vasculature. As a result, no increase in neuronal apoptosis was detected in SCG of mice KO for either artemin or its receptors at the early stage of development. Increased death was detected when neurons become dependent from target derived NGF, suggesting that this effect is a secondary consequence of the failure of many neurons to innervate the target organ.
- Endothelin-3 (Edn3) has been reported to be expressed by the external carotid artery and a part of SGNs express its receptor EdnrA. Since axonal growth is completely absent in the external but not in the internal carotid artery of *ednrA*$^{-/-}$ mice, Edn3 is relevant for axonal growth of a discrete subset of SGNs (Davies AM, 2009).
- NT3 is a neurotrophin expressed and released by the vasculature and SGNs express its receptor (TrkC). NT3 enhances outgrowth of sympathetic processes *in vitro* (Davies AM, 2009). Consistently, 50% of SNs survived after birth in *NT3*$^{-/-}$ mice (Francis N, 1999) (Wyatt S, 1997). Moreover, no innervation defects or increased neuronal death was observed in *TrkC*$^{-/-}$ mice (Fagan AM, 1996), suggesting that NT3 effects on SNs are achieved through TrkA signaling rather than TrkC receptor at the early developmental stage. Despite these observation, since neuronal loss in *NT3*$^{-/-}$ or *NGF*$^{-/-}$ mice occurs at the same developmental stage and is not higher in double KO mice when compared to *NGF*$^{-/-}$ mice (Francis N, 1999), it seems more likely that in *NT3*$^{-/-}$ mice, SNs die because they fail to reach the target organ and do not receive the adequate supply of pro-survival NGF. For this reason, NT3 signaling seems to be important during axonal growth along the vasculature. Moreover, SNs show a developmental change in their responsiveness from NT3 to NGF that is mediated by NGF signaling. When neurons are starting to innervate their target, $p75^{NTR}$ is much lower than TrkA and it is upregulated to similar TrkA

levels after birth (Wyatt S, 1997). Since $p75^{NTR}$ is known to increase TrkA affinity to NGF and to inhibit SN responsiveness to NT3, it seems that $p75^{NTR}$ upregulation is involved in the change of neuronal dependence from NT3 to NGF (Davies AM, 2009).

Since SGNs do not express TrkB (Fagan AM, 1996), BDNF or NT4/5 do not exert prosurvival effects, but might rather affect neuronal apoptosis through $p75^{NTR}$, as described before.

2.4. NE-NGF link

The existence of a crosstalk between neurotransmitter and neurotrophin signaling has been proposed in the case of the neuromuscular junction (NMJ), in which on the one hand the motor neuron activates the muscle by releasing acetylcholine and on the other, myofibers signal back to the neuron through release of the neurotrophin NT4. In the *in vitro* model between *Xenopus* motor neurons and muscles overexpressing NT4, the release of the neurotrophin from myocytes caused potentiation of presynaptic neurotransmitter release and the enhancement of postsynaptic response. Moreover, repetitive synaptic activity induced NT4 release by the myocyte, further potentiating synaptic transmission (Wang XH, 1997). A similar role of synaptic potentiation was described for NGF. In this case, stimulation of neurons in SGN/CM co-cultures caused a rise in CM contraction rate at increasing NGF concentrations. This effect was observed after either acute or chronic NGF stimulation (Lockhart ST, 1997). Moreover, increased NGF expression was demonstrated in astrocytoma cells treated with the non-selective β-agonist isoproterenol (Mocchetti I, 1989), suggesting that in different cell types interplay between β-adrenergic signaling and NGF transcription takes place. However, neither a similar interplay between NE released by the neuron and postsynaptic NGF expression nor the effect of the interaction between β-adrenergic signaling and NGF dependent signaling has been addressed so far in the neuro-cardiac axis.

2.5. The sympathetic nervous system in cardiac pathology

As described above, NGF expression correlates with target organ innervation (Korsching S, 1983) suggesting that NGF levels are regulated to match the requirement

of peripheral innervation. Evidence shows that NGF levels are altered in diseased hearts, causing aberrant innervation patterns. In a model of pulmonary hypertension-induced right ventricle hypertrophy, NGF expression was upregulated, leading to sympathetic nerve 'rejuvenation' (Kimura K I. M., 2007), which involves the expression of immature neuron-specific markers (e.g. PSA-NCAM). In congestive heart failure, although NGF levels were downregulated and innervation was reduced, sympathetic hyperactivity was assessed. Since CM exposure to 10µM NE led to NGF downregulation, this paradox was explained by a dynamic adaptive response to increased sympathetic activity (Kaye DM, 2000). Considering myocardial infarction (MI), NGF expression was increased in a canine model, causing cardiac nerve sprouting and hyperinnervation by sympathetic nerve (Zhou S, 2004), and such altered innervation pattern is one of the mechanisms increasing arrhythmogenesis in the post-MI heart. In further support of this, treatment of infarcted dogs with NGF caused altered sympathetic innervation, leading to ventricular tachycardia/fibrillation and sudden cardiac death. Untreated dogs with MI showed ventricular tachycardia but none of them died suddenly (Cao JM C. L., 2000).

Despite the involvement of NGF deregulation and abnormal innervation pattern have been described for different models of heart disease, a direct correlation between sympathetic innervation and fibrosis has never been investigated, nor the possibility that denervation may affect fibrosis in diseased hearts.

2.6. Objectives

Although the effects of SNs on CM trophism, channel expression and post-translational regulation have been characterized, not much is known about sarcomere dynamics. So the first aim of the project was the comprehension of the changes of sarcomeres under pro-hypertrophic or pro-atrophic stimuli.

The presence of an interaction between SNs and cardiac cells has been suggested by several papers. However the description a direct and stable interaction between the sympathetic axon and the CM nor the existence of a structure that is established between the two cells has never been described. For this reason, the second aim of this PhD thesis was to understand whether SGNs interact directly with CMs.

Considering NGF retrograde signaling, it is well accepted that the heart is able to produce and release NGF in low amounts; nevertheless NGF signaling at the ST is required for neuronal survival. However it is not known whether neurons are dependent on CM released NGF, whether neurotrophic signaling requires a contact site between two cells or occurs in the interstitial space and, eventually, its concentrations. For these reasons, our third aim was to investigate NGF signaling between neurons and cardiomyocyte.

The effects of different NGF concentrations on synaptic transmission have been described; however it is not clear whether adrenergic signaling may regulate NGF synthesis affecting neuronal survival. So, the fourth aim was the evaluation of the existence of a cross-talk between NE and NGF signaling for synaptic potentiation.

Finally, despite abnormal denervation has been detected in many models of heart disease, the role of the SNs on cardiac fibrosis has not been evaluated so far. So our last aim was to evaluate the effects of SNs in diseased hearts characterized by fibrosis.

3. Materials and Methods

3.1. Materials

Product	Company	Catalog number
0.25% Trypsin	Invitrogen	15050057
0.25% Trypsin-EDTA	Invitrogen	25200056
1.5mL tubes	Sarstedt	72690001
10mL serological pipettes	Sarstedt	861255001
100mm tissue culture dish	BD biosciences	353003
13mm coverslips	Vetrotecnica	90052176313
15mL tubes	Sarstedt	62554502
24 well plates	Sacco s.r.l.	F3047
24mm coverslips	Vetrotecnica	01.4150.31
25mL serological pipettes	Sarstedt	861254001
5mL serological pipettes	Sarstedt	861253001
50mL serological pipettes	Sarstedt	861689001
50mL tubes	Sarstedt	62547254
6-hydroxy-dopamine hydrochloride	Sigma-Aldrich	H4381
6well plates	Sacco s.r.l.	F3046
ABI 4800 Applied Biosystems	Applied Biosystems	
Absolute ethanol	Sigma-Aldrich	02860
Acetone	Polysciences	01921
Agglutinin alexa 555	Invitrogen	W32464
Agglutinin alexa 588	Invitrogen	W11261
Anti actin	Sigma-Aldrich	A5060
Anti DBH	Abcam	AB43868
Anti distrophin	Abcam	AB15277
Anti goat cy3	Jackson	705-165-147
Anti HA	Sigma-Aldrich	H6908

Anti LC3	Cell signaling	12741
Anti mouse alexa 647	Invitrogen	A21239
Anti mouse cy3	Jackson	115-165-1660
Anti mouse-HRP	Bio-rad	170-6464
Anti NGF	Abcam	AB6199
Anti pan cadherin	Abcam	AB6529
Anti prolyl-OH	Acris	AF5110
Anti rabbit alexa 488	Jackson	111-545-1440
Anti rabbit alexa 647	Jackson	711-605-1520
Anti rabbit cy3	Jackson	111-165-144
Anti rabbit-HRP	Bio-rad	170-6463
Anti sheep TRITC	Jackson	713-025-147
Anti synapsin I	Millipore	AB1543
Anti synaptophysin	Dako	M0776
Anti TOH (rabbit)	Millipore	AB152
Anti TOH (sheep)	Millipore	AB1542
Anti trkA	[1]	
Anti troponin I	[2]	
Anti troponin T	[3]	
Anti ubiquitin	Cell signaling	3936
Anti VAMP2[4]	Synaptic system	104211
Anti α actinin	Sigma-Aldrich	A7732

[1] Anti-Trka antibody was a gift from Dr. Louis Reichardt (University of California, San Francisco).

[2] Anti-Troponin I antibody was a gift from Prof. Stefano Schiaffino (University of Padova, Padova).

[3] Anti-Troponin T antibody was a gift from Prof. Stefano Schiaffino (University of Padova, Padova).

[4] Anti-VAMP2 antibody was provided by the lab of Dr. Claudia Lodovichi (VIMM, Padova).

Anti β catenin	Abcam	AB16051
AraC	Sigma-Aldrich	C6645
BamHI	New England Biolabs	R0136S
Blotting-grade blocker	Bio-Rad	170-6404
Bovine serum albumin	Sigma-Aldrich	A7906
Burker chamber	VWR	631-1123
C1000 Thermal Cycler	Bio-rad	
Cable for heater controller	Warner Instruments	CC-28
Carestream® Kodak® biomax® xar films	Sigma-Aldrich	F5388
ChemiKine NGF sandwich ELISA Kit	Chemicon	CYT304
Clenbuterol	Sigma-Aldrich	C5423
Collagen	Sigma-Aldrich	C9791
Collagenase A	Roche	10103586001
Complete EDTA-free	Roche	05056489001
Cryostat CM1950	Leica	
Culture dish incubator	Warner Instruments	dh-35iL
D-(+)-Sucrose	Sigma-Aldrich	84100
Dako pen	Dako	S2002
DAPI	Invitrogen	D3571
DMEM without phenol red	Invitrogen	21063029
DMEM, high glucose	Invitrogen	41965039
DMEM, high glucose, hepes	Invitrogen	42430025
DMSO	Sigma-Aldrich	D2650
DPBS without Ca^{2+} and Mg^{2+}	Invitrogen	14190094
DTT	Invitrogen	43816
ECL western blotting substrate	Tema ricerca	32132
Eclipse TE200	Nikon	
EDTA	Sigma-Aldrich	E6758
Eukitt®	Sigma-Aldrich	03989
Epoxidic resin	Sigma-Aldrich	31185
FBS	Invitrogen	10270106

GeneAmp 7500 Sequence Detection System	Applied Biosystems	
Genelute gel extraction kit	Sigma-Aldrich	NA1111
Glutaraldehyde	Sigma-Aldrich	49626
Glycerol bioxtra	Sigma-Aldrich	G6279
HATU	Chempep	120801
HBSS	Invitrogen	24020117
HBSS without phenol red	Invitrogen	14025134
Heater controller	Warner Instruments	TC-324B
Hematoxylin and eosin staining kit	Bio-optica	04-061010
Hoechst 33342	Invitrogen	H3570
HS	Invitrogen	16050122
Human recombinant β-NGF	Sigma-Aldrich	SRP3015
ImageJ	NIH	
K252a	Sigma-Aldrich	K1639
KpnI	New England Biolabs	R0142S
L-glutamine 200mM	Invitrogen	25030024
Laminin	Sacco s.r.l.	CPB40232
LB	Sigma-Aldrich	L3022
Leica DMI4000B	Leica	
Leica DMI6000B	Leica	
Lipofectamine 2000	Invitrogen	11668027
M199	Invitrogen	31150022
M199 without phenol red	Invitrogen	11043023
Magnesium chloride	Sigma-Aldrich	M8266
Maxi prep	Sigma-Aldrich	NA0310
Methanol	Sigma-Aldrich	32213
NCS	Invitrogen	16010159
NheI	New England Biolabs	R0131S
NuPage antioxidant	Invitrogen	NP0005
NuPage MES SDS running buffer (20 ×)	Invitrogen	NP0002
NuPAGE® 4-12% gradient bis-tris gel	Invitrogen	NP0321BOX

NuPage® LDS sample buffer	Invitrogen	NP0007
NuPage® transfer buffer 20×	Invitrogen	NP0006
OCT	Kaltek	0782
Olympus BX60	Olympus	
Olympus IX50	Olympus	
Osmium tetroxide	Sigma-Aldrich	75632
p-benzyloxybenzyl alcohol resin	Novabiochem	855002
Pancreatin	Sigma-Aldrich	P-1750
Paraformaldehyde	Sigma-Aldrich	P-6148
Penicillin/Streptomycin	Invitrogen	15070063
Phalloidin alexa 568	Invitrogen	A12380
Phalloidin alexa 633	Invitrogen	A22284
PhosStop	Roche	04906845001
Phusion	New England Biolabs	M0530L
Poly-D-lysine hydrobromide	Sigma-Aldrich	P6407
Polystyrene tubes	Sarstedt	55.1579.002
Polyvinyl alcohol	Sigma-Aldrich	P8136
Prep Nova-Pak HR C18	Waters	
Propidium iodide	Sigma-Aldrich	P4864
Propylene oxide	Sigma-Aldrich	82320
Protein assay dye reagent	Bio-rad	5000006
PVDF	GE Healthcare	GEHRPN303F
Reynolds lead citrate	Sigma-Aldrich	15326
RPMI	Invitrogen	52400025
Scanner Epson Photo Perfection V330	Epson	
Scrapers	VWR	391-3010IT
SDS	Sigma-Aldrich	L3771
SeeBlue® Plus2 Prestained Standard	Invitrogen	LC5925
SIC001	Sigma-Aldrich	SIC001
Sodium cacodylate	Sigma-Aldrich	C0250
Sodium chloride	Sigma-Aldrich	S7653

Superfrost plus microscope slides	Thermo scientific	4951PLUS4
Superscript III	Invitrogen	18080044
SV total RNA isolation	Promega	Z3100
Syro II peptide synthesizer	MultiSynTech GmbH	
T4 DNA ligase	New England Biolabs	M0202S
T75 tissue culture flasks	Sacco s.r.l.	F3136
TissueLyserII	Qiagen	
Total RNA isolation System	Promega	Z3100
Transfectin	Bio-rad	170-3351
Tris	Sigma-Aldrich	T1378
Triton X-100	Sigma-Aldrich	93420
TrkA-DsRed2 construct	Addgene	21216
Trypan blue solution	Invitrogen	T8154
Tween20	Sigma-Aldrich	P1379
Uranyl acetate	Sigma-Aldrich	73943
Uridine	Sigma-Aldrich	U3750

3.2. Cells

For this PhD thesis, many cell types were used. For experimental set up we used cultures of cell lines, such as HeLa [5] and PC12 [6]. For the final experiments, cardiomyocytes, sympathetic neurons and cardiac fibroblasts were isolated from neonatal rats according with European Commission guidelines. Protocols for culture preparation have been approved by the local ethical committee and the relevant Italian authority (Ministero della Salute, Ufficio VI), in compliance of Italian Animal Welfare Law (Law n 116/1992 and subsequent modifications), and complying with the Directive 2010/63/EU of the European Parliament.

3.2.1. Culture of neonatal cardiomyocytes

Neonatal cardiomyocytes were isolated from p2-p3 rat hearts. Before extraction, coverslips were sterilized with absolute ethanol, incubated with 20µg/mL laminin at 37°C for 1 hour and washed twice with 1× PBS. Hearts were isolated and collected in a 50mL tube containing 10mL of ice cold 1× ADS (table 1). The supernatant was removed under a biological hood and samples were minced using a surgical scissor. After mechanical dissection, heart fragments were put in a 50mL tube with a magnetic stir bar. After ADS removal, 7mL of digestion solution (table 2) were added to the samples and the suspension was incubated 5 minutes at 37°C on a stirrer to remove damaged cells from the surface of the heart pieces. At the end of this soft digestion, the supernatant was discarded and 7.5mL of digestion solution were added to the cells that were incubated 20 minutes at 37°C on a stirrer. The supernatant that contained cardiomyocytes was collected in a 15mL tube adding 1mL of heat inactivated HS, and centrifuged at 1500g for 5 minutes without brake. After supernatant removal, cells were resuspended in 2mL of fresh first day medium (FDM, table 3) and maintained in the incubator until the end of the digestions. About 7.5mL of digestion solution were added to the remaining non-digested heart pieces to begin a new digestion step. Digestions were repeated until the total dissolution of heart fragments was obtained.

[5] HeLa cells were a gift from Prof. Fabio Mammano (University of Padova, Padova).

[6] PC12 cells were a gift from Prof. Cesare Montecucco (University of Padova, Padova).

At the end of tissue digestion, cell suspensions were collected and seeded in a new 100mm tissue culture dish. The pre-plating was performed at 37°C for 1 hour. In this step, cardiac fibroblasts are separated from cardiomyocytes because of their faster adhesion to the plate. The supernatant enriched in cardiomyocytes was collected in a 50mL tube; count was achieved by diluting cells in a 1:5 solution of Trypan Blue:1× PBS and using a Bürker chamber. CMs were seeded on laminin-coated coverslips at a cellular density of 316cells/mm^2. The 3rd day of culture, the medium was changed and cardiomyocytes were incubated with second day medium (SDM) supplemented with 10µM AraC for 24 hours (table 3). The 4th day, AraC was removed and fresh SDM was added. Medium was changed every 2-3 days.

1× ADS

Component	Concentration
NaCl	106mM
Hepes	20mM
Na_2HPO_4	0.8mM
KCl	5.3mM
$MgSO_4(7H_2O)$	0.4mM
Glucose	5mM

The solution was brought to pH 7.4 and sterilized by using 0.22 µm filters.

Table 1 Composition of 1× ADS solution used for neonatal CM isolation.

Digestion solution

Component	Amount
Collagenase A	22.5mg
Pancreatin	50mg

Enzymes were resuspended in 50 mL 1× ADS and sterilized by using 0.22 µm filters.

Table 2 Composition of the enzymatic solution used for the disaggregation of heart pieces.

First day medium (FDM)		Second day medium (SDM)	
Component	**Concentration**	**Component**	**Concentration**
DMEM Hepes	66%	DMEM Hepes	75.4%
M199	17%	M199	17.1%
Heat inactivated HS	10%	Heat inactivated HS	5%
Heat inactivated NCS	5%	Heat inactivated NCS	0.5%
Glutamine (200mM)	1%	Glutamine (200mM)	1%
P/S	1%	P/S	1%

Table 3 Composition of CM culture media.

3.2.2. Culture of neonatal sympathetic ganglia neurons

Sympathetic ganglia neurons were isolated from the superior cervical ganglia of p2-p3 rats. Before extraction, coverslips were sterilized with absolute ethanol, incubated with 20µg/mL laminin at 37°C for 1 hour and washed twice with 1× PBS. Ganglia were collected in complete medium (table 4) and maintained in ice during the isolation. Samples were centrifuged at 1000g for 1 minute without brake, resuspended in 0.25% trypsin without EDTA, minced with surgical scissors and incubated at 37° C on a stirrer for 15 minutes. To improve cell isolation, the suspension was pipetted for 5 minutes. Enzymatic digestion was stopped by adding 4mL of heat inactivated HS and followed by a centrifugation at 1500g for 5 minutes without brake. Cells were resuspended in 500µL of final medium (table 4), counted as previously described and seeded on laminin-coated coverslips using a density of 105 cells/mm^2. The 3rd day of culture, the medium was changed and SNs were incubated with SDM supplemented with 8nM NGF and 10µM AraC for 24 hours to reduce fibroblast proliferation. From the 4th culture day, NGF was removed or maintained in the medium, accordingly to the experimental plan. The culture medium was changed every 2-3 days.

Complete medium		Final medium	
Component	**Concentration**	**Component**	**Concentration**
RPMI	84%	RPMI	97.4%
Heat inactivated HS	10%	Heat inactivated HS	1%
FBS	5%	Uridine (10mM)	0.1% (10µM)
P/S	1%	FDU (30mM)	0.3% (10µM)
		P/S	1%
		NGF (4µM)	0.2% (8nM)

Table 4 Composition of complete and final medium used for SGN isolation.

3.2.3. SGN/CM co-culture

Co-cultures were prepared by seeding together CMs and SGNs in a ratio of 3 to 1 on laminin-coated coverslips, as previously described. The 3rd day of co-culture, the medium was changed and cells were incubated with SDM supplemented with 8nM NGF and 10µM AraC for 24 hours. From the 4th culture day, NGF was maintained or removed, accordingly to the experimental plan. Medium was changed every 2-3 days and cultures were maintained for 12-14 days.

3.2.4. Cardiac fibroblast culture

Cardiac fibroblasts were obtained from the pre-plating phase during the neonatal cardiomyocyte preparation. Briefly, cells attached to the plate were washed twice with 5mL of fresh 1× ADS and detached by a 3 minute long incubation with 1 mL of 0.25% trypsin with EDTA at 37°C. To block enzymatic digestion, 3mL of FDM (table 3) were added and cells were collected in a new 50mL tube. The plate was further washed with other 3mL FDM that were put together with the previous suspension. Cells were centrifuged at 1500g for 5 minutes, trypsin was removed and cells were resuspended in 3mL of fresh FDM. Cells were counted and seeded in laminin coated 6 well plates at a density of 100 cells/mm^2. The 3rd day, cells were washed 3 times and SDM was added.

3.2.5. HeLa culture

We maintained HeLa cells in HeLa medium (see table 5) in T75 tissue culture flasks and split them when they reached a 70-80% confluence. Split was achieved by washing cells twice with 3mL of 1× PBS and by incubating them with 1mL of 0.25% Trypsin with EDTA for 3 minutes at 37°C. Enzymatic digestion was stopped with 3mL of HeLa medium; cells were collected in a 50mL tube. Other 3mL of HeLa medium were added to wash the flask and the remaining cells were collected in the 50mL tube. Collected cells were centrifuged at 1500g for 5 minutes with brakes and resuspended in 3mL of HeLa medium. Cell count was performed as previously described. To expand the culture, a 1:5 dilution of the cellular suspension was resuspended in 10mL of fresh HeLa medium and seeded in a T75 tissue culture flask. For freezing procedure, 700 µL/vial of cellular suspension were added to 300 µL/vial of a 2:1 solution FBS:DMSO and stored at -80°C in a polystyrene box after split. Each vial contained a 1:5 dilution of the initial culture.
For experiments, HeLa cells were seeded at a density of 100 c/mm^2 on laminin-coated coverslips.

HeLa medium

Component	Concentration
DMEM	89%
Heat inactivated FBS	10%
P/S	1%

Table 5 Composition of the medium used for HeLa cell culture.

3.2.6. PC12 culture

PC12 cells are a cell line derived from rat pheochromocytoma and can be differentiated in sympathetic like neurons in the presence of 8nM NGF. PC12 cells were maintained in an undifferentiated state in UM (see table 6) on 100mm tissue culture dishes that were previously coated with 0.064mg/mL collagen for 2 hours at room temperature. Medium was changed every 2-3 days. When cells were 70-80%

confluent, they were split. Briefly, undifferentiated PC12 were washed twice with 5mL 1× PBS, adding 2mL of fresh UM. Cells were detached from the plate using a 1mL pipet. Cellular suspension was collected in a 50mL tube, pipetted repeatedly for 10-15 minutes to disrupt clusters and counted by using a Bürker chamber. Cells were seeded on a new collagen coated dish at a dilution of 1:5 to expand the cell line. PC12 cells were frozen by using the same protocol of HeLa cells.

For differentiation in sympathetic like neurons, PC12 cells were resuspended in DM (see table 6). Cells were seeded at a density of 100 cells/mm^2 on coverslips that were previously coated with poly-D-lysine 0.01mg/mL for 1 hour and collagen 0.064mg/mL for 2 hours at room temperature. Medium was changed every 2-3 days and cells were differentiated for 6 days in the presence of 8nM NGF.

Undifferentiating medium (UM)		**Differentiating medium (DM)**	
Component	**Concentration**	**Component**	**Concentration**
RPMI	83%	RPMI	96.8%
Heat inactivated FBS	5%	Heat inactivated HS	1%
Heat inactivated HS	10%	Glutamine (200mM)	1%
Glutamine (200mM)	1%	P/S	1%
P/S	1%	NGF	0.2% (8nM)

Table 6 Composition of UM and DM used for PC12 cultures.

3.3. Immunofluorescence (IF)

One of the techniques used during this PhD thesis, was the IF staining, both on cell cultures and mouse and rat heart cryosections. It is a technique that allows the localization of specific proteins thanks to the binding of a primary antibody to one or more epitopes of the target protein. Fluorochrome bound antibodies that recognize the primary antibody, are used to detect the localization of the protein of interest.

3.3.1. Immunofluorescence staining on cell cultures

Cell cultures were fixed with 4% PFA for 30 minutes at 4°C and washed twice with 1× PBS for 10 minutes. Cells were permeabilized with 1× PBS supplemented with 1% BSA and 0.1% TX-100 for 3 minutes at room temperature and washed 3 times for 5 minutes using 1× PBS. Cells were incubated for 2 hours at 37°C with primary antibodies diluted in 1× PBS, 1% BSA as indicated in table 7. For double IF staining, a mix of 2 different antibodies was used. At end of primary antibody incubation, 3 washes of 5 minutes with 1× PBS were done and cells were incubated for 30 minutes at 37°C with the secondary antibody diluted in 1× PBS, 1% BSA (table 7). In double IF staining, the washes and this step were repeated using another secondary antibody against the other primary antibody. The sequence of the secondary antibody was chosen to reduce the risk of cross reactivity. Cells were washed 3 times for 5 minutes using 1× PBS, incubated for 15 minutes at room temperature with DAPI at 1:1000 dilution, washed twice with 1× PBS and mounted using elvanol. If a staining with dyes was required, dyes were incubated at the concentration and conditions listed in table 7 before the DAPI staining and washed 3 times with 1× PBS for 5 minutes.
Control samples were used to evaluate background and cross reactivity of secondary antibodies.

3.3.2. Immunofluorescence staining on rat and mouse heart slices

Hearts were isolated from 3 month old male mice and rats and put in ice cold 1× PBS to wash tissues from blood. Samples were cut transversally at the mid portion of the ventricles and fixed in 1% or 2% PFA (for mouse and rat hearts respectively) for 15 minutes at room temperature on a shaker. At the end of the fixation, samples were washed 3 times for 5 minutes with 1× PBS on a shaker at room temperature and incubated ON in 30% sucrose to allow tissue dehydration. The following day, hearts were frozen on liquid nitrogen after OCT treatment and stored at -80°C. Ten µm thick cryosections were cut using Leica cryostat, placed on superfrost slides and stored at -80°C.
Samples were thawed for 10 minutes at room temperature and slices were circled with Dako pen. Then, cryosections were rehydrated for 10 minutes in 1× PBS for

rehydration and incubated ON at 4°C with the primary antibody diluted to the concentration indicated in table 7 in 1× PBS supplemented with 1% BSA and 0.5% Tx-100. When a double IF staining was performed, slices were incubated with a mix of the two antibodies. The following day, cryosections were washed 3 times with 1× PBS for 5 minutes and incubated with the secondary antibody for 30 minutes at 37°C at the concentrations listed in table 7. At the end of the incubation, cryosections were washed 3 times with 1× PBS for 5 minutes and the steps of secondary antibody incubation and washes were performed again in the case of a double IF staining. Nuclei were counterstained with a 1:1000 dilution of DAPI (15 minutes) at room temperature; sections were washed 3 times with 1× PBS for 5 minutes and mounted using elvanol. If a staining with dyes was necessary, dyes were incubated at the concentration and conditions listed in table 7 and washed 3 times with 1× PBS for 5 minutes.

Primary antibodies

Target	Company	Host species	Dilution
DBH	Abcam	rabbit	1:200
Distrophin	Abcam	rabbit	1:500
HA	Sigma-Aldrich	rabbit	1:100
LC3	Cell signaling	rabbit	1:200
NGF	Abcam	rabbit	1:100
Pan cadherin	Abcam	rabbit	1:6000
Prolyl-OH	Acris	mouse	1:500
Synapsin I	Millipore	rabbit	1:600
Synaptophysin	Dako	mouse	1:50
TOH	Millipore	rabbit	1:400
TOH	Millipore	sheep	1:100
TrkA	[7]	rabbit	1:200

[7] Anti-Trka antibody was a gift from Dr. Louis Reichardt (University of California, San Francisco).

Troponin I	[8]	mouse	1:200
Troponin T	[9]	mouse	1:200
Ubiquitin	Cell signaling	mouse	1:50
VAMP2	Synaptic system	mouse	1:200
α actinin	Sigma-Aldrich	mouse	1:200
β catenin	Abcam	rabbit	1:4000

Secondary antibodies

Target	Company	Host species	Dilution
Anti goat cy3	Jackson	donkey	1:300
Anti mouse alexa 647	Invitrogen	rabbit	1:300
Anti mouse cy3	Jackson	goat	1:200
Anti rabbit alexa 488	Jackson	goat	1:200
Anti rabbit alexa 647	Jackson	donkey	1:200
Anti rabbit cy3	Jackson	goat	1:200
Anti sheep TRITC	Jackson	donkey	1:100

Dyes

Name	Company	Incubation	Dilution
Agglutinin alexa 488	Invitrogen	1 hour, 37°C	1:300
Agglutinin alexa 555	Invitrogen	1 hour, 37°C	1:300
Phalloidin alexa 568	Invitrogen	1 hour, 37°C	1:1000
Phalloidin alexa 633	Invitrogen	1 hour, 37°C	1:200

Table 7 List of primary, secondary antibodies and dyes used during IF stainings.

[8] Anti-Troponin I antibody was a gift from Prof. Stefano Schiaffino (University of Padova, Padova).

[9] Anti-Troponin T antibody was a gift from Prof. Stefano Schiaffino (University of Padova, Padova).

3.4. Hematoxylin and eosin staining

Hematoxylin and eosin staining was used to evaluate the histology of mouse hearts. The Hematoxylin and eosin staining kit (Bio-optica) was used. Heart cryosections were thawed for 10 minutes at room temperature and treated for 30 seconds with hematoxylin. The reagent was recovered and three washes with deionized water were performed to remove the excess of hematoxylin. Then, slices were incubated for 5 seconds in the toning solution for hematoxylin, washed 3 times with deionized water and incubated with eosin for 1 minute. After three washes with deionized water, heart cryosections were dehydrated with 95% ethanol for 5 seconds, 100% ethanol for 2 minutes and 100% xylene for 5 minutes. Final mounting was performed using Eukitt®.

3.5. Transmission electron microscopy

TEM analysis was performed both on rat SN-CM co-cultures and adult mouse heart slices.

3.5.1. Sample preparation for *in vitro* TEM

For *in vitro* TEM, cells were seeded directly on the plastic of 24 well plates that were previously coated with laminin. Samples were fixed by using a solution of 0.1M sodium cacodylate supplemented with 2.5% glutaraldehyde, at pH 7.2 for 40 minutes at 4°C and washed twice for 30 minutes with 0.2M sucrose, 0.1M sodium cacodylate at pH 7.2 maintaining cells on ice. After fixation, samples were processed in the TEM facility at the University of Padova, by Valerio Gobbo. Post-fixation was done in 1% osmium tetroxide, 0.1 M sodium cacodylate, pH 7.2 for 2 hours at 4°C. Samples were then dehydrated in ascending ethanol series (50% for 15 minutes, 70% for 30 minutes, 90% for 30 minutes and 100% for 90 minutes), incubated with propylene oxide for 45 minutes and embedded in epoxy resin. Resin embedding was performed with three successive 45 minutes incubations with different solutions of acetone/resin (2:1, 1:1 and 1:2) and incubating cells with 100% resin for 1 hour. Then fresh resin was added. Polymerization was performed with 3 successive 24 hours incubations at 37°C, 45°C and 60°C. The resin was extracted from the wells and semithin sections were cut, stained with 1% toluidine blue and observed at the light microscope. Sections of

selected fields were stained with uranyl acetate, 50% ethanol and Reynolds lead citrate and examined with a FEI Tecnai 12 electron microscope.

3.5.2. Sample preparation for TEM on mouse heart slices

To perform TEM on mouse heart slices, 3 month old mice were anesthetized 25mg/kg Zoletil 100. The thoracic cavity was opened and the abdominal aorta was canulated with a 22-G needle. The inferior cava vein was cut to allow the outflow of the fixative. Hearts were retrogradely perfused with 20mL of 1× tyrode solution (see table 8) at a rate of 60mL/h, followed by fixation with 50 mL of a solution of 2.5% glutaraldehyde, 0.1M sodium cacodylate at pH 7.2. Hearts were removed, the right and left ventricles dissected, minced in $1mm^2$ pieces and further fixed with a solution of 0.1M sodium cacodylate supplemented with 2.5% glutaraldehyde at pH 7.2 for 2 h at 4°C. Samples were washed twice for 10 minutes with 0.2M sucrose, 0.1M sodium cacodylate at pH 7.2 in ice. Post fixation steps were performed as described in the previous paragraph.

1× tyrode solution

Component	Concentration
NaCl	136mM
Hepes	5mM
$NaH_2PO_4(H_2O)$	0.33mM
KCl	5.4mM
$MgCl_2(6H_2O)$	1mM
Glucose	10mM

The solution was brought to pH 7.4 and sterilized by using 0.22 μm filters.

Table 8 Composition of 1× tyrode solution.

3.6. Molecular biology

For this PhD thesis a construct encoding the RFP-NGF plasmid was produced. Moreover, we used siRNA against NGF (Ogawa H, 2012) and many plasmids, such as

AKAR3[10], TrkA-DsRed2, EGFP-LC3[11], Murf1-flag[12], EmGFP-shRNA[13] against Murf1 and RFP-zasp[14]. A schematic representation of used plasmids is reported in figure 6 and the sequence of NGF targeted siRNAs is reported in table 9. Scramble siRNA was purchased by Sigma-Aldrich (SIC001).

siRNA sequences

siRNA name	Sequence
si44	GGCAGAACCGUACACAGAUAGCAAU
si08	CAGUGCUGGGCGAGGUGAACAUUAA

Table 9 Sequences of siRNAs used to silence NGF in cultures.

3.6.1. Production of the RFP-NGF construct

In our NGF cloning strategy, the final aim was to obtain a plasmid that allowed simultaneous NGF overexpression and fluorescent labeling of the transfected cells. Since NGF expression, dimerization and binding to its receptor is highly sensitive to its folding, we decided not to interfere with NGF structure by developing an NGF-fluorescent protein chimera. So we produced a construct, in which the RFP sequence is fused to the pre domain of NGF sequence, using a strategy that allows the expression of 2 proteins under the same promoter (figure 6, panel a). As a result, the RFP sequence is cleaved during NGF synthesis, fluorescently labeling transfected cells.

[10] AKAR3 construct was a gift from Prof. Michael D. Allen (The Johns Hopkins University School of Medicine, Baltimore).

[11] EGFP-LC3 construct was a gift from Prof. Marco Sandri (University of Padova, Padova).

[12] Murf-flag construct was a gift from Prof. Marco Sandri (University of Padova, Padova).

[13] EmGFP-shRNA construct was a gift from Prof. Marco Sandri (University of Padova, Padova).

[14] RFP-zasp construct was a gift from Dr. Giulietta Di Benedetto (VIMM, Padova).

RNA was isolated from the heart of an adult C57/BL6 mouse and purified using the SV total RNA isolation kit, accordingly to manufacturer instructions. Single-strand cDNA was synthesized by SuperScript III. Primers containing restriction sites for KpnI and BamHI were designed using the software OligoAnalizer (http://eu.idtdna.com/analyzer/applications/oligoanalyzer/) and used in the PCR reaction to amplify murine NGF. Sequences of the primers are reported in table 10. NGF and RFP cloning in pcDNA3.1/Hygro were performed by Giulietta Di Benedetto. For PCR, Phusion high fidelity polymerase was used. PCR products and pcDNA3.1/Hygro were cut using KpnI and BamHI restriction enzymes, DNA fragments were purified using Genelute gel extraction kit and ligation was performed with T4 DNA ligase.

RFP sequence was excised from a plasmid that was present in the lab, using NheI and KpnI restriction enzymes. The same digestion was performed for pcDNA3.1/Hygro, in which NGF was cloned. DNA purification and ligation were done as described above.

NGF primers

Primer name	Sequence
NGF_Forward_KpnI	5'-GGGGTACCATGCTGTGCCTCAAGCC-3'
NGF_Reverse_BamHI	5'-CGGGATCCTTTCAGCCTCTTCTTGTAGC-3'

Table 10 Sequences of the primers used for NGF cloning in pcDNA3.1/Hygro.

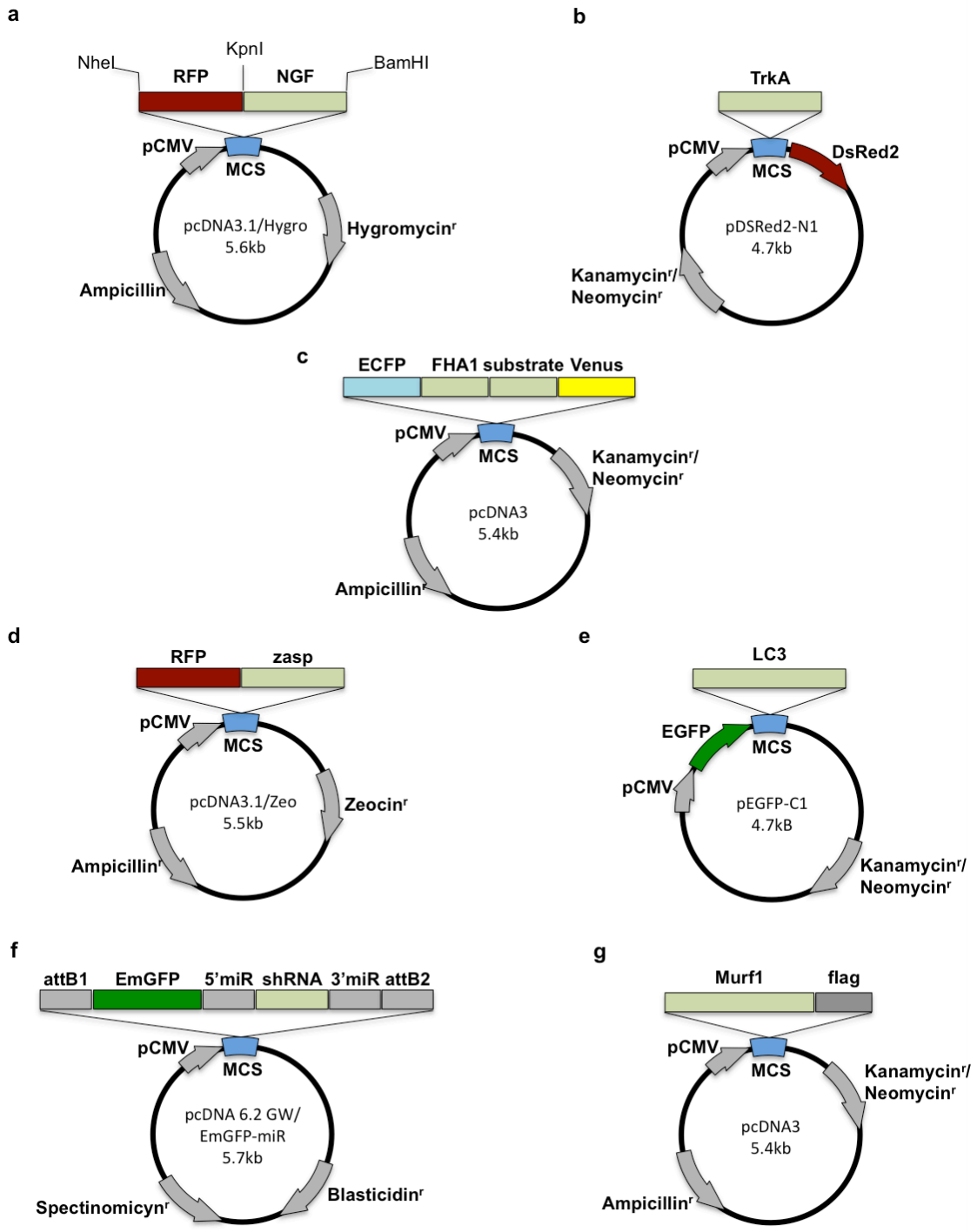

Figure 6 Schematic representation of used plasmids. (**a**) Plasmid containing the RFP-NGF sequence. (**b**) Plasmid encoding for TrkA-DsRed2 fusion protein. (**c**) AKAR3 construct. (**d, e, g**) Plasmids encoding for the sarcomeric RFP-zasp (**d**), EGFP-LC3 (**e**) and Murf1-flag (**g**) fusion proteins. (**f**) Plasmid used for Murf1 silencing.

3.6.2. Production of chemically competent *E. coli* bacteria

Competence is the natural ability of a cell to take up exogenous DNA from the environment. Bacteria become artificially competent using methods that make them passively permeable to DNA. The method that we used is based on the incubation of bacteria with the divalent cation $CaCl_2$, which increases cell permeability to DNA, promoting the binding of the plasmid DNA to lipopolysaccharides. The production of chemically competent bacteria is the basis for the amplification of plasmids. For this purpose, *E. coli* of the TOP 10 strain were inoculated in 3mL of sterile LB medium and grown ON at 37°C at 120rpm to provide good aeration. The second day, cells were diluted 1:100 in 200mL of sterile LB medium and incubated at 37°C at 120rpm until OD_{600} was between 0.3 and 0.4. Since competence can be increased using bacteria with a thinner cell wall, it is important to avoid excessive growth and to use cells in the logarithmic phase of their growth. To block cell division, bacteria were chilled quickly in an ice bath. Then samples were divided in 4 50mL tubes, centrifuged at 4000g for 5 minutes at 4°C and pellet were resuspended in a total volume of 100mL of ice-cold 0.1M $CaCl_2$. Cells should be well resuspended, disrupting any clumps by pipetting up and down. Finally, bacteria were kept in ice for 30 minutes, centrifuged at 2600g for 10 minutes at 4°C, resuspended in 10mL of ice-cold 0.1M $CaCl_2$, 10% glycerol and aliquoted into 50µL fractions. Aliquots were stored at -80°C until the use.

3.6.3. Transformation of competent TOP 10 *E. coli*

Transformation is the process, by which competent *E. coli* take up a desired plasmid from the environment. Since a prokaryotic origin of replication is included in the plasmid, transformed bacteria begin to expand the plasmid. Moreover, adding to the plasmid a gene that encodes a resistance for a selective agent, bacteria that have taken up the plasmid can be selected. The method of transformation that we used in this work is the heat shock transformation, by which $CaCl_2$ chemically competent bacteria are exposed to a short heat pulse to allow the crossing of cell membrane by calcium-DNA complexes.

Chemically competent bacteria were thawed in ice. 1-50ng of the desired plasmid were added to the bacteria that were left for 30 minutes in ice. For heat shock,

bacteria were incubated for 30 seconds at 42°C and left for 2 minutes at 4°C. Then, 450µL of LB medium were added and the bacterial suspension was incubated at 37°C for 1 hour. Finally, 250µL of bacterial suspension were plated on LB/Agar plates containing the appropriate antibiotics, depending on the plasmid. The plate was incubated ON at 37°C.

3.6.4. DNA extraction using Maxi prep kit

After bacteria were transformed with the desired plasmid, DNA amplification, extraction and purification were performed using the Maxi prep kit. Single colonies containing the plasmid were obtained thanks to the bacterial growth in a plate with the selective agent. A single colony was picked up and put in 3mL of antibiotic containing LB medium, to ideally obtain clones of the first cell that was transformed. The suspension was incubated over day at 37°C at 120rpm. After cell growth was verified, the suspension was diluted 1:1000 in 150mL of LB medium and incubated ON at 37°C at 120rpm. The next day, bacteria were chilled in an ice-cold bath and divided in 3 50mL tubes. The suspensions were centrifuged for 10 minutes at 4000g for 15 minutes at 4°C and cells were resuspended in 12mL of resuspension solution, pipetting up and down. 12mL of lysis solution were added to the cell suspension, inverting 8 times to mix and allowing clearing for 5 minutes. In the meanwhile, the plunger was removed from a filter syringe the barrel was placed in an upright position. Then, 12mL of neutralization solution were added to the lysed cells, gently inverting 8 times to mix. 9mL of binding solution were added to the suspension, inverting twice, and immediately the mix was added to the barrel of the filter syringe, letting sit for 5 minutes. In the meantime, the binding column was placed into a collection tube; 12mL of column preparation solution were added to the column that was centrifuged at 3000g for 2 minutes. The flow through was discarded and the cleared lysate was added to the column after inserting the plunger in the syringe. The column was centrifuged at 3000g for 2 minutes and the flow through was discarded. The remainder of the cleared lysate was added to the column repeating the spin and discarding the flow through. After these steps, the DNA remains linked to the membrane of the column. It is washed adding 12mL of wash solution 1, spinning the column at 3000g for 2 minutes

and discarding the flow through. A second wash was performed adding 12mL of wash solution 2 and spinning the column at 3000g for 7 minutes. Another centrifuge at 3000g for 5 minutes was performed to better remove ethanol from the DNA. Finally, the column was transferred to a new collection tube, 3mL of elution solution were added and the column was centrifuged at 3000g for 5 minutes. The eluted DNA was divided in aliquots and stored at -20°C.

3.6.5. Plasmid transfection in cell lines

Since cell line viability is not much affected during transfection processes, lipofectamine was used. Briefly, cells were seeded at a density of 100cells/mm^2 on 24mm coverslips. The second day, two solutions were prepared in polystyrene tubes to avoid plasmid adhesion to the surface of the tube. The first solution contained 5µL of lipofectamine and M199 to a final volume of 250µL per coverslip. The second solution contained 3µg of plasmid and M199 to a final volume of 250µL per coverslip. Solutions were left 5 minutes at room temperature and then mixed together, adding the DNA solution to the lipofectamine solution, and incubated 20 minutes at room temperature to allow liposome formation. In the meantime, cells were washed twice using M199 to remove serum that is known to lower transfection efficiency in lipofectamine based protocols, and left in 500µL of M199. Finally, 500µL of transfection solution were added to the cells drop by drop and plates were incubated for 4 hours at 37°C, 5% CO_2. At the end of the incubation, cells were washed twice with M199 and fresh medium was added. Transfection of 13mm coverslips was performed dividing transfection volumes to 5.

3.6.6. Plasmid and siRNA transfection in cardiomyocytes

Since CMs are more sensitive to transfection agents, transfectin was used. CMs were seeded at a density of 316cells/mm^2 for plasmid or siRNA transfection and subsequent SGN seed, or 600cells/mm^2 for RT-qPCR experiments. The second day, cells were washed twice using M199 and incubated with 1mL of SDM for 2 hours at 37°C, 5% CO_2 for allowing cell adaptation to the new medium. Later, two solutions were prepared. The first one contained 5µL of transfectin and M199 to a final volume of 250µL per

coverslip. The second solution contained 3µg of plasmid or 100pmol of siRNA and M199 to a final volume of 250µL per coverslip. Solutions were left 5 minutes at room temperature, then mixed together, adding the DNA/siRNA solution to the transfectin solution, and incubated 20 minutes at room temperature. Finally, 500µL of SDM were removed from cells and 500µL of the transfection solution were added drop by drop. CMs were incubated for 4 hours at 37°C, 5% CO_2. If a co-culture of neurons and transfected CMs was needed, SGNs were prepared in the meantime. At the end of the transfection, CMs were washed twice using M199 and 2mL of SDM were added. In case of co-culture, 1mL of SDM and 1mL of neuronal suspension were added to CMs after washes. Transfection of 13mm coverslips was performed dividing transfection volumes to 5.

For siRNA/plasmid co-transfection, the same protocol was used, mixing together 3µg of the plasmid and 10pmol of the siRNA. These quantities were chosen to avoid the production of liposomes containing the siRNA and not the plasmid.

3.6.7. Plasmid transfection in sympathetic neurons

Neurons were transfected using a specific protocol that was developed in our laboratory because of neuronal resistance to standard transfection protocols. After 24mm coverslips were coated with 20µg/mL laminin and washed twice with 1× PBS, 500µL FDM were left on coverslips and transfection solution were prepared as described for CM transfection. At the end of the 20-minute incubation at room temperature, 500µL of transfection solution were added to coverslips drop by drop and liposomes were left to deposit for 2 hours at room temperature on a table. During this period it is important to avoid plate movements and vibrations that can resuspend liposome. In the meantime, SGNs are prepared as described before. At the moment of the seed, the transfection solution was gently removed from coverslips using a 1mL pipet and 1mL of FM was added. Finally, 1mL of neuronal suspension was seeded drop-by-drop and incubated at 37°C, 5% CO_2. The second day, 1mL of FM was replaced either with 1mL of FDM to prepare a neuronal culture, or 1mL of CM suspension to prepare a co-culture with transfected neurons. The third day, cultures were washed 5 times and SDM with or without 8nM NGF was added to cells. Since imaging was

performed from 48 to 72 hours after neuronal transfection, no AraC was added to the cultures.

3.6.8. RT-qPCR

For analysis of NGF expression in CMs, RT-qPCR was performed. Extracts were prepared from cultured CMs seeded at a density of 600cells/mm^2 in 6 well plates that were previously coated with 20µg/mL laminin. RNA isolation and purification was performed using the SV total RNA isolation kit, accordingly to manufacturer instructions. Briefly, cells were washed twice with 1mL of ice cold 1× PBS and incubated for 5 minutes with 85µL of RNA lysis buffer maintaining plates on ice. Lysed cells were collected using a scraper and samples were frozen in 1.5mL tubes at -80°C. RNA purification, retrotranscription and RT-qPCR were performed by Nicola Pianca. Single-strand cDNA was synthesized by SuperScript III. RT-qPCR was performed using a C1000 Thermal Cycler BioRad coupled with a GeneAmp 7500 Sequence Detection System. To evaluate differences in gene expression the relative quantification method was used (Pfaffl MW, 2001), normalizing values to the expression of the internal reference. As reference, genes were chosen, whose expression did not change among the different experimental conditions, and in particular GAPDH and β-actin. Gene-specific primer pairs were designed using Primer 3 software (http://frodo.wi.mit.edu/cgi-bin/primer3/primer3_www.cgi); choosing sequences of distinct exons to avoid amplifying contaminant genomic DNA. Primer sequences are listed in table 11.

Primers

Primer name	Sequence
Rat NGF Forward	5'-TGACAGTGCTGGGCGAGGTGAA-3'
Rat NGF Reverse	5'-TCAATGCCCCGGCATCCACTCT-3'
Rat GAPDH Forward	5'-AGGGCTGCCTTCTCTTGTGAC-3'
Rat GAPDH Reverse	5'-TGGGTACAGTCATACTGGAACATGTAG-3'
Rat β-actin Forward	5'-CTGGCTCCTAGCACCATGAAGAT-3'

Rat β-actin Reverse	5'-GGTGGACAGTGAGGCCAGGAT-3'

Table 11 Sequences of primers used for RT-qPCR.

3.7. Western blot

Western blot analysis was performed on protein extracts from CMs or mouse hearts. Rat neonatal CMs were seeded on 100mm tissue culture plates at a density of 600 cells/mm^2 after laminin coating. CMs were cultured as described before. Protein extraction was performed the 5^{th} day of culture. Briefly, cells were washed twice with ice cold 1× PBS and 250µL of protein lysis buffer (table 12). Frozen tissues were incubated in 200µL of lysis buffer and disrupted by using the tissue lyser for 1 minute. Cell and heart lysates were collected in 1.5mL tubes and incubated for 1 hour at 4°C. Proteins were denatured for 10 minutes at 70°C on a shaker (1250rpm). This step was followed by a centrifugation at 4°C, 100g for 10 minutes. The supernatants were collected and quantified by using the Bradford assay. Samples were aliquoted and stored at -80°C until use.

Protein lysis buffer

Component	Concentration
Tris pH 7.5 (1M)	0.05M
NaCl (3M)	0.15M
$MgCl_2$ (1M)	0.01M
DTT (0.1M)	0.0005M
EDTA (0.5M)	0.001M
Glycerol (100%)	10%
SDS (10%)	2%
Triton (100%)	1%
Anti phosphatases (10×)	1×
Anti proteases (50×)	1×

Clean mQ H_2O was added to reach the desired volume.

Table 12 Composition of protein lysis buffer used for western blot analysis.

For SDS page, from 20 to 80 µg of protein samples per lane were prepared in loading buffer (table 13) and incubated for 10 minutes at 70°C on a shaker (1250rpm). The sample and the SeeBlue® Plus2 Prestained Standard were loaded in 4-12% gradient gels. SDS page was performed using 1× MES as running buffer at 150mV for the times required by the optimal identification of the protein band.

Loading buffer	
Component	**Concentration**
DTT (20×)	1×
SB (4×)	1×

1% SDS was added to reach the desired volume.

Table 13 Composition of loading buffer used for preparing samples for SDS page.

Proteins were transferred on a PVDF membrane of 0.2µm porosity that was previously activated with methanol, by using transfer buffer (see table 14). Protein transfer was performed at 4°C, 400 mA. Then, membranes were quickly washed in 0.1% TTBS (see table 14) and saturated for 60 minutes on a shaker with 0.1% TTBS supplemented with 5% milk to avoid aspecific binding of the primary antibody.

0.1% TTBS		**Transfer Buffer**	
Component	**Concentration**	**Component**	**Concentration**
Tris	0.05M	Methanol	20%
NaCl	0.15M	Antioxidant	0.05%
Tween20	0.1%	Transfer Buffer (20×)	1×

0.1% TTBS was brought to pH 7.6. Clean mQ H_2O was added to reach the desired volumes.

Table 14 Composition of 0.1% TTBS and transfer buffer that were used for membrane processing.

After saturation, membranes were incubated with primary antibodies as reported in table 15. Then, membranes were washed three times with 0.1% TTBS supplemented with 5% milk for 10 minutes on a shaker and incubated with the HRP conjugated secondary antibodies for 90 minutes at room temperature. Antibodies were used at the dilutions listed in table 15. Finally, 3 washes of 10 minutes with 0.1% TTBS were performed on a shaker and the reactivity was revealed by incubating blots for 5 minutes in ECL and by using Kodak films.

Primary antibodies

Target	Company	Host species	Dilution	Solution
Actin	Sigma-aldrich	rabbit	1:2500	0.1% TTBS, 5% milk, 2h RT
LC3	Cell signaling	rabbit	1:1000	0.1% TTBS, 5% milk, ON 4°C
NGF	Abcam	rabbit	1:1000	0.1% TTBS, 5% BSA, ON 4°C
Troponin I	[15]	mouse	1:5000	0.1% TTBS, 5% milk, ON 4°C
Troponin T	[16]	mouse	1:5000	0.1% TTBS, 5% milk, ON 4°C
α actinin	Sigma-Aldrich	mouse	1:1000	0.1% TTBS, 5% milk, ON 4°C

Secondary antibodies

Target	Company	Dilution	Solution
Anti mouse-HRP	Bio-Rad	1:5000	0.1% TTBS, 5% milk, ON 4°C
Anti rabbit-HRP	Bio-Rad	1:10000	0.1% TTBS, 5% milk, ON 4°C

Table 15 List of primary and secondary antibodies used for western blot.

[15] Anti-Troponin I antibody was a gift from Prof. Stefano Schiaffino (University of Padova, Padova)

[16] Anti-Troponin T antibody was a gift from Prof. Stefano Schiaffino (University of Padova, Padova)

3.8. ELISA

ELISA is a highly sensitive assay that we used to measure NGF concentration in medium conditioned by CMs or HeLa that were prepared and stored at -80°C. We used a sandwich ELISA kit and performed the assay accordingly to manufacturer instructions. Briefly, the desired number of NGF strips was placed in the strip well plate holder. Standards were prepared in assay diluent at different concentrations (0, 15.6, 31.25, 62.5, 125, 250, 500 and 1000pg/mL). 100µL of standards and samples were added to each well in duplicate. The plate was sealed with the plate sealer and incubated ON at 4°C. The second day, the plate sealer was removed and the plate was washed 4 times. Washes were performed adding 250µL/well of wash buffer, inverting the plate over a sink, flicking the fluid out of the wells and blotting the plate on clean paper towels. 100µL/well of the anti-mouse NGF monoclonal antibody (1:100) were added to each well. The plate was covered, incubated at room temperature for 2 hours on a shaker, washed 4 times as described previously and 100µL/well of 1:1000 diluted anti-mouse-HRP antibody were added to each well. The plate was covered and incubated for 2 hours at room temperature on a shaker. Finally, samples were washed 4 times and 100µL/well of TMB were added to each well and incubated for 10 minutes at room temperature. The reaction was stopped adding 100µL/well of stop solution. Absorbance was read at 450nm and absorbance at 560nm was used as reference wavelength. After plotting the calibration curve, NGF concentration in the samples was estimated.

3.9. Preparation of c(92-96) peptide

The cyclic peptide c(92-96) (YCTDEKQCY) was synthesized in the lab of Prof. Oriano Marin, University of Padova, by using a solid-phase technique with a multiple peptide synthesizer (Syro II) on a *p*-benzyloxybenzyl alcohol resin (Wang resin). The Fmoc strategy (Fields GB, 1990) was used throughout the peptide chain assembly, utilizing HATU as coupling reagent (Carpino LA, 2002). Crude peptide was purified by reverse phase HPLC on a preparative column (Prep Nova-Pak HR C18). Purified peptide was oxidized (0.1mg/ml) in 100mM NH_4HCO_3 buffer (pH 8.2) for 72 hours, and

repurified. The formation of disulphide bridges was verified by mass spectrometry analysis using a MALDI TOF/TOF instrument (ABI 4800).

3.10. Imaging

IF stainings were acquired by using the inverted fluorescence microscopy. Confocal microscopy was used to increase the resolution of image acquisition. In live FRET and confocal imaging was also performed. Before sample imaging, controls were used to adjust parameters through the evaluation of background and antibody cross-reactivity. For quantification purposes, random field images were acquired using the same parameters within the same experiment.

3.10.1. Fluorescence microscopy

To acquire images of the IF stainings and for quantification of the area occupied by myofibrils, we used the Olympus BX60 microscope with the 40× objective. For the different fluorochromes we used WU (330-385 nm), WIBA (460-490 nm), MF (560/55 nm) filters.

For the quantification of the mean neuronal density and of the area occupied by sympathetic axons, we used the Leica DMI4000B. Images were acquired with the 10× objective and A4 (excitation: 360/40nm, emission: 470/40nm) and L5 (excitation: 480/40nm, emission: 527/30nm) filters.

3.10.2. Confocal microscopy on fixed samples

To increase the acquisition resolution, to perform z-stacks and to analyze IF stainings with 4 fluorochromes, we used the confocal microscope Leica TCS SP5. In this case, imaging was performed using 63× and 40× immersion objectives and Argon, Diode 405, DPSS 561 and HeNe lasers. Excitation and emission wavelength that we used are listed in table 16. To avoid excitation/emission interferences between different fluorochromes, acquisition was performed in the sequential manner. For z-stack acquisition, a distance of 0.4µm between planes was used.

Fluorochrome excitation/emission

Fluorochrome	Excitation wavelength	Emission wavelength
DAPI	405nm	415-490nm
Alexa fluor 488, EGFP	488nm	498-570nm
Alexa fluor 568, 555, TRITC, cy3	561nm	571-650nm
Alex fluor 633, 647	633nm	643-750nm

Table 16 Emission/excitation wavelength used for confocal image acquisition with the Leica TCS SP5.

3.10.3. In live imaging of PC12 viability

To analyze PC12 viability upon NGF withdrawal or anti-NGF treatment, cells were incubated for 30 minutes with a solution of 1µg/mL Hoechst 33342 and 2µg/mL propidium iodide prepared in the same culture medium to avoid cellular damage. After 2 washes, PC12 were incubated with the same culture medium and random images were acquired using the microscope Leica DMI6000B. 10× objective was used as well as the A4 (excitation: 360/40nm, emission: 470/40nm) and N21 (excitation: 515-560nm, emission> 590nm) filters.

3.10.4. Real time imaging of TrkA-DsRed2 in SGNs and of RFP-zasp in CMs

Since movements of TrkA enriched endosomes are highly dependent on the viability state of SGNs, we decided to perform TrkA-DsRed2 imaging using conditions that were more similar to those of the incubator. During imaging experiments, cells on the coverslip were placed in a culture dish incubator coupled to a heater controller that kept the temperature at 37°C, in a 5% CO_2, 95% O_2 atmosphere. Moreover, cells were maintained in SDM without phenol red to avoid background. Since we needed to perform long time imaging on CMs to analyze sarcomeric growth and disassembly, the same was done with RFP-zasp transfected CMs.

The culture dish incubator was coupled to the confocal microscope Nikon Eclipse TE200 (Ultraview, see figure 7), using the immersion 60× objective. For RFP imaging we used 568/10nm excitation and 607/45nm emission filters, while for GFP imaging we used 488/10nm excitation and 525/50nm emission filters. Z-stacks were performed using a distance between planes of 0.4μm.

3.10.5. FRET imaging of PKA activity in CMs

For evaluation of PKA activity, CMs were transfected with a plasmid encoding for AKAR3 (Allen MD, 2006). The functioning of AKAR constructs is based on energy transfer between CFP and YFP upon phosphorylation by PKA (figure 7). In live FRET imaging was performed on AKAR3 transfected CMs placed in the culture dish incubator. Cells were coupled to the heater controller and maintained in SDM without phenol red. Since we needed to add stimuli to the cells, no atmosphere control was done. Moreover, the inverted microscope Olympus IX50 and the immersion 40× objective were used. Images were acquired using the software Roboscope. AKAR3 was excited at a wavelength of 433nm and the ration between emission at 527 and 476nm was considered.

3.10.6. TEM

FEI Tecnai 12 electron microscope was used to acquire images.

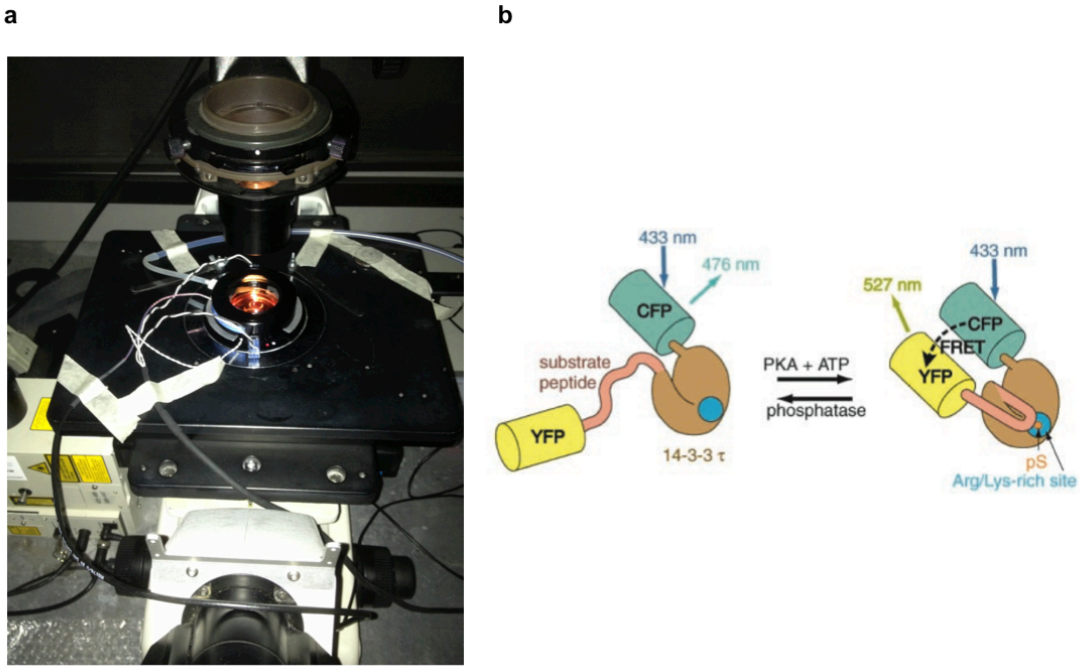

Figure 7 (**a**) Culture dish incubator coupled to the confocal microscope Nikon Eclipse TE200. (**b**) Representative scheme of AKAR functioning during FRET experiments, from (Zhang J, 2001).

3.11. Image analysis

For non-automatic image analysis, ImageJ software was used and all analysis were performed in a blind manner. To measure the area occupied by sarcomeres in CMs or by the synaptic bouton, ROIs were manually traced and areas were calculated using ROI manager tool of ImageJ.

To quantify the number of LC3 marked vesicles, IF images where thresholded to remove background. Manual count of the vesicles was then performed.

For WB densitometry, we used the ImagJ function called 'Gels', selecting and plotting the lanes and labeling peaks. Values were normalized to the housekeeping protein.

For analysis of β catenin and cadherin enrichment under the sympathetic process, background subtraction was performed. After getting the plot profiles of TOH and cell-to-cell adhesion molecules, signals were normalized and plotted.

To measure the mean neuronal density, a threshold was imposed to the images for background subtraction and nuclei inside TOH positive cell bodies were counted.

For evaluating the presence of NGF uptake by SNs, linear ROIs were traced along processes in bright field images and a reslice of both bright field and fluorescent

images was performed. After imposing a threshold to eliminate background, NGF positive vesicles inside axons were counted.

For TrkA-DsRed2 measures, kymographs of time-lapse image series were developed using the ImageJ plugin kymograph. TrkA trajectories were manually drawn and velocities were measured using the same plugin.

For analysis of FRET imaging, a ROI was manually drawn on the transfected cell and the fluorescence intensity was measured in the ECFP and Venus channels over time.

For evaluation of β catenin and cadherin enrichment along processes, linear ROIs were manually traced and plot profiles of both TOH and the cell-to-cell adhesion molecule were obtained. Pixel intensities were used for the final plot.

To perform a semi-automated image analysis, we developed Matlab® implemented programs. When it is possible, this type of image analysis has many advantages, such as high speed, user independent and high throughput analyses. Programs were developed to analyze the area occupied by sympathetic processes in spotted co-cultures and cell viability after Hoechst/PI staining. In the first case, the software performs a binary conversion of processes using a preselected threshold, and evaluates the total area of the image that is positive for TOH. Cell bodies are subtracted from the image after manual drawing. In the second case, Hoechst positive nuclei are segmented using the method of regional minima selection. PI signal is thresholded to eliminate background, and imposed on the segmented nuclei to evaluate the ratio between PI marked and total nuclei.

3.12. Statistical analysis

For data analysis, Excel® and Origin® programs were used. To describe distributions, the mean and the standard error of the mean were considered. For comparisons between two distributions, the t-test was used. For comparisons between more than two distributions, the one-way anova and the Bonferroni correction were used. P-values were considered statistically significant, when included between 0.05 and 0.01 (*), highly significant when lower than 0.01 (**).

4. Results and discussion

The result section of this PhD thesis focused on the experiments aiming at investigating the effects of both anterograde and retrograde signals between sympathetic neurons and cardiomyocytes.

In the first part we considered the effects of the noradrenergic anterograde signaling cardiac trophism with particular emphasis on sarcomere dynamics.

In the second part we studied the effect of a direct neuro-cardiac interaction on NGF mediated retrograde signaling between CMs and SNs.

In addition, we obtained a set of preliminary data suggesting that a cross-talk between β adrenergic and NGF signaling might operate in the sympathetic nervous system-to-myocardium interaction.

Finally, the role of alterations in the sympathetic neuron to CM coupling is being investigated in cardiac disease models and the preliminary data and aims are discussed in the paragraph describing the future perspectives.

4.1. From the neuron to the heart

It is well known that cardiac SNs control cardiac contractility and electrophysiology, and recently has been shown that neuronal input to the heart also has a trophic effect mediated by the regulation of protein degradation. Both the hypertrophic and atrophic remodeling are characterized by changes in sarcomere structure. However, the mechanism whereby adrenergic signaling regulates sarcomere dynamics is still unclear. The first part of this PhD work was focused on the effects of adrenergic signaling on cardiomyocyte trophism, and in particular on sarcomere dynamics.

4.1.1. Analysis of sarcomere synthesis and dismantlement

To analyze sarcomere synthesis, rat neonatal CMs were transfected with a construct encoding RFP-tagged zasp (figure 8, panel a) to label sarcomeric Z-disks and incubated with a set of different adrenergic stimuli known to have pro-hypertrophic effect. In particular, we used 10μM clenbuterol (CL), a β2 adrenergic receptor agonist, 10μM phenylephrine (PH), an α adrenergic receptor agonist, and 100nM norepinephrine, that acts on all cardiac adrenergic receptors. Since long term incubation with NE is

known to have a pro-apoptotic effect (Fu YC, 2004), we used a relatively low NE concentration (100nM). For every agonist, cells were treated for 24-48h before fixation and confocal immunofluorescence analysis. After image acquisition, the total cell area occupied by sarcomeres was quantified, and the results are shown in figure 8, panel b; even if small increases in the total sarcomeric area were measured, we did not detect significative changes upon incubation with any of the stimuli within 2 days of treatment.

To evaluate the effects of pro-atrophic stimuli, cells were nutrient and serum deprived by incubating them with HBSS. Nutrient deprivation, as well as denervation, is known to activate autophagy and the ubiquitin proteasome system in the heart. Even if the upstream mechanisms differ between nutrient deprivation and denervation, both pro-atrophic stimuli share common downstream signaling effects, including activation of the ubiquitin ligase Murf1 transcription, a process inhibited by treatment with β-adrenergic agonists, as shown in figure 8, panel c (Zaglia T, 2013). Thus, for what concerns the changes in sarcomeric structure we can make a parallel between starvation and autonomic denervation.

RFP-zasp transfected CMs were starved with HBSS for 20h, and such treatment resulted in significant (61.54 ±8.89%) decrease in the area occupied by sarcomeres (figure 8, panel d, e), suggesting that dismantlement process is faster than assembly. Moreover, cells were stained with FITC-conjugated wheat germ agglutinin (WGA) to evaluate changes in the total cell area induced by nutrient/serum deprivation. As reported in figure 8, panel f, g, we detected a small decrease after cell incubation with HBSS, which however fell short of statistical significance. Taken together, these results suggest that sarcomere dismantlement may precede cytoplasm rearrangement upon induction of atrophic remodeling by starvation.

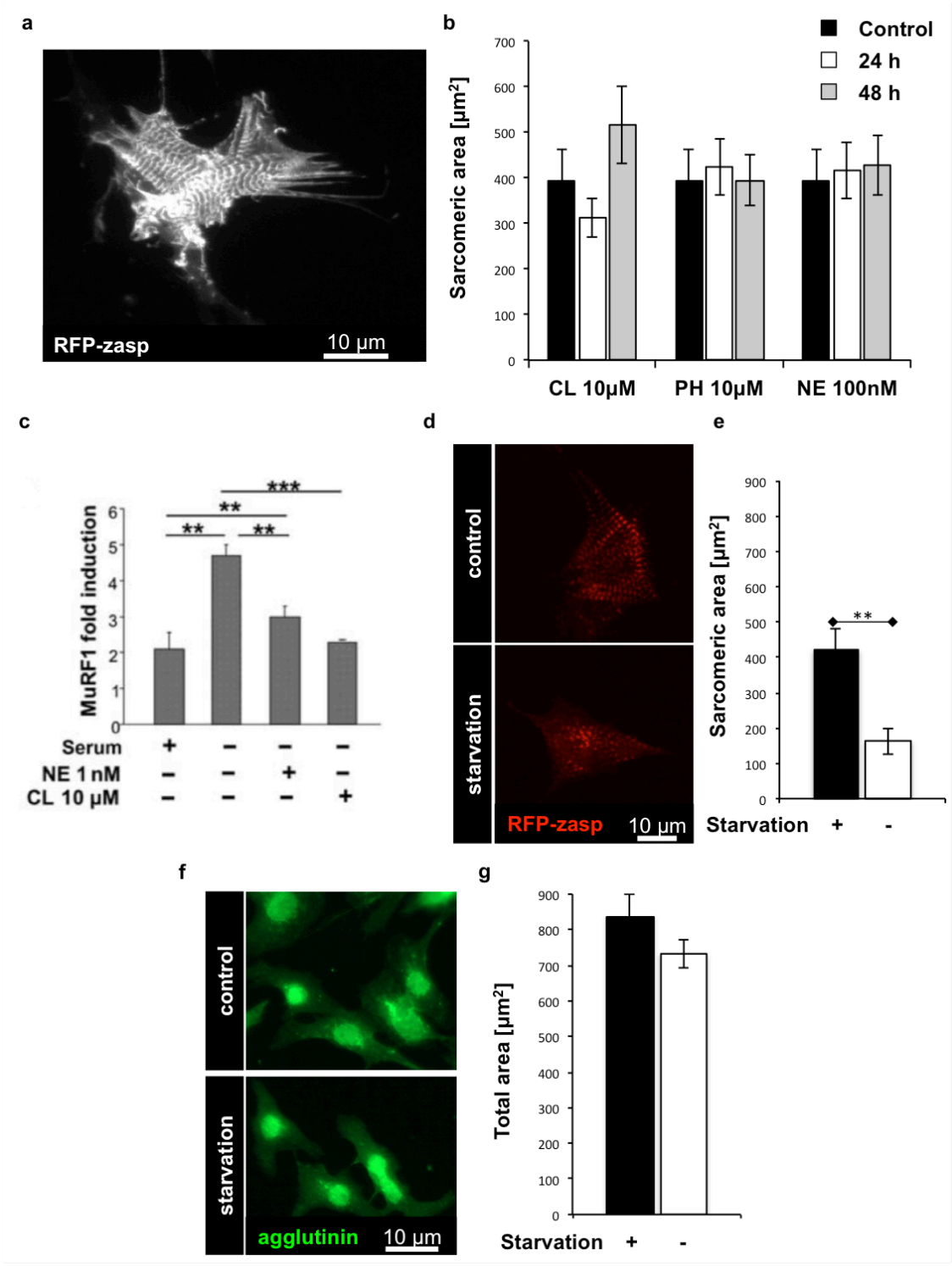

Figure 8 Sarcomere changes in cells treated with pro-hypertrophic or pro-atrophic stimuli. (**a**) Confocal z-projection of a CM transfected with the RFP-zasp construct (gray signal). Scale bar: 10µm. (**b**) Evaluation of sarcomere area upon CM treatment with different pro-hypetrophic stimuli for 24-48 h (error bars represent s.e.m., n=20 cells per condition). (**c**) RT-qPCR analysis of Murf1 induction in starved CMs, from (Zaglia T, 2013). Murf1 induction by starvation is rescued by NE or CL treatment. (**d, e**) Confocal z-projection of control and starved CMs transfected with RFP-zasp plasmid (red signal) (**d**) and

quantitative analysis of the area occupied by sarcomeres (**e**, error bars represent s.e.m., ** p<0.01, n=20 cells per condition). Scale bar: 10µm. (**f, g**) IF staining for agglutinin (green signal) on control and starved CMs (**f**) and quantitative analysis of the total CM area (**g**, error bars represent s.e.m., n=135 cells per condition). Scale bar: 10µm.

4.1.2. HBSS incubation causes sarcomere dismantlement

To directly analyze the dynamics of sarcomeric remodeling during the onset of cardiomyocyte atrophy, we set up an imaging protocol to monitor variations in the sarcomeric structures in real time, in living CMs. Briefly, CMs were seeded the first day, transfected the second day with the RFP-zasp construct and incubated with HBSS the third day for 16 hours. For imaging, cells were next transferred in an imaging chamber equipped with an incubator coupled to a heater controller, in a controlled atmosphere (5% CO_2, 95% O_2). Cells were continuously observed with a spinning-disk confocal microscope during 4-hours long experiments, thus in the last four of a 20 hours nutrient/serum deprivation protocol. One example of this experiment is reported in figure 9, panel a, b. In the control cell, incubated with the standard, serum containing culture medium, no changes were detected in the sarcomeric structure. Conversely, the HBSS treated cell showed sarcomere disassembly and disappearance of whole Z-disks (figure 9, the enlargements of panel a). These qualitative observations were confirmed by the quantitative analysis (figure 9, panel b): while the fraction of the total cell area occupied by sarcomeres is almost constant in control cells, a 54.63% decrease was detected in the starved cell, further supporting that starvation induces sarcomere dismantlement.

It has to be underlined that this type of starvation does not preclude sarcomere functionality. While during incubation with HBSS cell contraction was greatly reduced, cells immediately started contracting at restoration of nutrient and serum level in the medium.

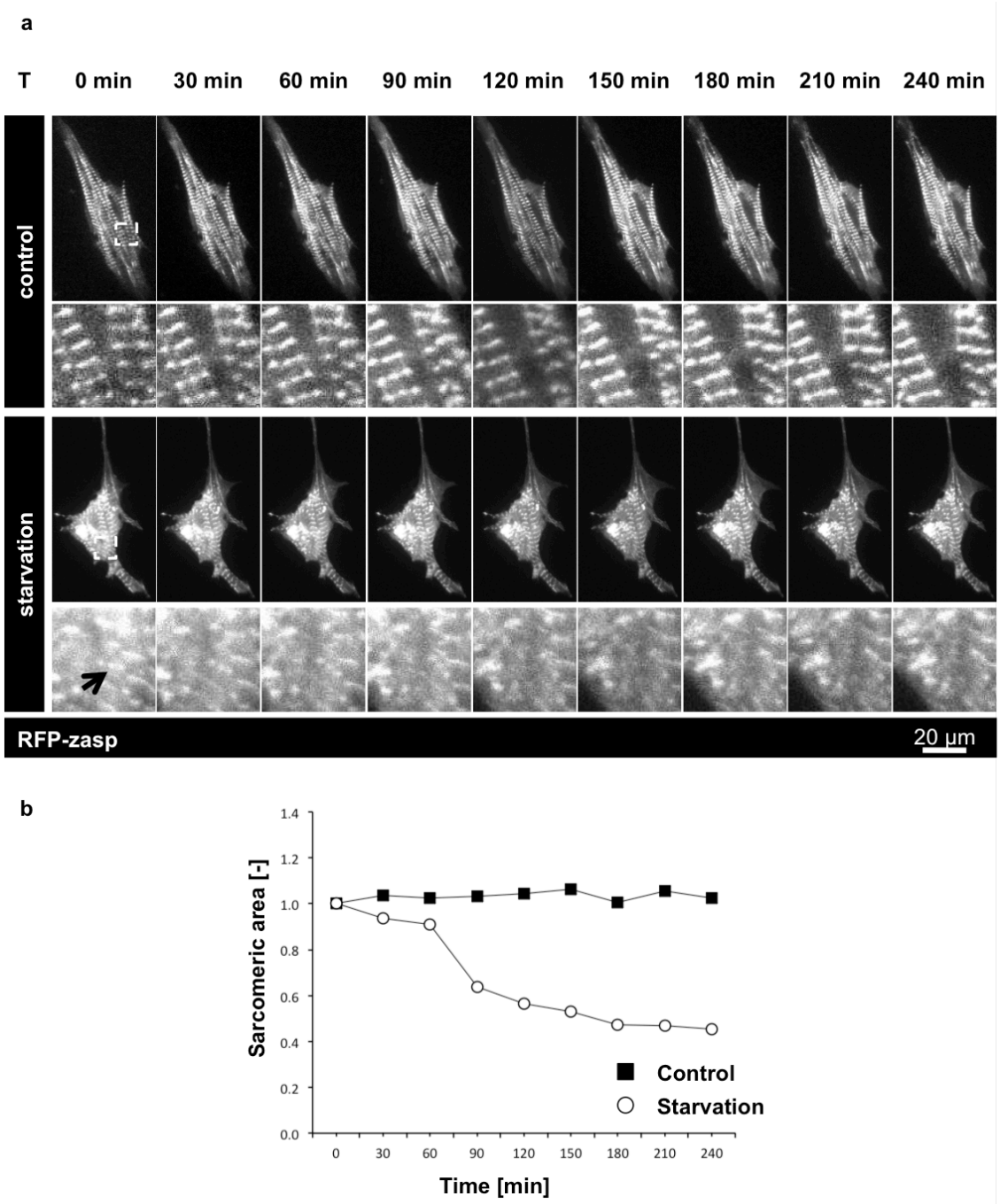

Figure 9 Incubation with HBSS causes sarcomeric dismantlement. (**a**) Confocal z-projection of RFP-zasp transfected CMs (gray signal) incubated with SDM or HBSS. Magnifications of white boxes in the images are reported. The arrow indicates a sarcomere that is degraded during the imaging. Scale bar: 20µm. (**b**) Quantitative analysis of the area occupied by sarcomeres of the cells shown in (**a**). The ratio between the area at a certain time and the initial area is reported.

4.1.1. Selective delocalization and degradation of a subset of sarcomeric proteins by nutrient/serum deprivation

The results described above were obtained considering the sarcomeric protein zasp, which is localized in the Z-disk. We thus sought to understand the dynamics of other sarcomeric constituents during atrophic disassembly.

For this analysis we considered different proteins:

- α actinin, another Z-disk protein;
- actin, the protein that constitutes thin filaments and that can be stained using fluorescently labeled phalloidin;
- cTnT and cTnI, which are placed along thin filaments, regulating myosin head binding to actin.

Desmin was also considered, but it was discarded because in rat neonatal CMs no sarcomeric localization was detected, probably due to the incomplete differentiation stage of cultured CMs.

We first focused on protein localization during nutrient and serum deprivation, and to this aim, IF stainings were performed in CMs starved for 20h for each of the proteins indicated above and the area occupied by marked sarcomeres was quantified. As shown in figure 10 panel a and b, HBSS induced delocalization does not involve all the proteins. Sarcomeric area decrease was detected for α actinin, actin and cTnI that showed respectively 47.43%, 33.12% and 33.28% reduction when compared to the control maintained in SDM. Only cTnT remained constant upon CM starvation, suggesting that not all sarcomeric proteins are degraded with the same kinetics upon atrophy induced by nutrient/serum deprivation.

We next evaluated the effect of HBSS treatment on protein degradation by WB analysis. Since nutrient/serum deprivation causes degradation of many cellular proteins, including the ones that are normally used as loading control in WB experiments, protein expression was compared among samples by loading lysates obtained from the same number of cells. In line with the IF data, α actinin and cTnI protein levels were decreased by 43.74% and 46.31%, respectively, while cTnT levels were not affected by starvation (figure 11, panel a and b). Unexpectedly, actin levels did not change and for this reason we considered it a good housekeeping protein for

analysis of protein levels upon starvation. This might be due to the fact that actin is not only present in sarcomeres, but is also mainly the constituent unit of microfilaments. While in IF analysis we considered the minor part of actin that localized in the sarcomere and that was degraded, using the WB we looked at the total content of actin of the cell that did not change.

Altogether, these data support that sarcomeric proteins are degraded with different kinetics, suggesting that dismantlement of sarcomere components is a regulated process with precise timing and target specificity.

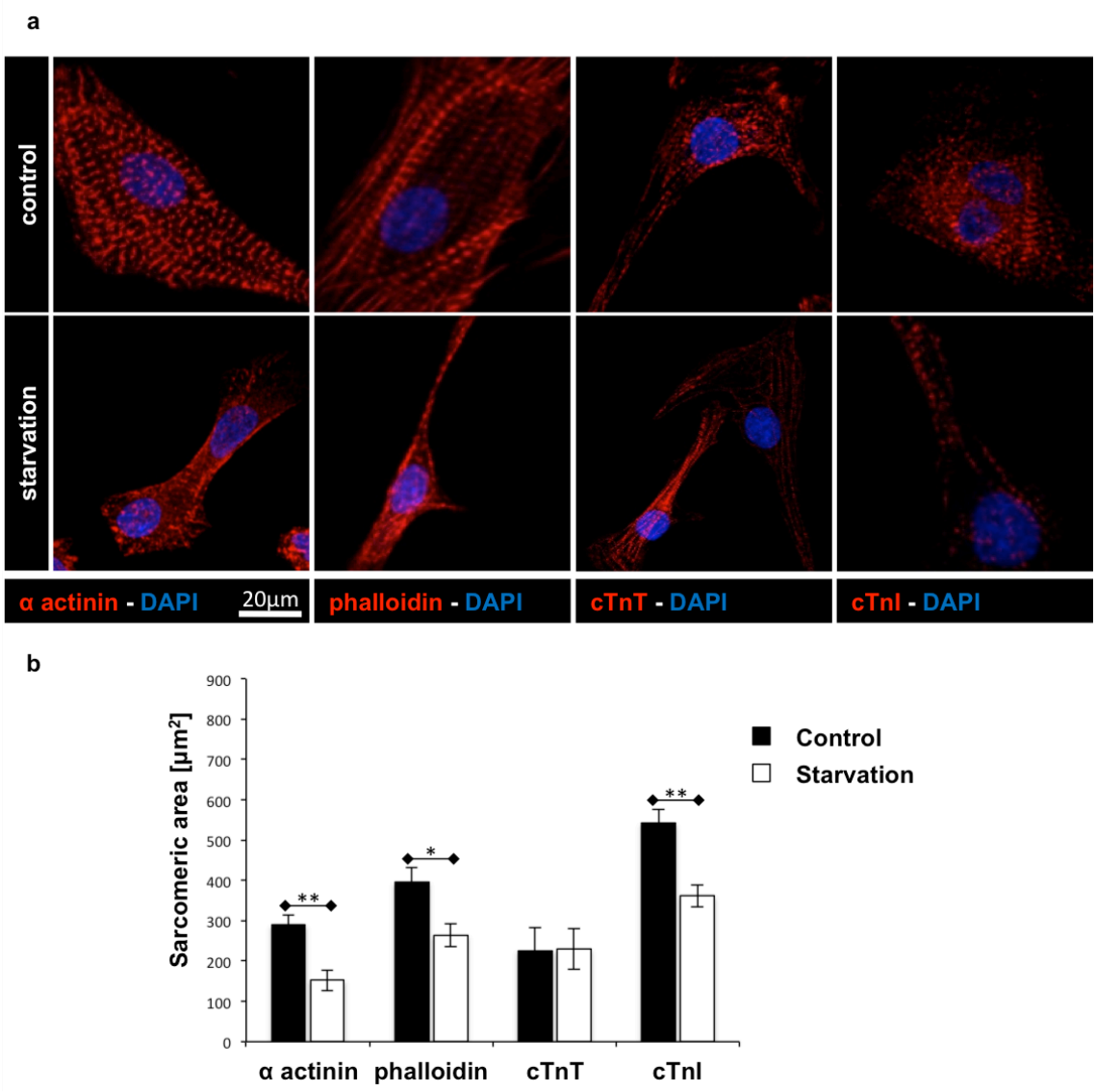

Figure 10 HBSS treatment causes α actinin, actin and cTnI delocalization. (**a**) Confocal IF stainings for α actinin, phalloidin, cTnT, cTnI (red signals) and nuclei (blu signal) on starved and control CMs. Scale bar:

20µm. (**b**) Quantitative analysis of the area occupied by sarcomeres after IF stainings described in panel (**a**) (error bars represent s.e.m., *0.01<p<0.05, ** p<0.01, n=30 cells per condition).

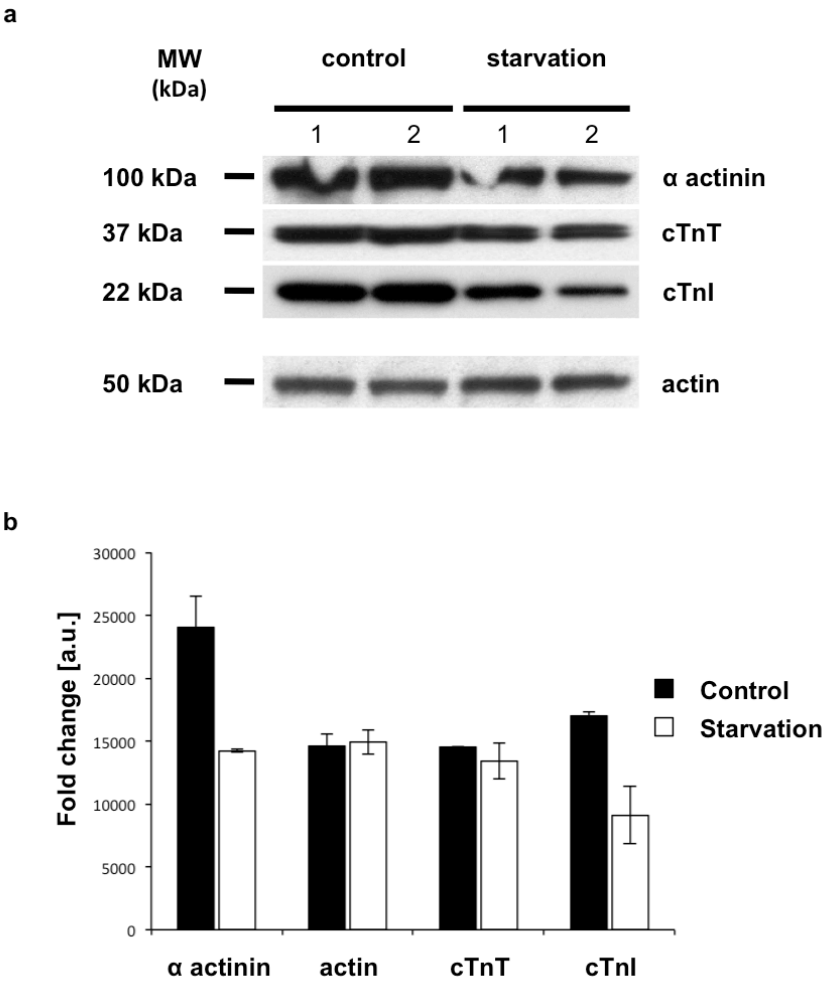

Figure 11 HBSS treatment causes decrease in protein levels of α actinin and cTnI. (**a**) WB analysis for α actinin, phalloidin, cTnT, cTnI on lysates from starved and control CMs. (**b**) Densitometry of the WB showed in panel (**a**) (error bars represent s.e.m., n=2 cultures per condition).

4.1.2. HBSS treatment activates both autophagy and UPS

As described previously, nutrient deprivation activates autophagy and UPS that are the two main routes of protein degradation. So we evaluated whether those systems were activated also in nutrient/serum deprived (HBSS incubated) CMs. Autophagy activation was assessed by western blot analysis and IF staining (figure 12, panel a-d). For WB analysis, equal concentrations of protein lysates were separated with PAGE, and we looked at LC3-II/LC3-I ratio, whose increase indicates autophagy induction. As shown

in figure 12, panel a, we detected an enrichment in the low molecular weight LC3-II band upon starvation that was confirmed by the densitometric analysis in panel b (0.5 ±0.5 vs 1.31 ±0.35 of LC3-II/LC3-I ratio in control and starved CMs respectively). Moreover, IF quantification analysis demonstrated that the LC3-positive vesicles were 2.52 times more concentrated in CMs treated with HBSS, when compared to controls (figure 12, panel c, d) in further proof that nutrient/serum deprivation of cultured cardiomyocytes induced autophagy.

For the evaluation of UPS induction, we performed IF staining with anti-ubiquitin antibody and phalloidin on CMs, and as shown in figure 12, panel e, we detected an increase in the fluorescence level of ubiquitin staining upon starvation, supporting that, in addition to autophagy, UPS is activated by HBSS treatment.

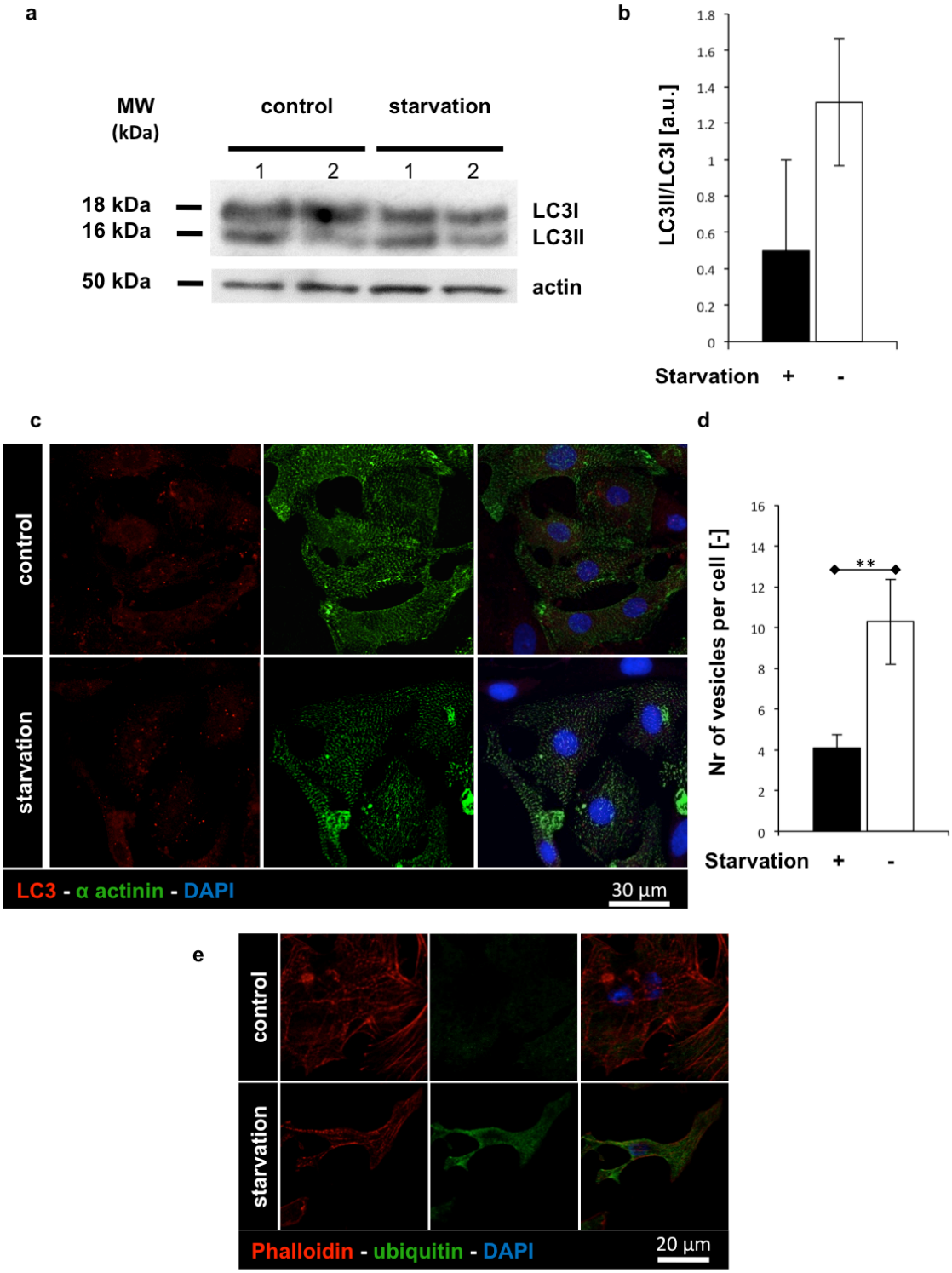

Figure 12 Induction of UPS and ALS upon HBSS treatment. (**a, b**) WB analysis (**a**) and densitometry (**b**) for LC3 in control and starved CMs (error bars represent s.e.m., n=2 CM cultures per condition). (**c**) Confocal IF staining for LC3 (red signal), α actinin (green signal) and nuclei (blue signal) on CMs incubated or not with HBSS. Scale bar: 30µm. (**d**) Quantitative analysis of the number of LC3 positive vesicles in control or starved CMs (error bars represent s.e.m., ** $p<0.01$, n=10 cells per condition). (**e**) Confocal IF staining

for phalloidin (red signal), ubiquitin (green signal) and nuclei (blue signal) on CMs after HBSS treatment. Scale bar: 20μm.

4.1.3. Role of autophagy in sarcomere degradation

Since we detected activation of both autophagy and UPS upon HBSS treatment, we investigated the involvement of these proteolytic systems in nutrient/serum-deprivation dependent sarcomere degradation. Confocal IF staining for LC3 and α actinin, showed that HBSS treatment caused enrichment in LC3 positive vesicles close to sarcomeric α actinin (figure 13, panel a) suggesting that autophagy may be involved in sarcomeric disassemble. This result was confirmed by the real-time imaging experiments in cardiomyocytes co-transfected with both RFP-zasp and EGFP-LC3 (figure 13, panel b and c). 48 h after transfection, EGFP-LC3 was almost completely localized in the cytosol in controls, while a vesicular localization was apparent in nutrient/serum deprived cells, consistent with autophagy activation upon HBSS treatment. Moreover, image analysis demonstrated that LC3 and zasp were largely colocalized along sarcomeres in nutrient/serum deprived cells, while no colocalization was detected in controls.

Altogether, these data indicate that autophagy may be involved in the process of sarcomeric disassembly.

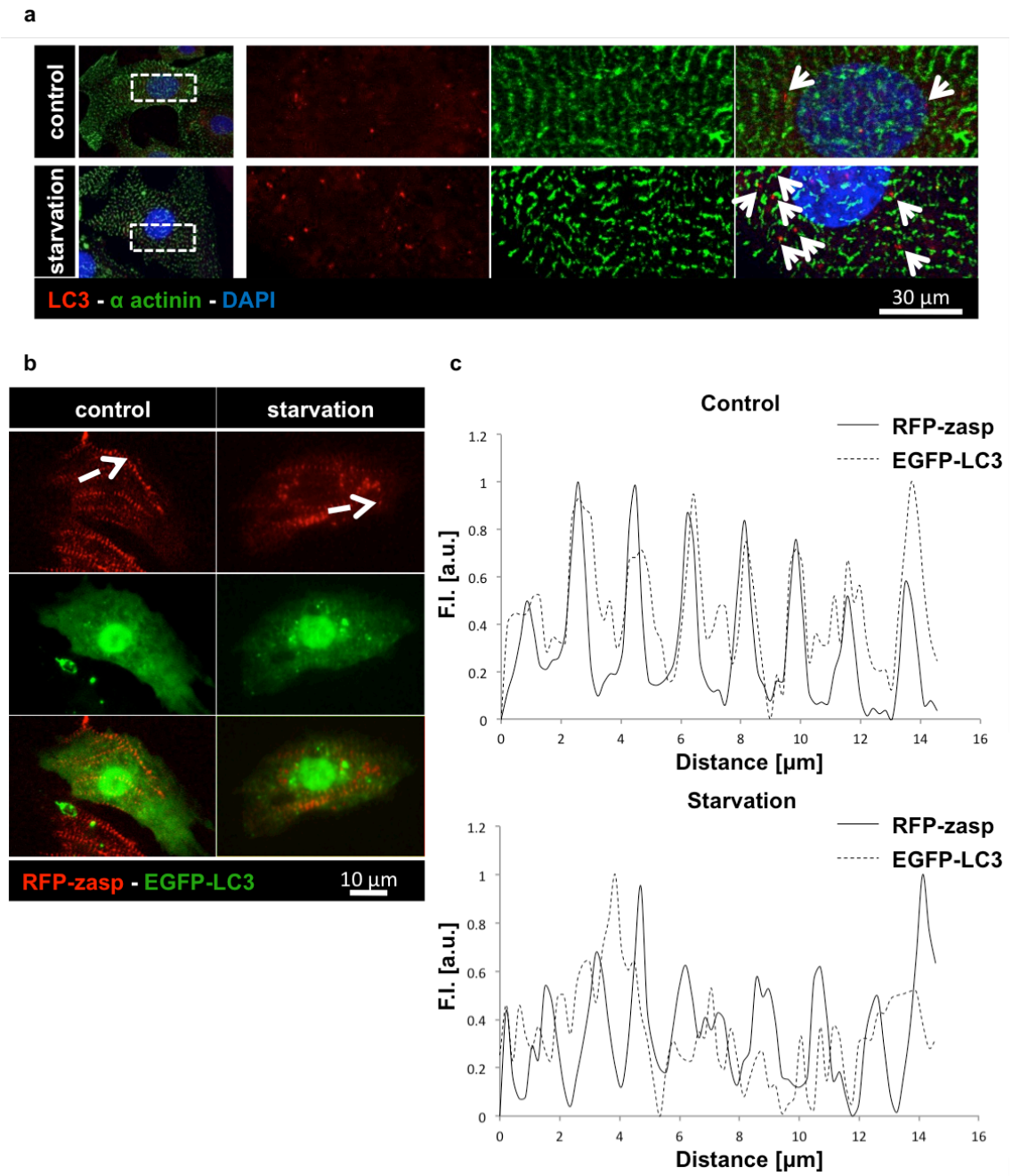

Figure 13 Role of autophagy in sarcomere disaggregation. (**a**) Confocal IF staining for LC3 (red signal), α actinin (green signal) and nuclei (blue signal). Magnifications of the white boxes are reported. Arrows indicate sites near sarcomeres where LC3 positive vesicles are enriched. Scale bar: 30µm. (**b**) Confocal imaging on CMs co-transfected with RFP-zasp (red signal) and EGFP-LC3 (green signal). Arrows indicate ROIs used for image analysis in (**c**). Scale bar: 10µm. (**c**) Plot profile analysis of RFP-zasp and EGFP-LC3 signals of the ROIs in (**b**).

4.1.4. The UPS participates to sarcomere disassembly

To understand whether the UPS has a role in sarcomeric dismantlement, we analyzed high resolution confocal images of ubiquitin IF of nutrient/serum deprived cardiomyocytes (figure 14, panel a). While ubiquitin staining was completely absent on sarcomeres of control CMs, ubiquitin immunoreactivity was enhanced in nutrient/serum deprived cardiomyocytes and predominantly accumulated between phalloidin positive sarcomere components, supporting that UPS may be involved in sarcomere dismantlement. Since phalloidin interacts with actin, which is mainly found in the I-band of the sarcomere, and ubiquitin staining was excluded from phalloidin marked sites, we concluded that the sites being ubiquitinated during starvation are localized along the A-band, near the M-line. A well-characterized ubiquitin ligase that is known to be localized in the M-line, is Murf1 (Powell SR, 2006), which as described above is potently induced by nutrient/serum deprivation both *in vitro* and *in vivo*. We therefore looked at the involvement of Murf1 in sarcomere dismantlement, and to this aim we set up Murf1 overexpression or silencing approach measuring the sarcomeric area after IF staining for α actinin (figure 14, panel b and c). Overexpression of the ubiquitin ligase alone in CMs maintained in SDM was sufficient to cause sarcomere degradation (446.19 ±35.65 vs 51.00 ±12.00 μm^2 of sarcomeric area in controls and Murf1 overexpressing CMs respectively). Moreover, we did not detect a complete recovery upon Murf1 gene silencing in CMs treated with nutrient/serum deprived medium (446.19 ±35.65 vs 144.91 ±26.25 μm^2 of sarcomeric area in controls and silenced CMs respectively), suggesting that Murf1-dependent degradation is not the only mechanism involved in sarcomeric disassembly.

The fact that Murf1 overexpression alone is sufficient to dismantle sarcomeres was confirmed by the imaging experiments in living CMs co-transfected with RFP-zasp and Murf1-flag constructs. After only 48 hours from transfection, sarcomeres were completely absent; this indicates the extent of Murf-1 mediated proteolysis, and also led us to perform the remainder imaging experiments in this model at an earlier time point (24 hours) after transfection. An example of the experiment is shown in figure 15, panel a, b. Consistent with previous data, Murf1 overexpressing CMs dismantle sarcomeres when compared to controls co-transfected with RFP-zasp and empty

pcDNA3.1, and this result was confirmed by the quantitative analysis of sarcomeric area (figure 15, panel b).

Taken together, these data support that the UPS, and in particular Murf1 in cardiomyocytes, mediate sarcomeric degradation in nutrient deprived cardiomyocytes. However, since silencing of Murf-1 did not prevent sarcomere degradation, our data also indicate that other ubiquitin ligases, or alternative proteolytic pathways (e.g. autophagy) may participate.

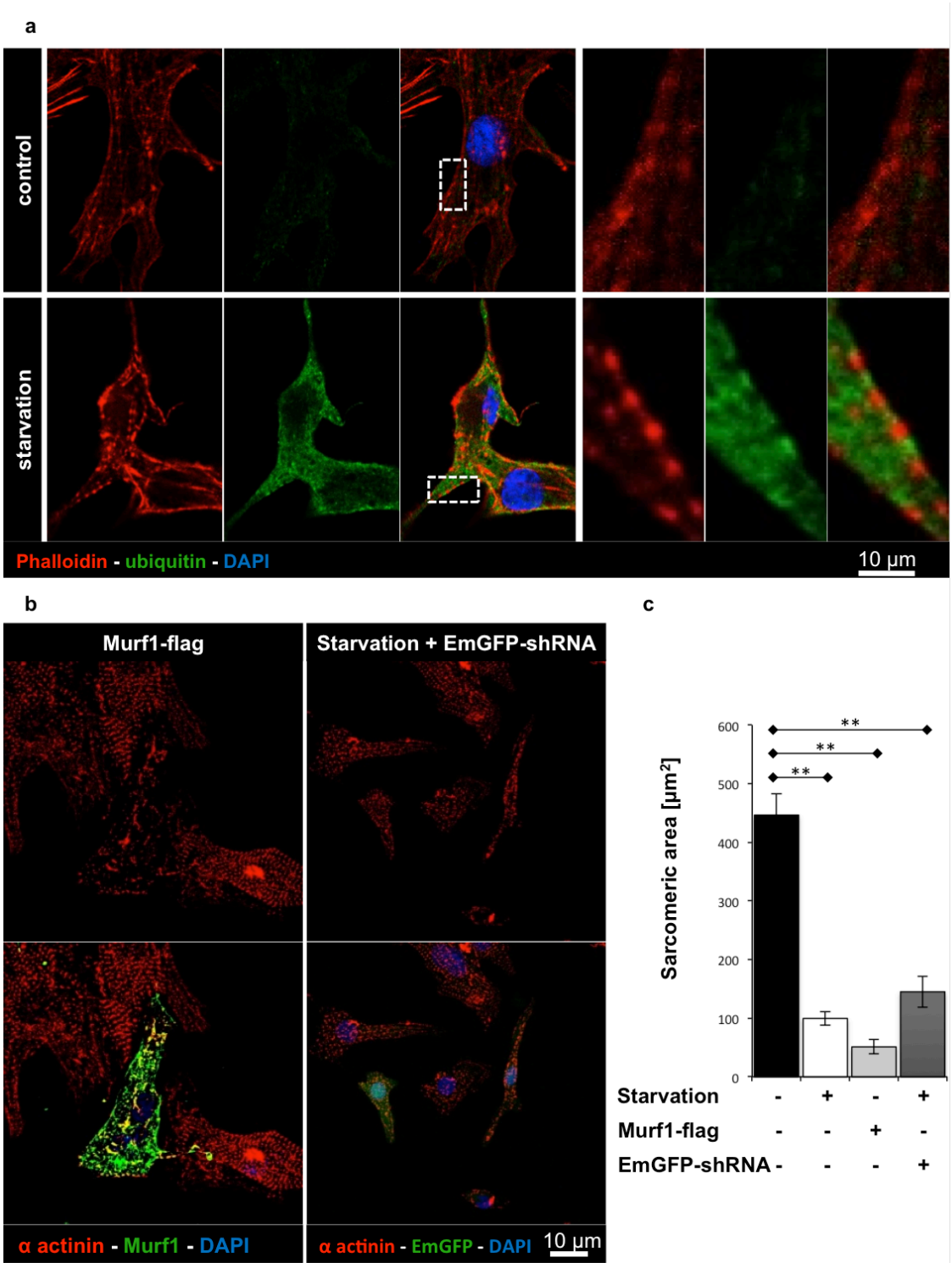

Figure 14 Murf1 is involved in sarcomere degradation. (**a**) Confocal z-projection of the IF staining for phalloidin (red signal), ubiquitin (green signal) and nuclei (blue signal) on CMs treated with HBSS or SDM. Magnifications of the white boxes in the images are shown. Scale bar: 10µm. (**b**) Confocal z-projection of the IF staining for α actinin (red signal), nuclei (blue) and Murf1 (green, right images) or EmGFP (green, left images) on CMs transfected with Murf1-flag or EmGFP-shRNA constructs. Scale bar:

10µm. (**c**) Quantitative analysis of the sarcomeric area in CMs overexpressing or downregulating Murf1 (error bars represent s.e.m., ** p<0.01, at least n=18 cells per condition).

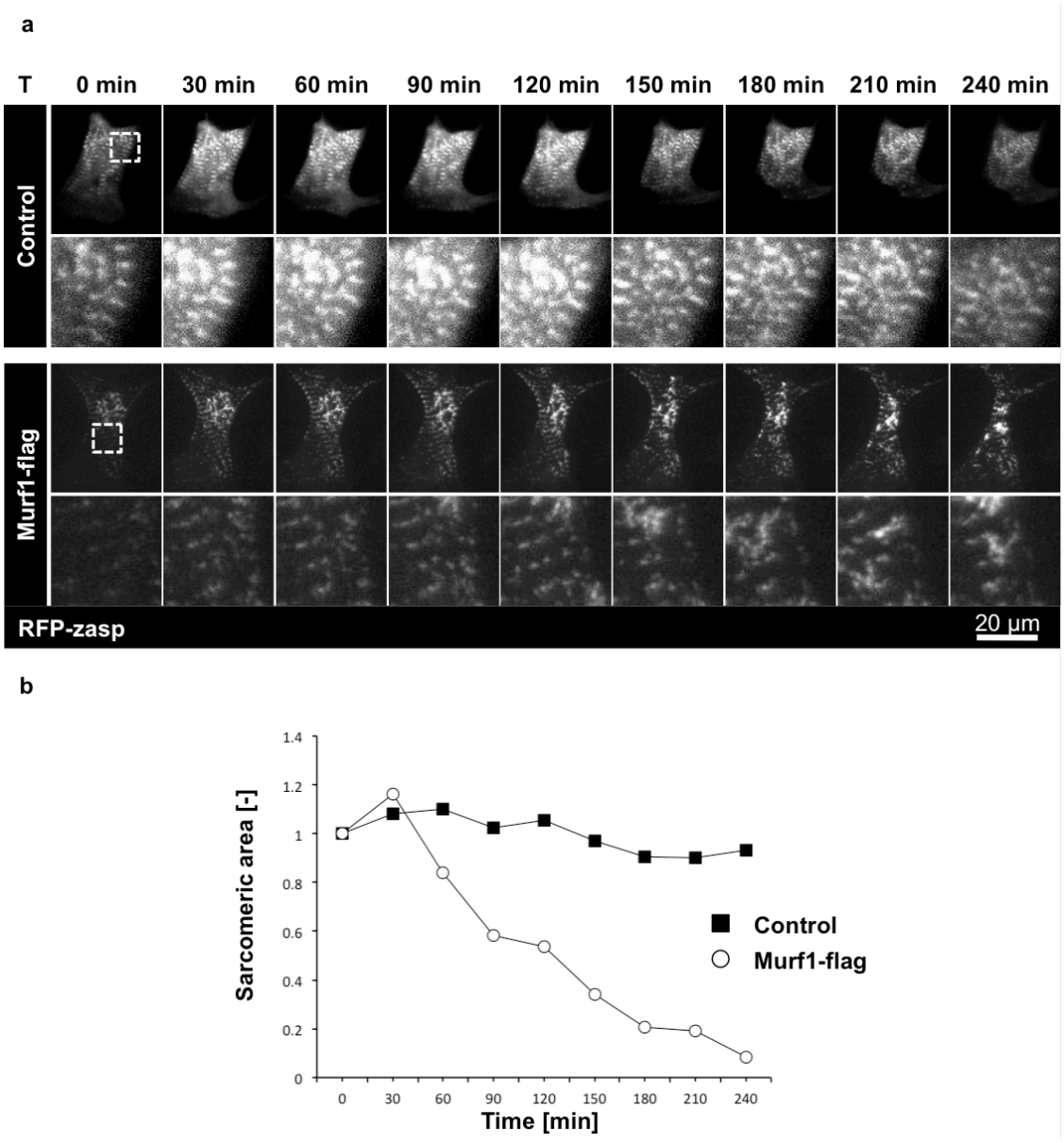

Figure 15 In live imaging of RFP-zasp degradation upon Murf1 overexpression. (**a**) Confocal z-projection of CMs in SDM and co-transfected with RFP-zasp (gray signal) and Murf1-flag. Magnifications of the white boxes in the images are reported. Scale bar: 20µm. (**b**) Quantitative analysis of the area occupied by sarcomeres shown in (**a**). The ratio between the area at a certain time point and the initial area is reported.

4.2. From the heart to the sympathetic neurons

The dependence of SN survival on target derived NGF is known. Moreover, the existence of an interaction between SNs and CMs was hypothesized by several papers. However, whether a direct interaction based on a specific structure is established, and what is the functional effect of such interaction on neurotrophic signaling is yet unclear. The second part of this PhD work focuses on the neuro-cardiac interaction and on its role on NGF mediated pro-survival signaling to the neurons.

4.2.1. CMs are closely associated with SNs *in vivo*

The first part of this work we aimed to understand the cellular interaction partners for myocardial STs. The two most represented cell types in the heart are cardiomyocytes and cardiac fibroblasts. CMs occupy approximately the 75% of cardiac volume, but they comprise only the 30-40% of cell number (Vliegen HW, 1991). The remaining cells are mainly cardiac fibroblasts, the biggest cardiac cell population, accounting for about two third of the cells (Fan D, 2012). Other permanent cell types (i.e. endothelilal cells and smooth muscle cells) or transient cell populations (i.e. lymphocytes, mast cells and macrophages) represent smaller populations. We thus focused on SN interaction with either CMs or CFs, and we started by performing IF analysis on adult rat heart cryosections, using antibodies against TOH and POH to identify sympathetic neurons and fibroblasts respectively. Moreover, sarcomeric phalloidin staining was used to mark CMs. As shown in the representative confocal image reported in figure 16, panel a, STs are preferentially found close to CMs, suggesting that the preferential interaction occurs between these two cell types, and such observation was corroborated by quantitative analysis (figure 16, panel b, 71.18 ±6.09% vs 25.97 ±5.71% of the axonal length was in contact with CMs and CFs respectively). Moreover, proximity between SNs and CM membranes was detected in the IF staining for TOH and agglutinin in mouse heart cryosections (figure 16, panel c). For a more detailed morphological characterization, we performed the IF staining for agglutinin and synapsin 1, a marker for active releasing sites, (figure 16, panel d). STs display regular features, such as 1 active releasing site every 4 ±0.04µm, and every CM membrane was contacted by approximately 5 synaptic boutons. Interestingly, we detected many

active sites of the ST close to the CM membrane, supporting that the two cell types are directly interacting and that this interaction may be functional. To further increase the resolution of our analysis, we performed TEM analysis on mouse heart (figure 16, panel e) and detected sites of ST-CM interaction characterized by membrane thickenings, neurotransmitter vesicle accumulation and cell-to-cell distance of approximately 70-100 nm. Taken together, these results suggest that a direct interaction is preferentially established between CMs and SNs. For its similarity with the well known neuromuscular junction (NMJ) we defined such interaction neuro-cardiac junction (NCJ).

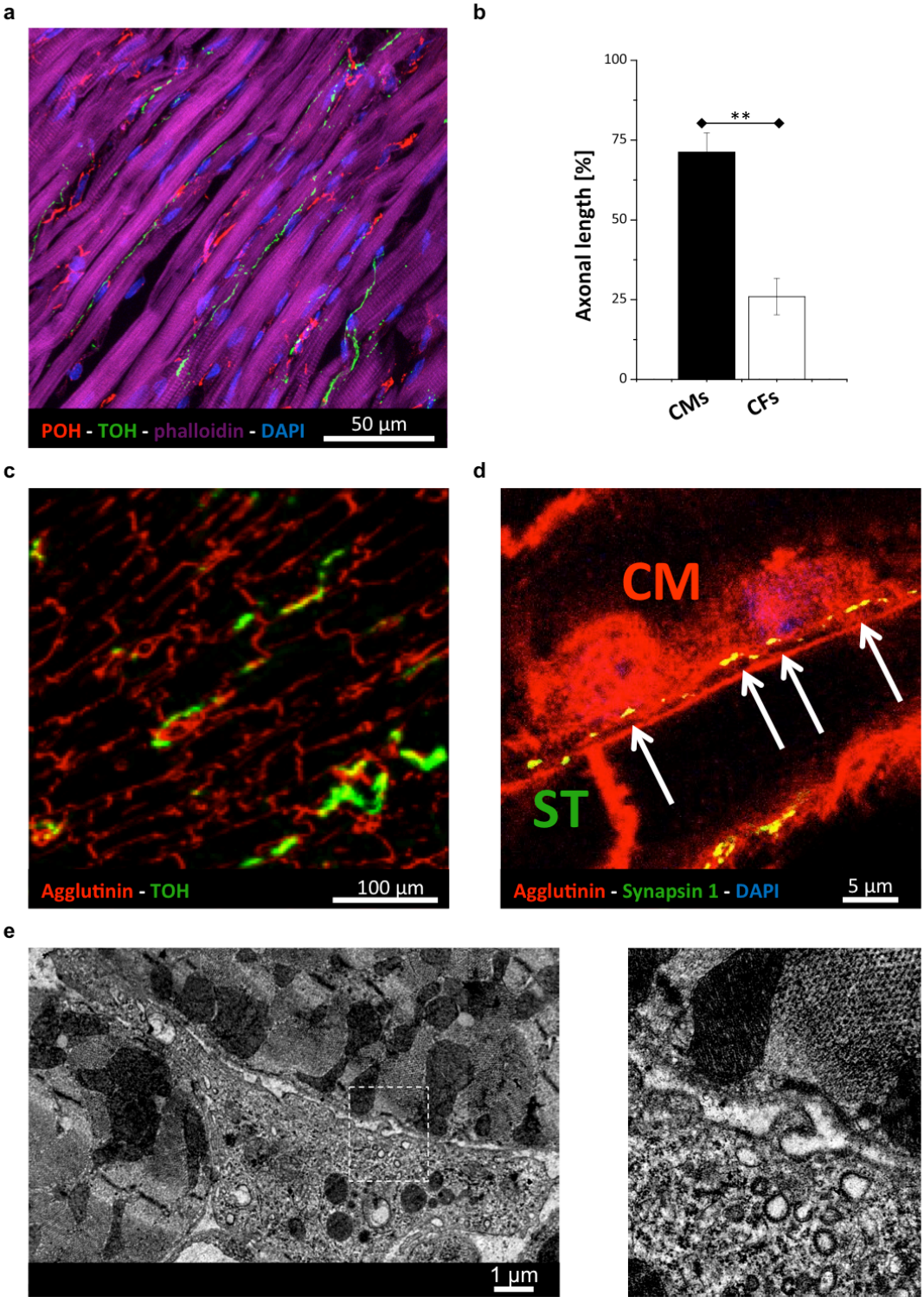

Figure 16 A preferential interaction between STs and CMs is established in rat and mouse myocardium. (**a**) Confocal z-projection of the IF analysis on an adult rat heart cryosection stained for POH (red signal), TOH (green signal), phalloidin (violet signal) and nuclei (blue signal). Scale bar: 50µm. (**b**) Quantitative analysis of the interaction between sympathetic axons and CMs or CFs (error bars represent s.e.m., ** $p<0.01$, n=14 terminals). (**c**) Confocal IF analysis on mouse heart cryosections stained with agglutinin (red signal) and an antibody for TOH (green signal). Scale bar: 100µm. (**d**) Confocal IF analysis on mouse

heart cryosections stained with agglutinin (red signal) and an antibody for synapsin 1 (green signal) and DAPI (blue signal). Arrows indicate sites of contact between the ST and the CM membrane. Scale bar: 5µm. (**e**) TEM analysis on mouse right ventricle, showing a ST surrounded by CMs. The magnification of the white box is reported in the left side of the image. Scale bar: 1µm.

4.2.2. Generic cell-to-cell adhesion molecules are enriched at the NCJ

To gain insight into the structural features of the NCJ, we established a versatile experimental model based on SGN/CM co-cultures, obtained by mixed culture of CM from the hearts and sympathetic neurons from the superior cervical ganglia of p2-p3 rats. The two cell types were characterized by staining CMs for α actinin and SNs for TOH and DBH (figure 17, panel a, b). Since isolated neurons were positive for DBH, we concluded that they were noradrenergic and not dopaminergic neurons. Moreover we performed IF staining on 12-day co-cultures for cTnI and TOH and detected neurons that contacted different CM clusters (figure 17, panel c). These results suggest that both isolated CMs and SGNs maintain their differentiation state and interact in co-cultures.

Co-cultures were further characterized for the enrichment of generic cell-to-cell adhesion molecules. Cadherins are calcium dependent homophilic cell adhesion molecules that, in the intercellular interaction sites in different systems, can link the pre- and post-synaptic membranes, thus promoting synapse stability. They are known to form complexes with β catenin that binds the cadherin complex to the actin cytoskeleton. It has been reported that both proteins are enriched under the sympathetic processes in SGN/CM co-cultures of 5 days (Shcherbakova OG, 2007). We performed an IF staining for TOH and cadherins or β catenin on both 5 day or 14 day old co-cultures, and demonstrated that such proteins are enriched under the sympathetic process in a time dependent manner (figure 18, panel a, b). While in 5 day co-cultures protein enrichment was not significant, in 14 day co-cultures it became more evident, suggesting that the interaction is characterized by time dependent maturation. Non CM cardiac cells did not show any enrichment of cell-to-cell adhesion molecule under the sympathetic process. Since a linear correlation between TOH and cadherin or β catenin enrichment was detected, these data support that the enzyme involved in NE synthesis is enriched in sites of cell-to-cell interaction.

Moreover, we asked whether such enrichment was specific for the CM-sympathetic neuron interaction. To answer this question, we cultured CMs with hippocampal neurons[17] (HN) or SGNs, and performed IF staining for presynaptic markers, e.g. VAMP2, and proteins enriched at the junctional site (i.e. cadherin, β catenin). To avoid excessive fibroblast growth from cells retained during the HN preparation, cells were fixed after 8 days of culture. As reported in figure 19, panel a-d, we detected no difference in cell-to-cell adhesion molecule enrichment in those culture models, suggesting that β catenin and cadherins are not specifically enriched at the contact site between neurons and CMs. Altogether, these results suggest that cell-to-cell adhesion protein enrichment occurs at the cell-cell interaction site in a time dependent manner, but it is not specific.

[17] Hyppocampal neurons were provided by the lab of Dr. Claudia Lodovichi (VIMM, Padova).

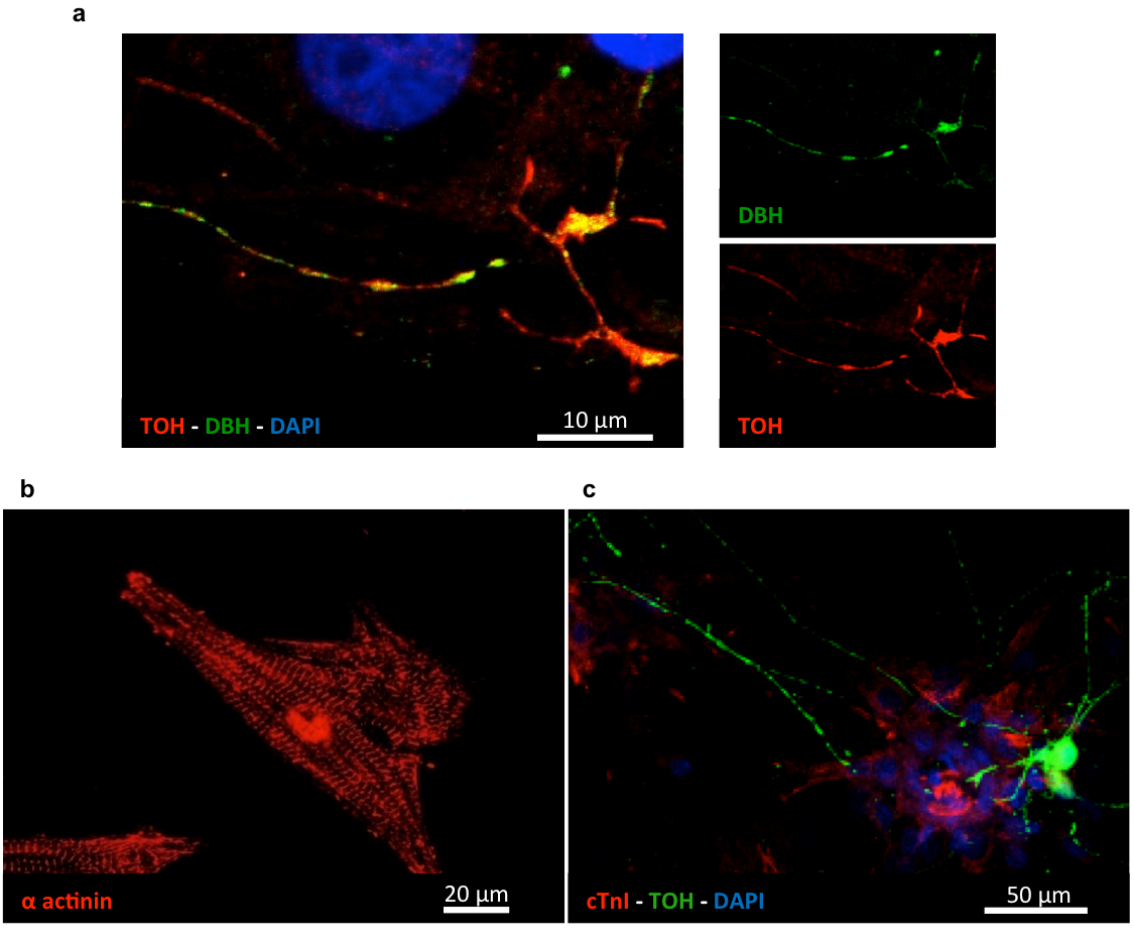

Figure 17 SGN/CM co-cultures. (**a**) Confocal z-projection of the IF staining for TOH (red signal), DBH (green signal) and nuclei (blue signal) on isolated SGNs. Scale bar: 10µm. (**b**) Confocal IF staining for α actinin (red signal) on isolated CMs. Scale bar: 20µm. (**c**) Confocal z-projection of the IF staining for cTnI (red signal), TOH (green signal) and nuclei (blue) on 12 day SGN/CM co-cultures. Scale bar: 50µm.

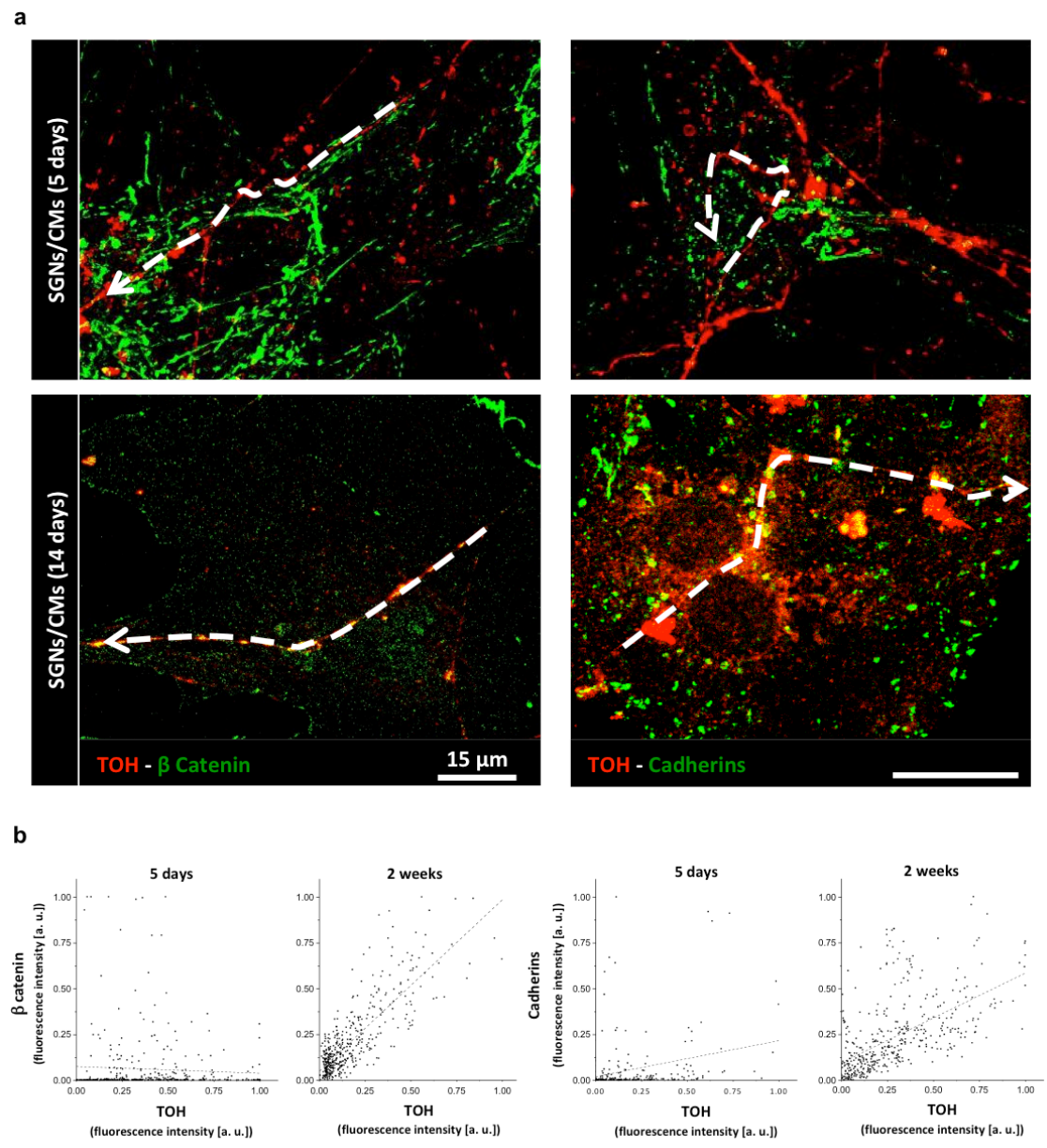

Figure 18 Cell-to-cell adhesion molecules are enriched at the NCJ in a time dependent manner. (**a**) Confocal z-projection of the IF staining on 5 or 12 day old co-cultures for TOH (red signal) and cadherins or β catenin (green signal). Scale bar: 15µm. (**b**) Graphs reporting β catenin and cadherin accumulation at the SGN/CM interaction site in 5 days or 2 weeks old co-cultures. One representative cell per condition is reported.

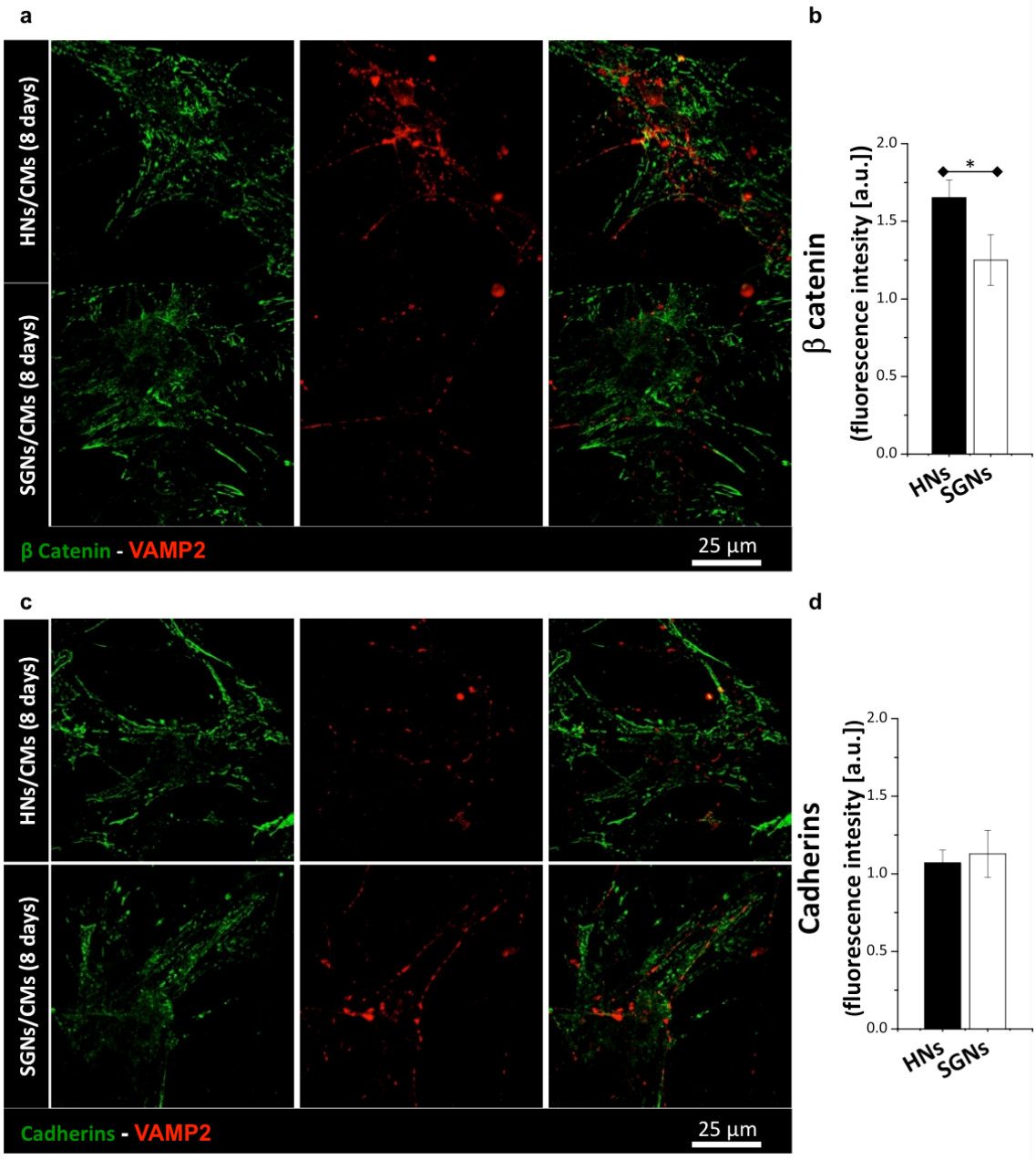

Figure 19 Cell-to-cell adhesion molecules do not enrich only at the NCJ. (**a**-**b**) Confocal z-projection of IF staining on 8 day co-cultures between CMs and HNs or SGNs using antibodies to β catenin (green signal) and VAMP2 (red signal, **a**) and quantification (**b**). Scale bar: 25µm (error bars represent s.e.m., * 0.01<p<0.05, at least n=13 processes per condition). (**c**-**d**) Confocal z-projection of IF staining on 8 day co-cultures between CMs and HNs or SGNs using antibodies to cadherins (green signal) and VAMP2 (red signal, **c**) and quantification (**d**). Scale bar: 25µm (error bars represent s.e.m., at least n=10 processes per condition).

4.2.3. Contact site enlargement and stabilization occur between SNs and CMs in co-cultures

To understand whether a preferential interaction is established between SNs and CMs *in vitro* in co-cultures, another model was set up using compartmented CM plating in culture coverslips. This method allowed to divide in the same coverslip areas (central) with enrichment in CM and others (peripheral) characterized by high density in non CM cardiac cells (mainly CFs). After plating, neurons were uniformly seeded throughout the coverslip (figure 20, panel a). When exogenous 8nM NGF was maintained in the medium, neuronal process sprouting was identical both on CMs and non CM cardiac cells. Process retraction was detected mainly on non CM cardiac cells upon NGF withdrawal (figure 20, panel b) and the area occupied by TOH-marked processes was significantly higher in the CM enriched regions (67.11 ±12.36% vs 3.79 ±1.12% of area occupied by processes on CMs or non CM cardiac cells respectively, figure 20, panel c), supporting the preferential interaction of SGNs with CMs. This result was confirmed by imaging of living co-cultures (figure 20 panel d). In the absence of NGF, neuronal processes also contacted non CM cardiac cells, however, these interactions were mostly unstable and detached within 4 hours. On the contrary, sympathetic processes in contact with CM clusters remained in direct contact with the cells for the duration of the experiment (4 hours), suggesting that this interaction is more stable. This idea is further supported by the observation that SGNs developed larger contact sites on CMs than on other cardiac cells of the same culture (figure 21, panel a and b, 82.88 ±1.3% decrease in contact area on non CM cardiac cells when compared to CMs). Taken together, all these data suggest that SGNs establish a direct and stable interaction with CMs and not other cardiac cells.

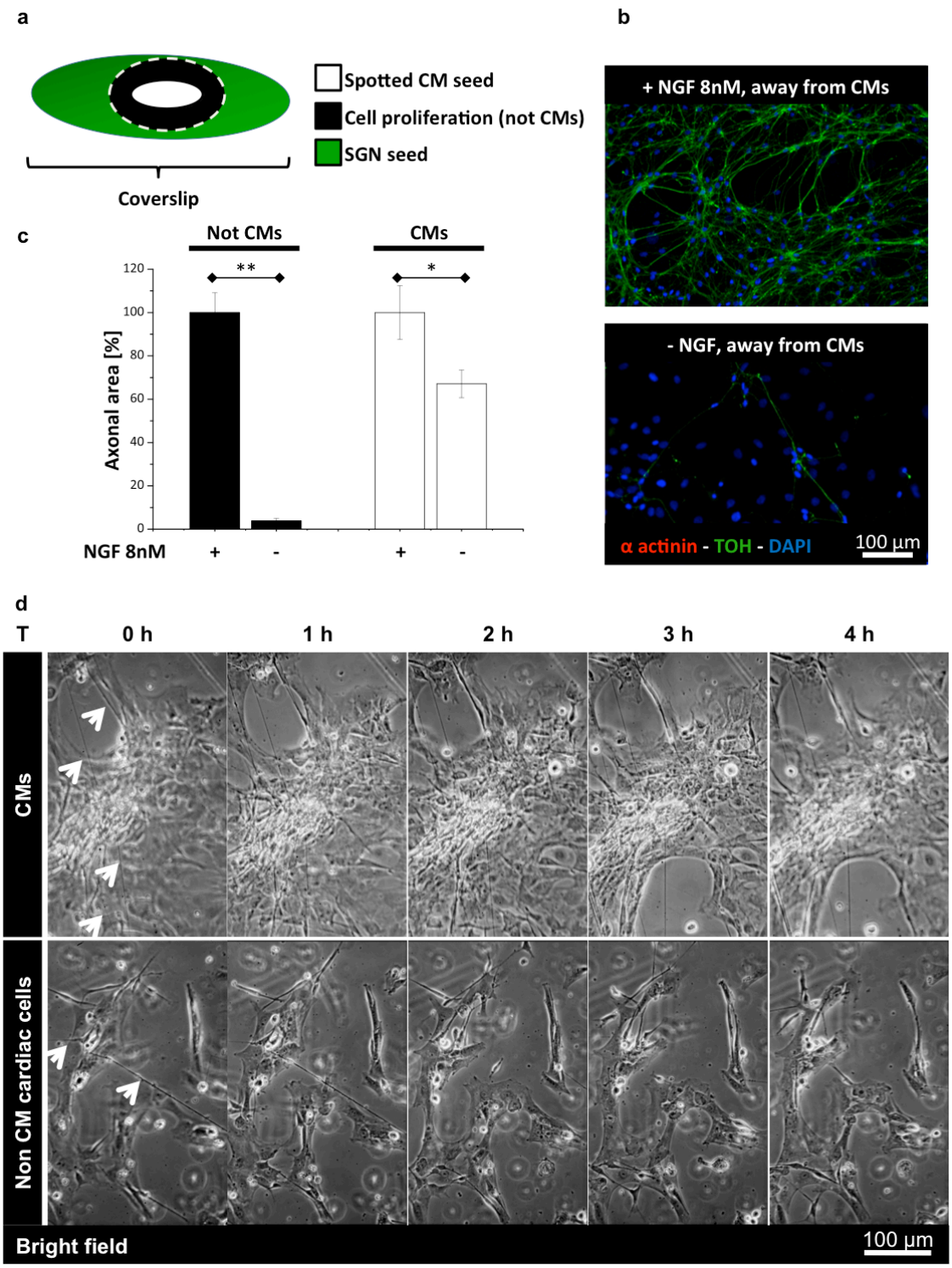

Figure 20 Contact stabilization occurs between SNs and CMs. (**a**) Schematic view of spotted co-cultures. (**b**) IF analysis on spotted co-cultures stained with DAPI (blue signal) and antibodies to α actinin (red signal) and TOH (green signal). Images of fields on non CM cardiac cells with or without NGF are reported. Scale bar: 100µm. (**c**) Quantification of the area occupied by sympathetic processes on CMs or other cardiac cells with or without NGF (error bars represent s.e.m., **p<0.01, *0.01<p<0.05, n=10 fields per condition). (**d**) Bright field images of the time lapse experiment on sympathetic processes on

CMs or other cardiac cells. Arrows indicate sympathetic processes in contact with cells. Scale bar: 100µm.

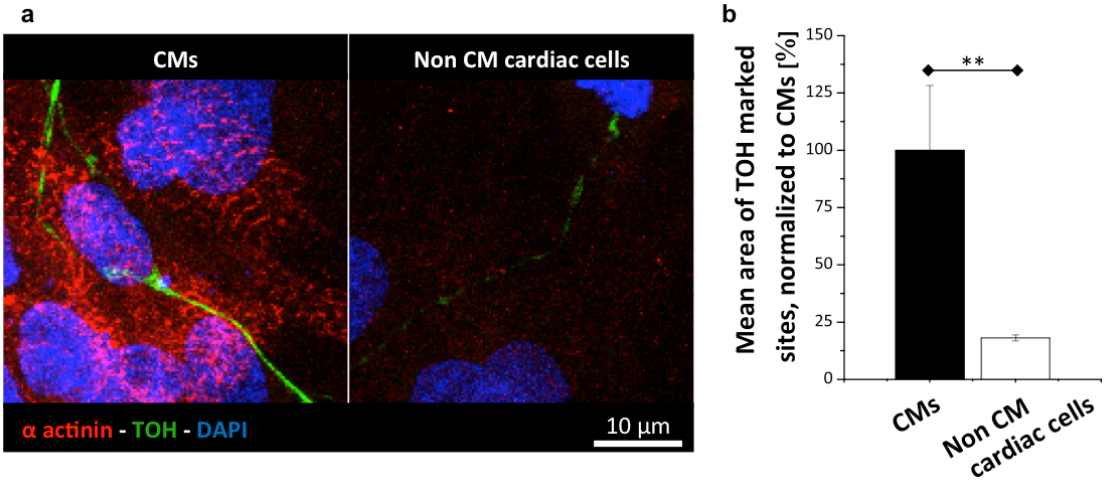

Figure 21 Contact site enlargement occurs between SNs and CMs. (**a**) Confocal z-projection of co-cultures stained with DAPI (blue signal) and antibodies to α actinin (red signal) and TOH (green signal). Scale bar: 10µm. (**b**) Quantification of the contact site size between sympathetic processes and CMs or other cardiac cells (error bars represent s.e.m., **p<0.01, n=33 boutons per condition)

4.2.4. Cardiac sympathetic neurons are dependent on NGF released by cardiomyocytes

Since the myocardium is known to produce NGF that is required for SN viability, we aimed to assess the functional role of the NCJ in NGF dependent signaling. NGF expression by the heart was demonstrated by western blotting, both in whole heart protein extracts, as well as cellular lysates from CM cultures (figure 22, panel a). To understand whether SNs are dependent on CM derived NGF, cultured CMs were transfected with siRNA against NGF. Si44 was the most efficient in NGF silencing, causing a 72.91% decrease in neurotrophin expression when compared to the scramble SIC001 (figure 22, panel b). A combination between different siRNA did not increase NGF silencing, so we used only si44 for the following experiments. Moreover, siRNA transfection did not affect CM viability and morphology (figure 23, panel a, b and c), since no significant differences in sarcomeres, CM area or density were measured.

When we transfected CMs with si44 and then seeded SGNs, we detected a 65.72 ±9.33% reduction in the mean neuronal density upon NGF withdrawal (figure 22, panel

c and d). This effect was rescued by the addition of exogenous 8nM NGF to the culture medium and supports that cultured sympathetic neurons are dependent on CM derived NGF.

To further analyze NGF signaling between SNs and CMs we monitored translocation of the NGF receptor TrkA in the co-cultures. It is well-accepted that NGF binding to its receptor enables its activation, endocytosis and retrograde transport to the neuronal soma. Studies on PC12 cells revealed increase in movements of GFP labeled TrkA upon NGF administration (Nomura M, 2011). We thus transfected the neurons with a construct encoding the fusion protein TrkA-RFP, and used confocal time lapse fluorescence imaging to monitor TrkA retrograde movements as an effect of receptor activation by NGF. In transfected neurons, TrkA-RFP was detected on the neuronal membrane, in particular in the terminal region, as well as in intracellular vesicular structures distributed along the neuronal processes. Immunofluorescence staining showed co-localization between TrkA and RFP in neurons (figure 24, panel a), suggesting that the fusion protein is correctly expressed. To analyze the effect of NGF presence on TrkA, the speed of retrograde TrkA-RFP dots was quantified through kymograph analysis of confocal images (figure 24, panel b, c, d and e). The results of our experiments demonstrate that the speed of retrograde TrkA-RFP movement is significantly reduced upon NGF withdrawal, as compared to control cells kept in NGF supplemented medium (figure 24, panel b and c, 0.32 ±0.06 vs 0.19 ±0.03µm/s in presence or absence of NGF). In line with the hypothesis that CM signal to the neurons through release of NGF and activation of TrkA receptors, retrograde TrkA translocation was faster in processes contacting CMs than in those contacting other cardiac cells (figure 24, panel d and e, 0.24 ±0.05 vs 0.11 ±0.02µm/s respectively).

Collectively, these data indicate that SGN survival requires CM derived NGF, and that neuronal NGF signaling is activated by CM and not by other cardiac cells.

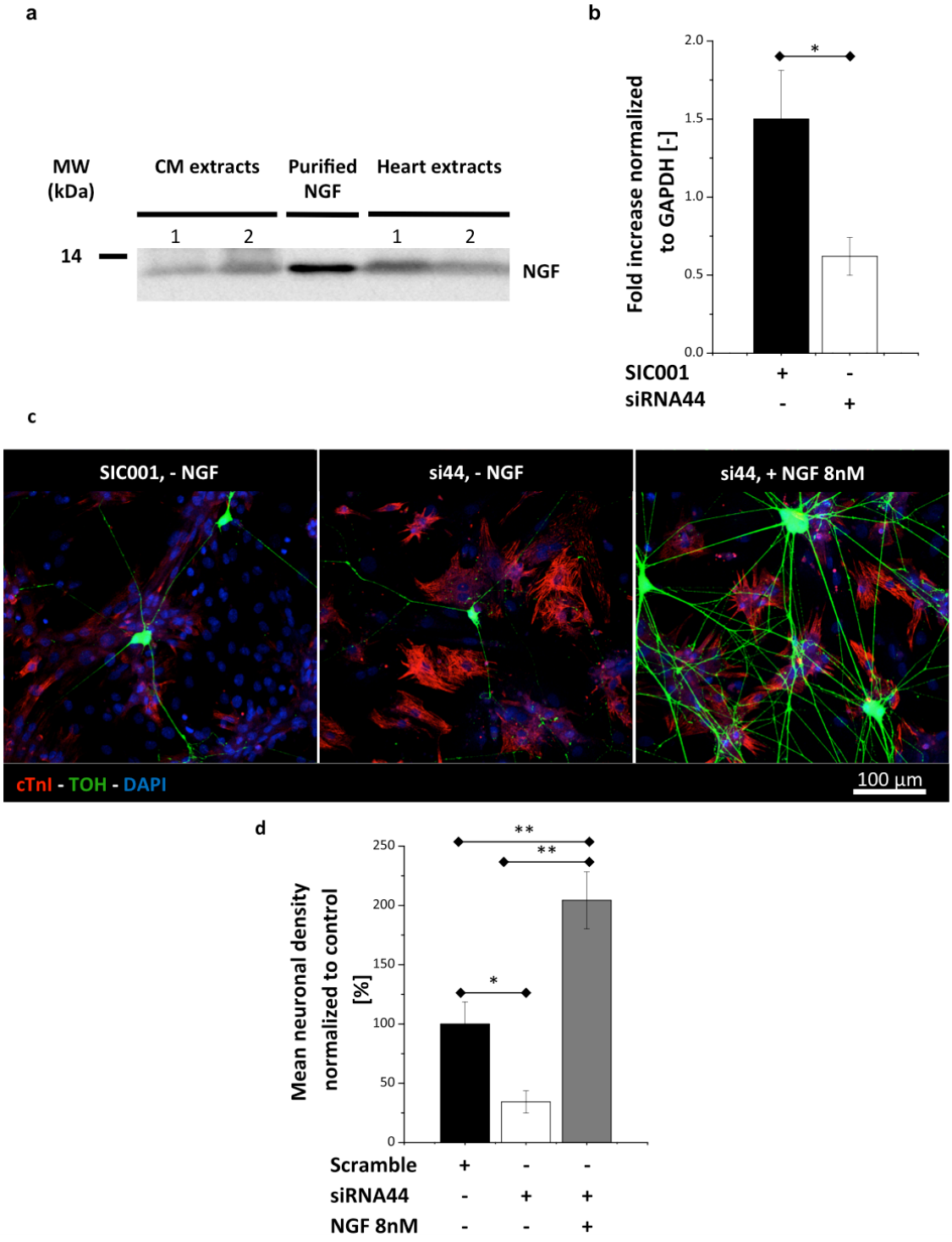

Figure 22 Cardiac sympathetic neurons are dependent on CM released NGF. (**a**) WB analysis for NGF on heart and CM protein extract. (**b**) RT-qPCR analysis for NGF expression on CMs transfected either with the scramble siRNA (SIC001) or with the NGF targeted siRNA (si44, error bars represent s.e.m., *0.01<p<0.05, n=6 CM cultures). (**c**) Confocal z-projections of co-cultures transfected with scramble and NGF targeted siRNAs and stained for DAPI (blue), cTnI (red signal) and TOH (green signal). Scale bar: 100µm. (**c**) Quantitative analysis of the mean neuronal density upon siRNA transfection in co-cultures (error bars represent s.e.m., **p<0.01, *0.01<p<0.05, n=16 fields per condition from 2 cultures).

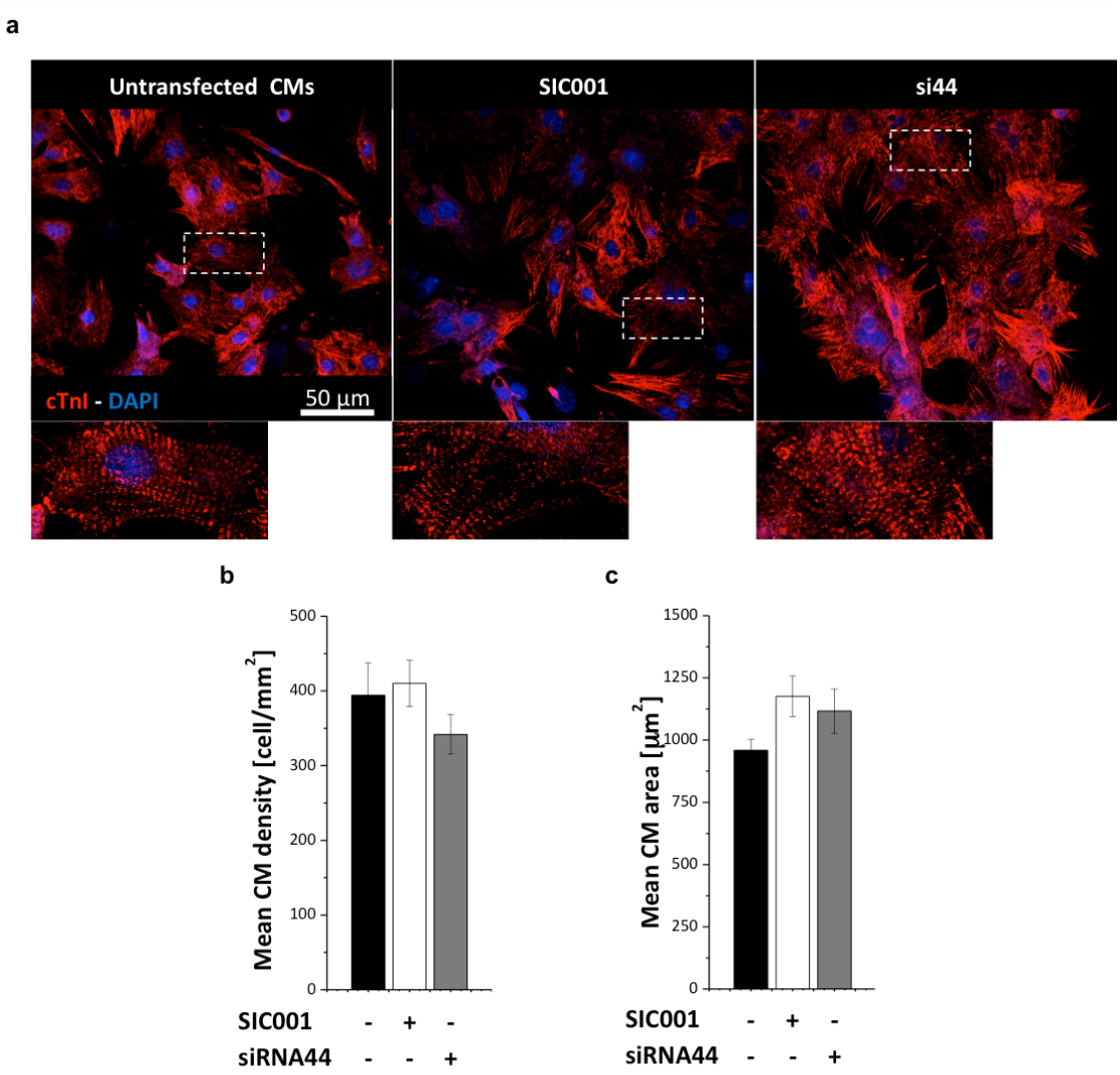

Figure 23 SiRNA transfection has no relevant morphological effects on CMs**.** (**a**) Confocal z-projections of the IF staining for cTnI (red signal) and nuclei (blue signal) on CMs transfected or not with si44 or SIC001. Magnifications of the white boxes are reported. Scale bar: 50µm. (**b**, **c**) Quantitative analyses of CM density (**b**) and area (**c**) upon siRNA transfection (error bars represent s.e.m., at least n=32 CMs per condition for size measures and n=6 fields per condition for CM density).

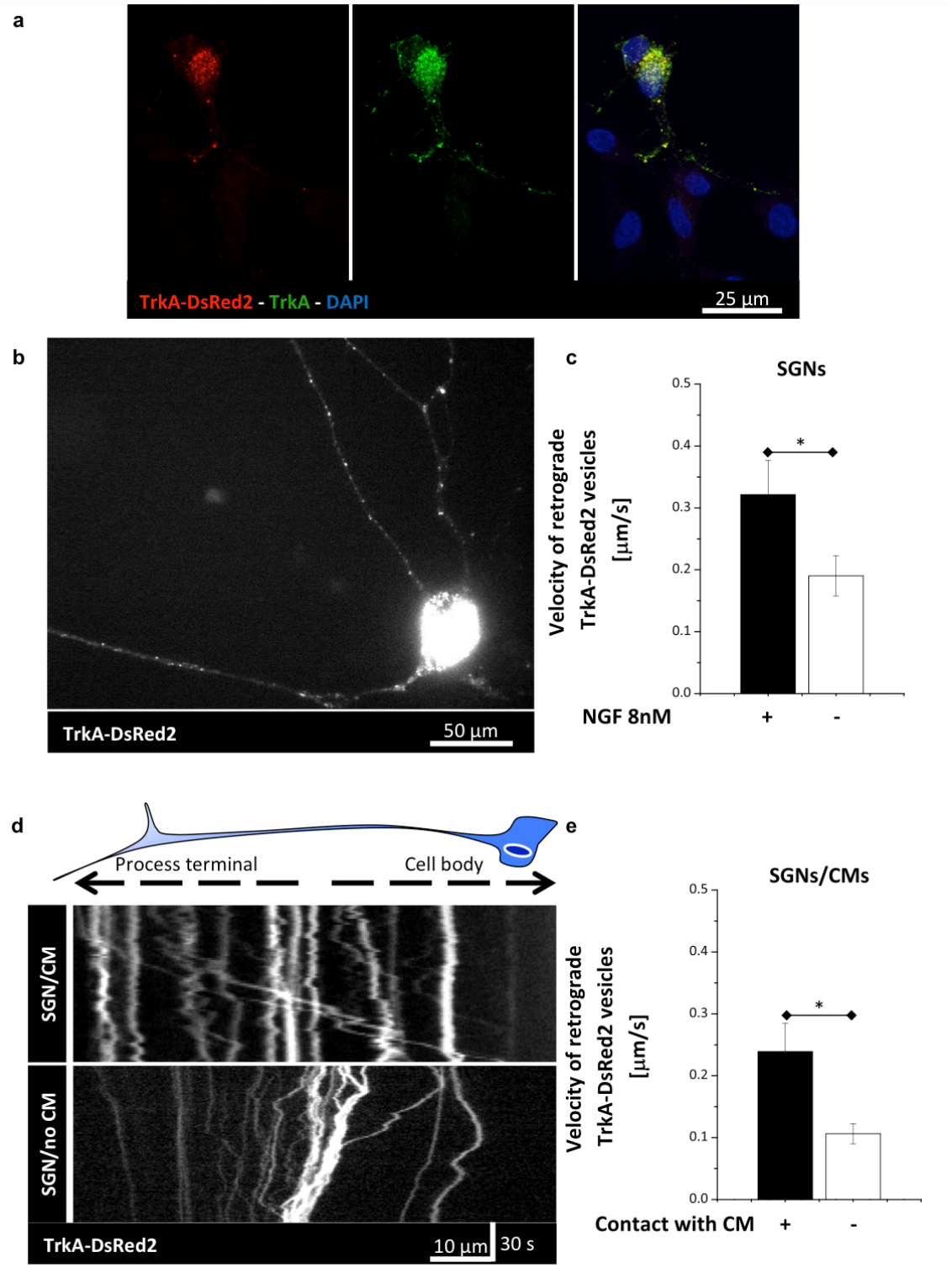

Figure 24 TrkA retrograde transport in neurons and co-cultures. (**a**) Confocal z-projection of the IF staining for TrkA (green signal) and nuclei (DAPI) on SGNs transfected with the TrkA-DsRed2 construct. Scale bar: 25µm. (**b**) Confocal image of TrkA-DsRed2 transfected SGNs. Scale bar: 50µm. (**c**) Quantification of the speed of TrkA-DsRed2 retrograde movements in transfected neurons in presence of NGF or after 24h of NGF withdrawal (error bars represent s.e.m., *0.01<p<0.05, at least n=4 sympathetic processes per condition). (**d**) Kymograph of TrkA-DsRed2 transfected processes on CMs or

other cardiac cells, without NGF. Scale bars: 10μm and 30s. (**e**) Quantification of the speed of TrkA-DsRed2 retrograde movements in processes contacting CMs or other cardiac cells without NGF in the medium (error bars represent s.e.m., *0.01<p<0.05, at least n=3 sympathetic processes per condition).

4.2.5. Direct SGN/CM interaction is required for NGF signaling

Since SGNs interact with CMs and depend on CM released NGF, we tested the hypothesis that the NGF mediated signaling at the NCJ is necessary for neuronal survival. Immunofluorescence staining of cryosections of adult rat hearts with anti-TrkA and anti-synaptophysin antibodies, showed that TrkA clustered at the site of interaction between the sympathetic terminal and the CM membrane, suggesting that the upstream events of the NGF signaling cascade may be triggered at the SN-CM contact site (figure 25, panel a). To test our hypothesis we used our co-cultures. As previously shown, SGN survival depends on the continuous stimulation of NGF signaling, and in the absence of the neurotrophin neurons undergo death. Removal of NGF after three days of SGN/CM co-culture resulted in the decrease of SN density to about one half (figure 25, panel b and c, SN density upon NGF withdrawal relative to NGF treated cultures: 47.4 ±5.77%). Interestingly, when NGF was removed from the cells after 7 days of NGF-treated co-culture, no neuronal loss was detected (figure 25, panel c). As shown above, we have demonstrated that the markers of membrane rearrangement at the contact site, including cell-to-cell adhesion molecules like cadherins and β catenin, accumulate in a time-dependent manner (Figure 18). Therefore, the difference in neuronal loss observed upon NGF withdrawal in three- or seven-day co-cultures could reflect the different degree of maturation of a functional interaction between SNs and CMs.

We then sought to understand whether the effect of cardiomyocytes on neuronal survival were due to the release of sufficient NGF in the culture medium or, on the contrary, if local CM-SN signaling was required. To this aim, we compared the mean neuronal density in neurons incubated with 7 day CM-conditioned medium, to that of NGF-deprived co-cultures, or co-cultures maintained in 10-fold diluted culture medium. CM conditioned medium did not prevent neuronal death (figure 25, panel d, 58.21 ±10.42% decrease in mean neuronal density when compared to SGN/CM co-cultures maintained without NGF), suggesting that NGF concentration in the medium is

not sufficient for neuronal survival. Consistently, we used an ELISA assay for NGF to measure the neurotrophin concentration in CM-conditioned medium, which was 0.13 ±0.08pM, 1000-fold lower than the minimal dose required for neuronal survival (0.4nM, as described by (Lockhart ST, 1997)).

To evaluate whether single cell-to-single cell NGF signaling occurs between SGNs and CMs, we analyzed neurotrophin-mediated effects at the level of the contact sites along the 'pearl and necklace' structure of the neuron. Neurons alone showed 31.84 ±4.49% decrease in the area of TOH labeled sites after NGF withdrawal, suggesting that NGF may regulate bouton size (figure 26, panels a, b). To analyze neurotrophin-dependent effects on SGN/CM contact sites, co-cultures were co-transfected with siRNA against NGF and a plasmid encoding for the GFP allowing identification of NGF-silenced CMs. Sympathetic processes interacting with NGF-silenced CMs showed a 19.56 ±4.01% decrease in the neuro-cardiac contact area when compared to that of processes interacting with untransfected CMs on the same coverslip. These results indicate that local cell-cell NGF signaling takes place at the junctional site whereby cardiomyocyte-released NGF regulates development of the interacting pre-junctional neuron (figure 26, panels c and d). This effect was rescued by the addition of 8nM NGF to the medium.

The presence of direct intercellular NGF signaling was further tested by overexpressing NGF in HeLa cells. NGF expression by RFP-NGF transfected HeLa was assessed by IF staining and showed a vesicular localization. Since the RFP sequence is fused to NGF pre-domain, it is cleaved and releases NGF and soluble RFP, thus resulting in diffuse red fluorescence (figure 27, panel a). HeLa clones with stable expression of RFP-NGF construct were generated (c5NGFRFP HeLa) and NGF release was assessed by measuring its concentration in the medium using an ELISA assay ($[NGF]_{c5NGFRFP}$ = 16.73 ±0.16pM vs. $[NGF]_{RFP\text{-}HeLa}$ < 0.8pM). These results suggest that NGF is expressed and released by RFP-NGF transfected cells.

Since endogenous NGF is expressed by CMs at low levels and cannot be detected with IF techniques, co-cultures were transfected with the RFP-NGF construct in order to detect NGF accumulation in sympathetic processes (figure 27, panel b). Only processes in contact with transfected CMs contained NGF puncta, while those in contact with

untransfected cells did not contain NGF (figure 27, panel c; 43.43 ±10.77 vs 4.17 ±4.1% of processes on transfected or un-transfected CMs). Taken together, these data support the presence of a local NGF signaling and suggest that the establishment of a neuro-cardiac interaction is necessary to allow NGF signaling.

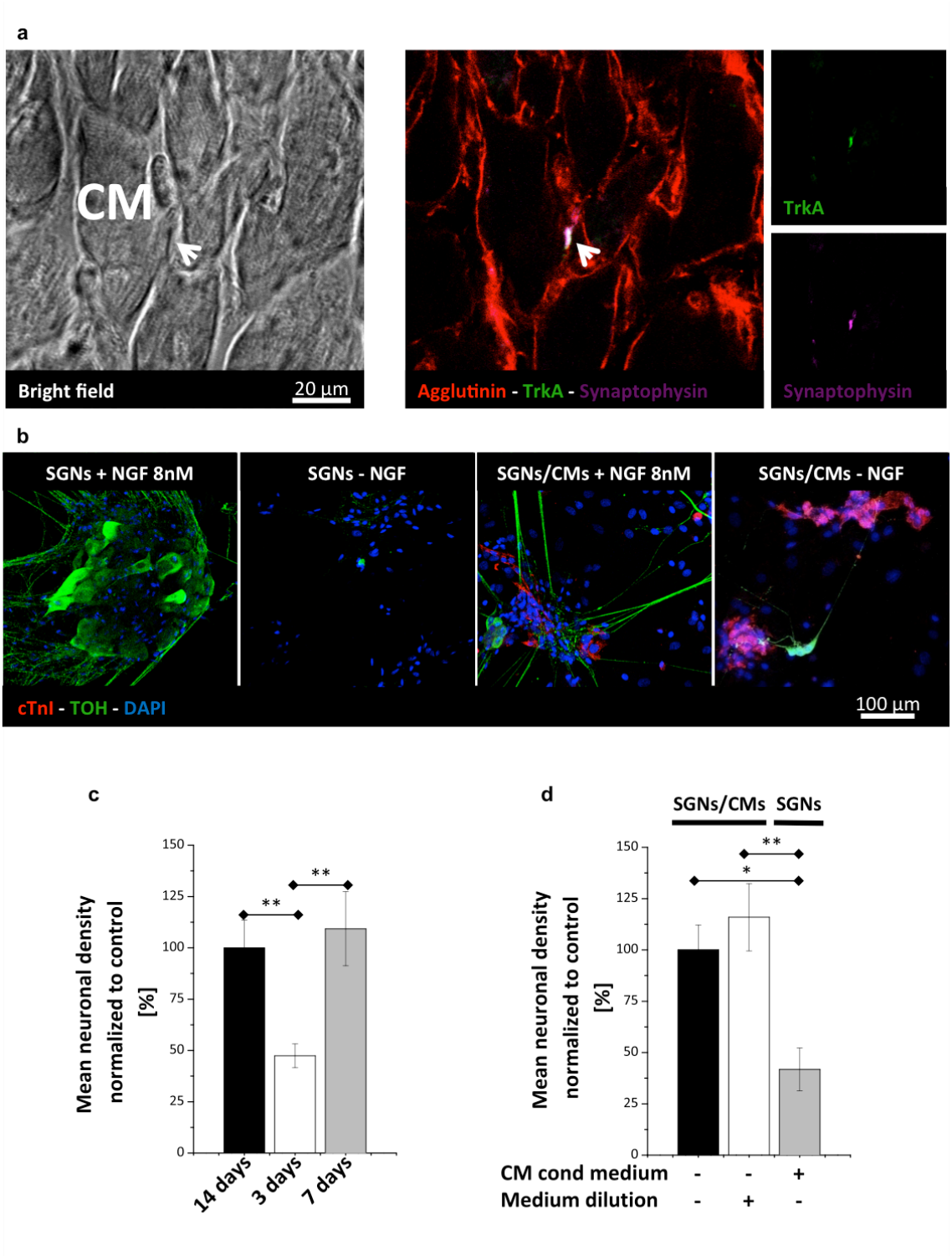

Figure 25 The NCJ is required for neurotrophic signaling. (**a**) Confocal IF staining for agglutinin (red signal), TrkA (green signal) and synaptophysin (violet signal) and bright field on heart cryosections from adult rat. The arrow indicates TrkA enrichment at the interaction site between the axon and the CM membrane. Scale bar: 20µm. (**b**) Confocal z-projections of the IF staining for cTnI (red signal), TOH (green signal) and nuclei (blue signal) on neuronal cultures and SGN/CM co-cultures. Scale bar: 100µm. (**c**, **d**) Quantification of the mean neuronal density of co-cultures incubated with NGF for different

periods (**c**) and neurons treated with CM conditioned medium (error bars represent s.e.m., **p<0.01, *0.01<p<0.05, at least n=15 fields per condition).

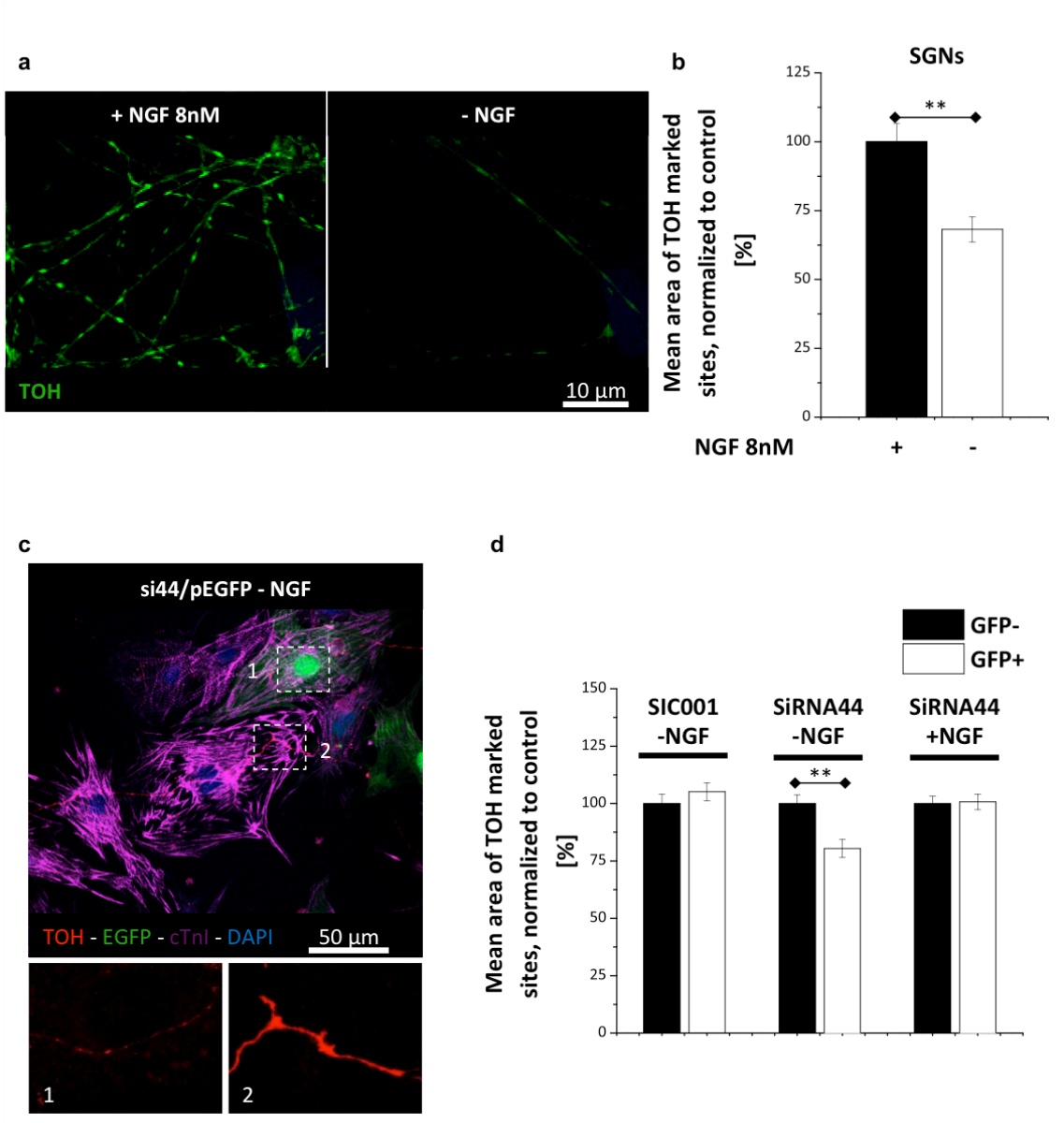

Figure 26 Evidence of cell-to-cell NGF mediated signaling. (**a**) Confocal z-projection of SGNs stained with antibodies to TOH (green signal) and maintained with or without NGF for 8 days. Scale bar: 10µm. (**b**) Quantitative analysis of TOH marked sites along sympathetic processes with or without NGF (error bars represent s.e.m., **p<0.01, at least n=154 sites per condition). (**c**) Confocal z-projection of a SGN/CM co-culture co-transfected with si44 and pEGFP and stained with DAPI (blue signal) and antibodies to TOH (red signal) and cTnI (violet signal). Magnifications of the white boxes are reported. Scale bar: 50µm. (**d**) Quantitative analysis of TOH marked sites on GFP positive or negative CMs, in co-cultures transfected either with si44 or SIC001 in presence or absence of NGF (error bars represent s.e.m., **p<0.01, at least n=389 sites per condition from 3 independent co-cultures).

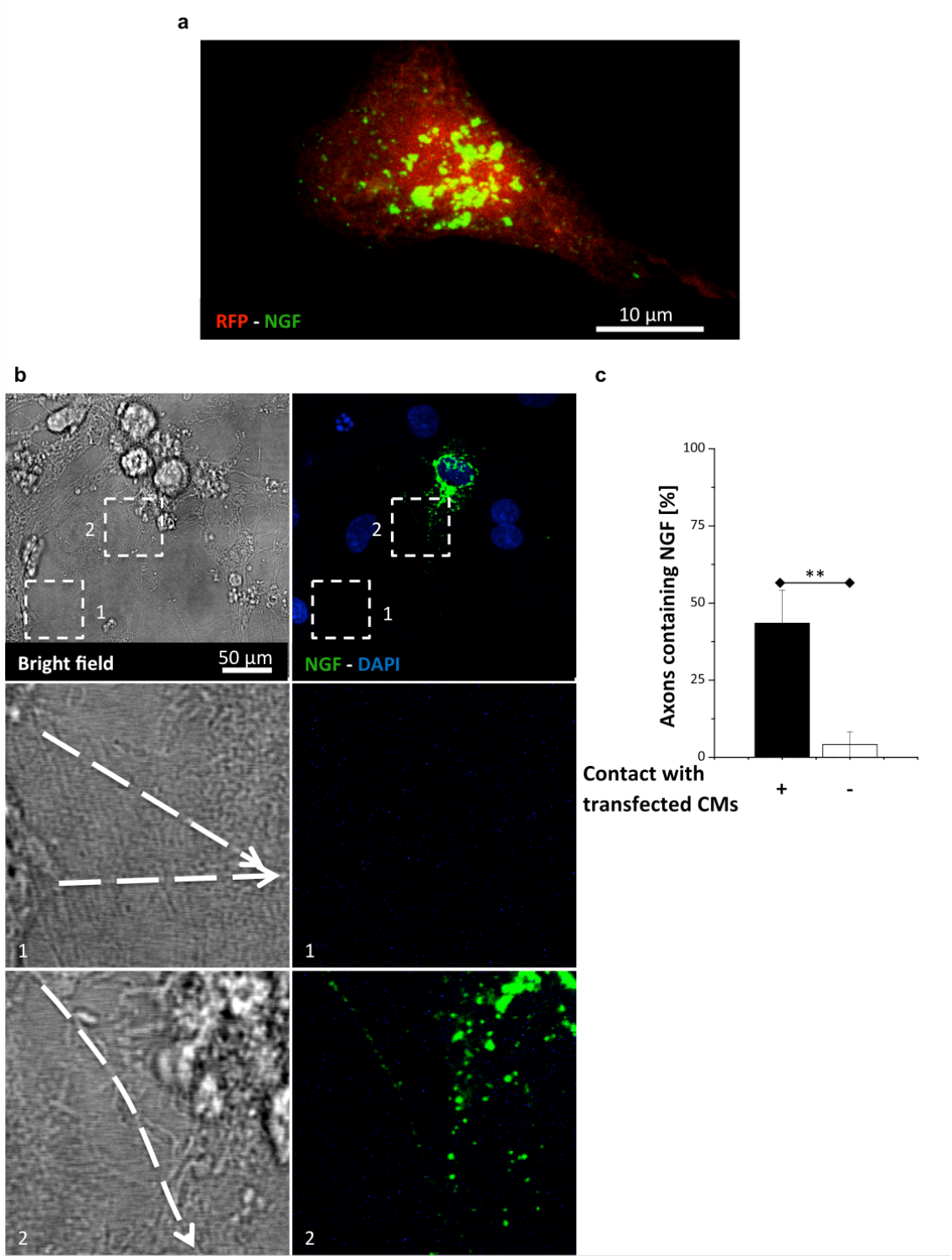

Figure 27 NGF uptake is detected only in SGNs contacting RFP-NGF transfected CMs. (**a**) Confocal z-projection of HeLa transfected with the RFP-NGF construct (red signal) and stained for NGF (green signal). Scale bar: 10µm. (**b**) Confocal z-projection of bright fields and IF staining for NGF (green signal) and nuclei (blue signal) on co-cultures transfected with the RFP-NGF construct. Scale bar: 50µm. (**c**) Quantification of NGF uptake by sympathetic processes contacting either RFP-NGF transfected or

untransfected CMs (error bars represent s.e.m., **p<0.01, at least n=41 axons per condition from 3 independent co-cultures).

4.2.6. The neuro-cardiac junction is an isolated microdomain of high NGF concentration

We next aimed to gain insight into the local NGF signaling domain forming at the neurocardiac junction. To assess whether the narrow space outlined by the juxtaposed membranes of interacting neuron/cardiomyocyte has a role on intercellular NGF signaling, we used a series of strategies to interfere with NGF signaling (figure 28, panel a). These approaches included: i) incubation with anti-NGF antibody to sequester NGF from the medium, ii) incubation with the NGF fragment c(92-96), that has been reported to bind to TrkA and inhibit its activation, and has been shown to antagonize NGF mediated neurite extension in PC12 cells (LeSauteur L, 1995); iii) incubation with the TrkA antagonist k252a that has a size comparable to that of c(92-96) and that is membrane permeable (Berg MM, 1992). All the molecules were able to mimic the effect of NGF withdrawal on SGNs viability, leading to a significant reduction in density of SGNs (figure 28, panel b and figure 29). The three molecules were also tested on PC12 cells, a cell line that becomes dependent on continuous NGF signaling after neurotrophin-induced differentiation in sympathetic like neurons (figure 30, panel a and b). Treatment of PC12 cells with anti-NGF antibody increased neuronal death (figure 30, panel c and d), while a control IgG had no effects (figure 30, panel e), further supporting the results of anti-NGF treatment on neurons alone.

Although the three molecules worked on SGN cultures, only k252a was able to reduce neuronal density in primary co-cultures (figure 28, panel c, figure 31, 73.24 ±4.18% decrease in mean neuronal density when compared to the control), suggesting that the antibody and c(92-96) are not able to enter the SGN/CM contact site.

To determine whether ultrastructural determinants of the NCJ could possibly render the intermembrane space inaccessible to either of the protein-based NGF antagonists, we used TEM imaging and analyzed the cell-cell interaction site at high resolution. TEM images in SGN/CM co-cultures (figure 28, panel d) showed 2 sites of 10nm cell-to-cell distance within the NCJ, characterized by increased electron density, in addition to the

features already discussed for mouse heart slices. This observation supports the hypothesis that such interaction sites may act as a barrier to diffusion thanks to protein enrichment and close membrane proximity.

No aspecific or side effects were detected on CM morphology caused by the antibody (figure 32, panel a, b) or c(92-96) (figure 32, panel c, d) treatment. Indeed, we did not observe any changes of the sarcomeric structure upon incubation with the molecules and control IgG and linearized c(92-96) did not decrease neuronal density. Moreover, since k252a has been reported to non-specifically inhibit several protein kinases, including PKA (Kase H, 1987), whose inhibition has effects on neuronal viability, we tested the effect of the drug on PKA dependent phosphorylation of the fluorescent exogenous target AKAR3 (A-kinase-activity-reporter). For this purpose, we transfected CM with a construct encoding AKAR3, and measured PKA activity upon incubation with the PKA-activating adrenergic agonist norepinephrine (NE), at increasing concentrations, in CMs incubated with k252a (overnight, 100nM). The results showed in figure 33, panels a and b, suggest that no inhibition of PKA occurs in these conditions, supporting that the effect measured on SGN viability were due to a specific effect of k252a on TrkA. CM morphology was also determined in cells treated with k252a, and while no changes in the sarcomeric structure were observed, modest but significant hypertrophy was detected at 1µM of k252a (figure 33, panel c). For this reason, k252a was used at 100nM.

Since k252a led to neuronal death both in neurons alone and in co-cultures, we used this inhibitor to antagonize NGF dependent prosurvival signaling, in the attempt to estimate the effective NGF concentration active at the junctional site between neurons and cardiomyocytes. The results were normalized to the neuronal density without k252a and compared to the results obtained in co-cultures, and are shown in figure 28, panel e. The estimated NGF concentration active at the contact site was 1.4 ±0.03nM, 3.5 times higher than the minimal dose required for neuronal survival, suggesting that the NCJ is characterized by high NGF concentration. These results would imply that the NGF concentration in the intermembrane cleft is higher than that in the medium by four orders of magnitude, supporting that the structure of the NCJ allows amplification

of intercellular NGF signaling. Without the NCJ, NGF would diffuse in the medium reaching a concentration that is not sufficient for neuronal survival.

Taken together, these results suggest that the NCJ is an isolated microenvironment protected from diffusion and characterized by high NGF concentrations.

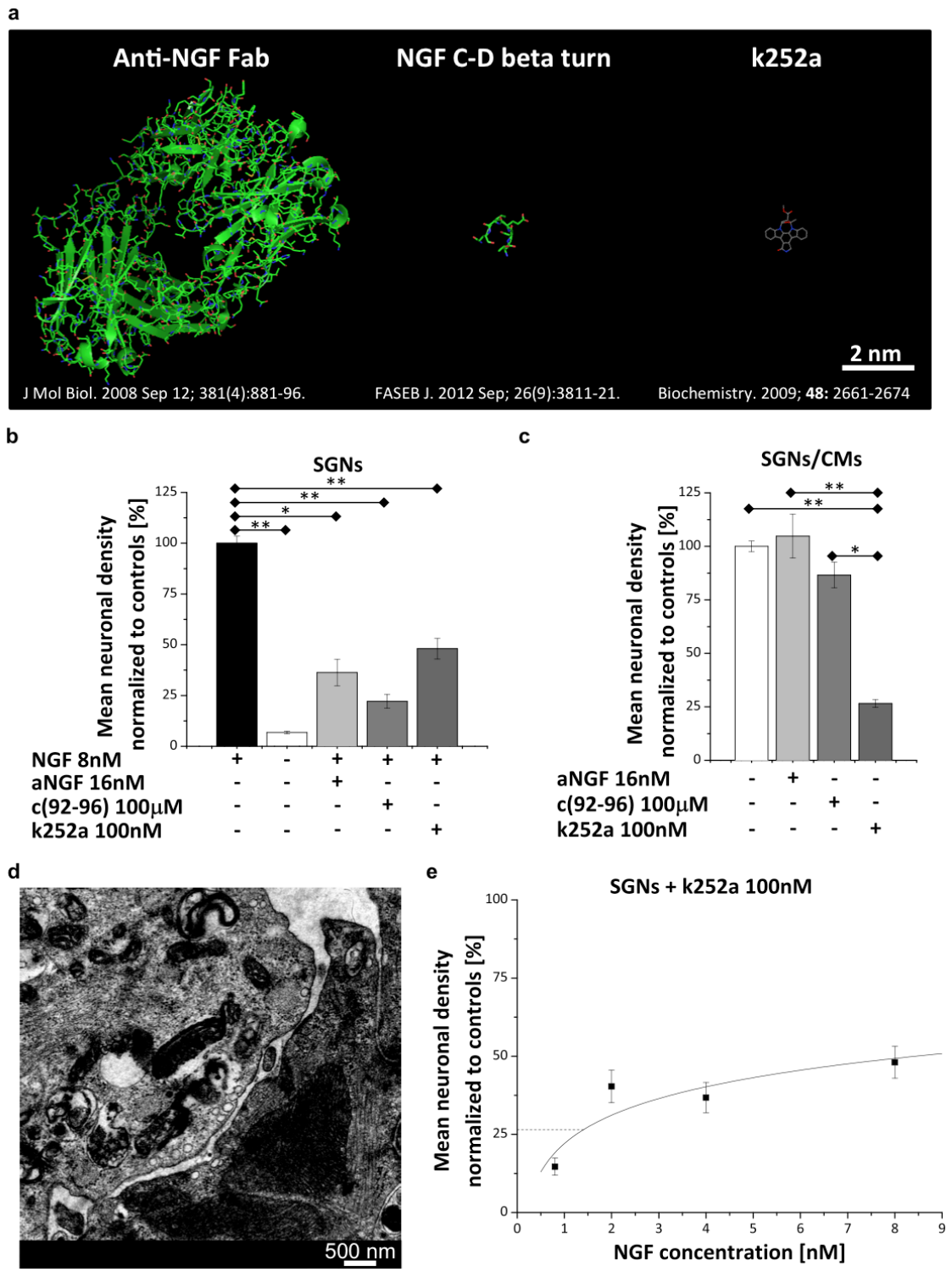

Figure 28 SGN/CM contact site is an isolated microdomain characterized by high NGF concentration. (**a**) Jmoll® 3D reconstruction of Fab domain of anti-NGF antibody, of NGF C-D β-turn, which is mimicked by c(92-96), and k252a. Scale bar: 2nm. (**b**) Quantification of the mean neuronal density upon treatment of SGN cultures with anti-NGF 16nM, c(92-96) 100µM and k252a 100nM (error bars represent s.e.m., **p<0.01, *0.01<p<0.05, at least n=24 fields per condition from 3 independent co-cultures). (**c**) Quantification of the mean neuronal density in co-cultures treated with indicated molecules (error bars

represent s.e.m., **p<0.01, *0.01<p<0.05, at least n=24 fields per condition from 3 independent co-cultures). (**d**) TEM analysis on *in vitro* co-cultures. Scale bar: 500nm. (**e**) Estimation of NGF concentration at the interaction site between SNs and CMs using increasing NGF concentrations (error bars represent s.e.m., at least n=24 fields per conditions from 3 independent co-cultures).

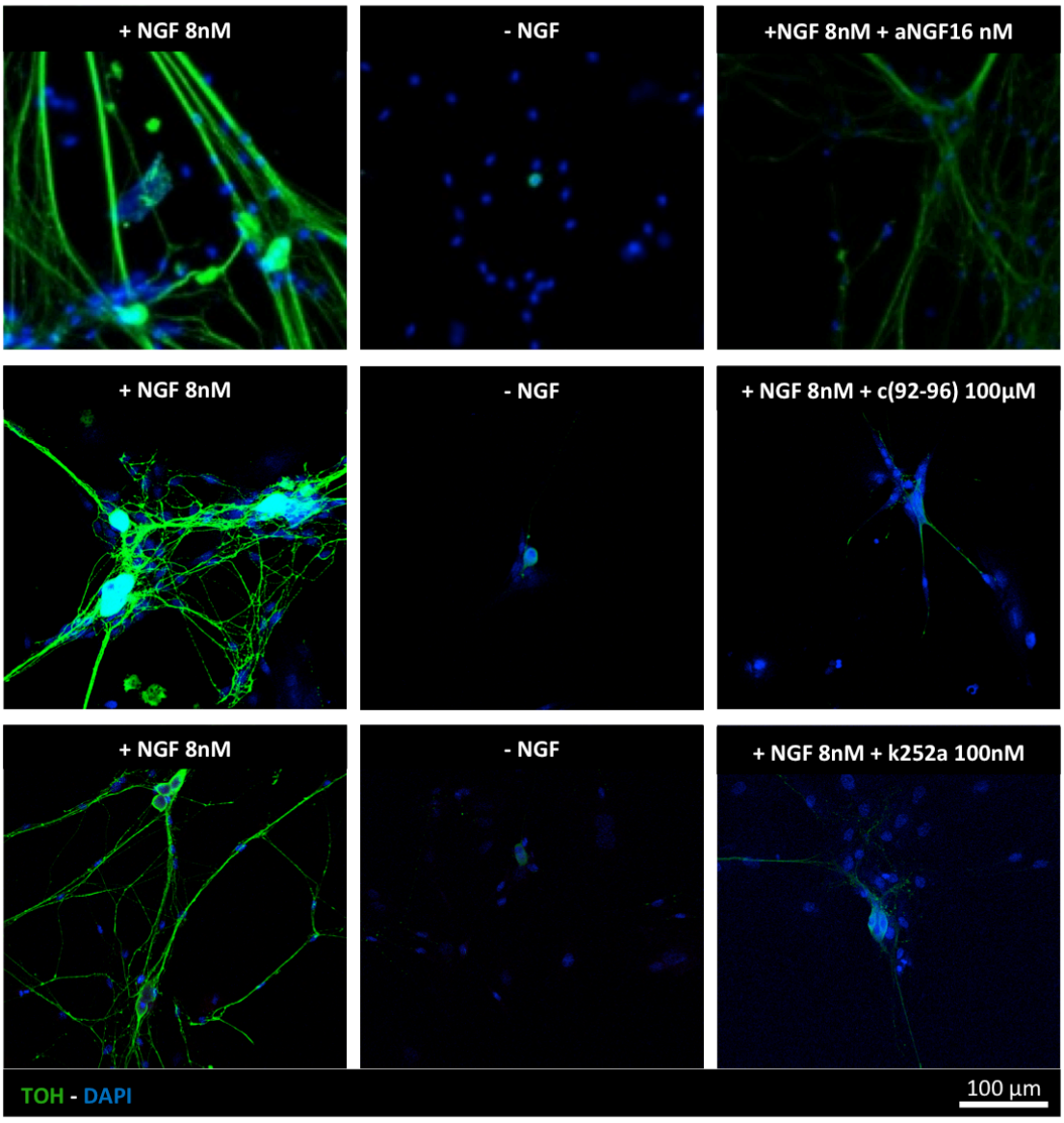

Figure 29 Anti-NGF antibody, c(92-96) and k252a treatment decreased the density of neurons alone. Confocal z-projection of SGNs upon NGF withdrawal or incubation with reported molecules and stained with DAPI (blues signal) and an antibody to TOH (green signal). Scale bar: 100µm.

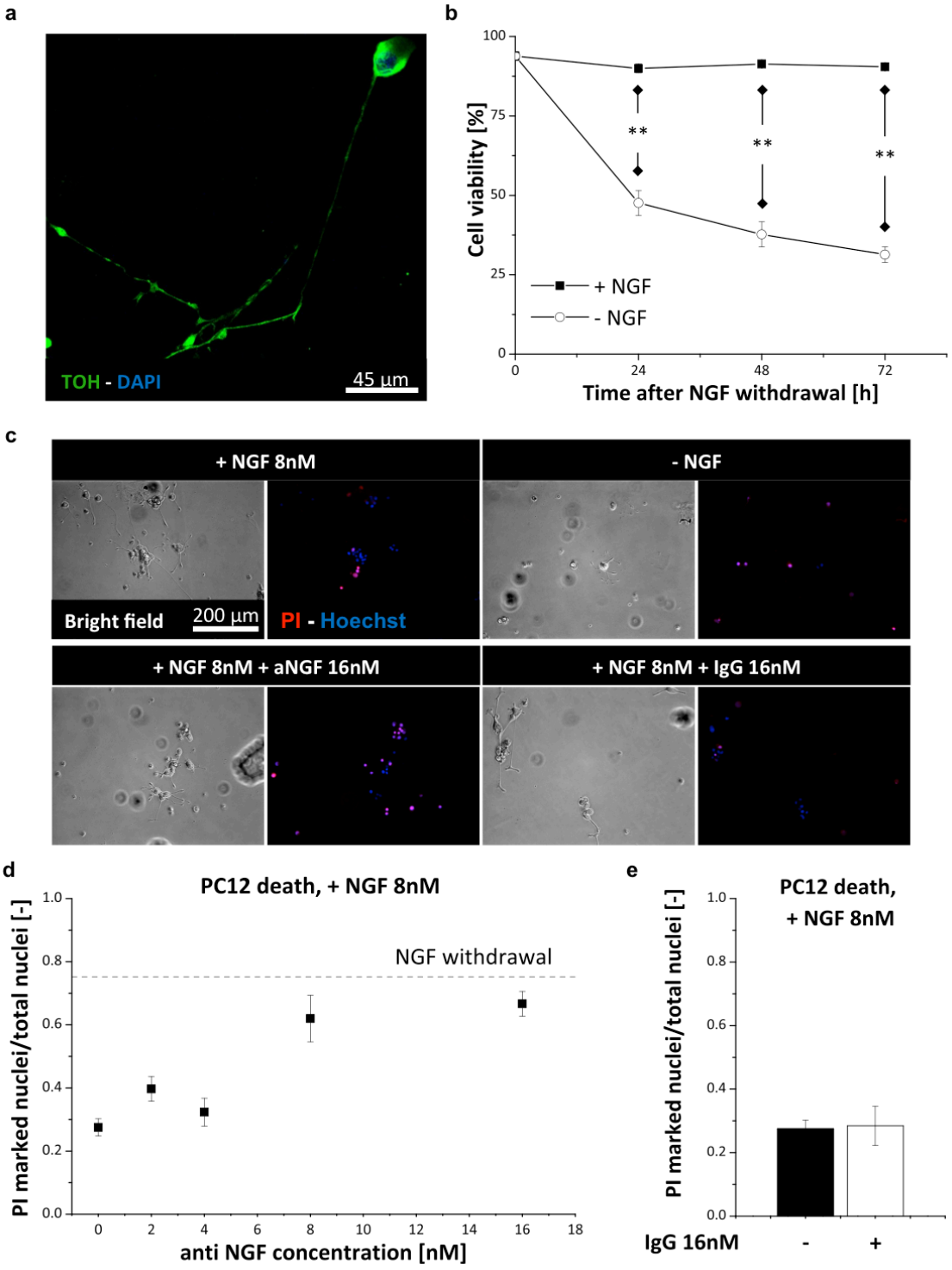

Figure 30 Test of anti-NGF antibody on PC12. (**a**) Confocal z-projection of PC12 cells differentiated for 5 days with 8nM NGF and stained with DAPI (blue signal) and an antibody to tyrosine hydroxylase. Scale bar: 45µm. (**b**) Trypan blue based quantification of PC12 viability upon NGF withdrawal after 5 days of differentiation (error bars represent s.e.m., **p<0.01, at least n=11 counts per condition). (**c**) Fluorescence and bright field images of PC12 treated with anti-NGF antibody or aspecific IgG and incubated with propidium iodide and Hoechst for viability evaluation. Scale bar: 200µm. (**d-e**)

Quantification of PC12 viability upon anti-NGF treatment. The ratio between PI and Hoechst marked nuclei was calculated (error bars represent s.e.m., at least n=12 fields per condition).

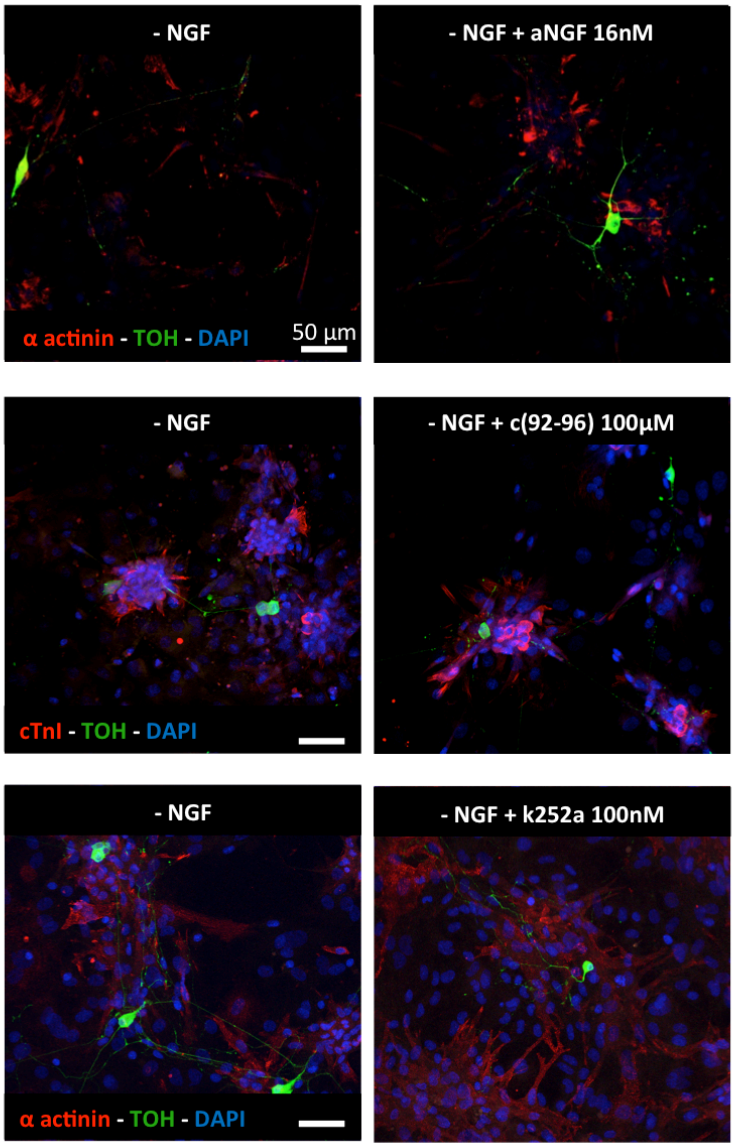

Figure 31 Only k252a decreased neuronal density in co-cultures. Confocal z-projection of the IF staining for α actinin or cTnI (red signal), TOH (green signal) and nuclei (blue) on co-cultures treated with anti-NGF antibody, c(92-96) or k252a. Scale bars: 50µm.

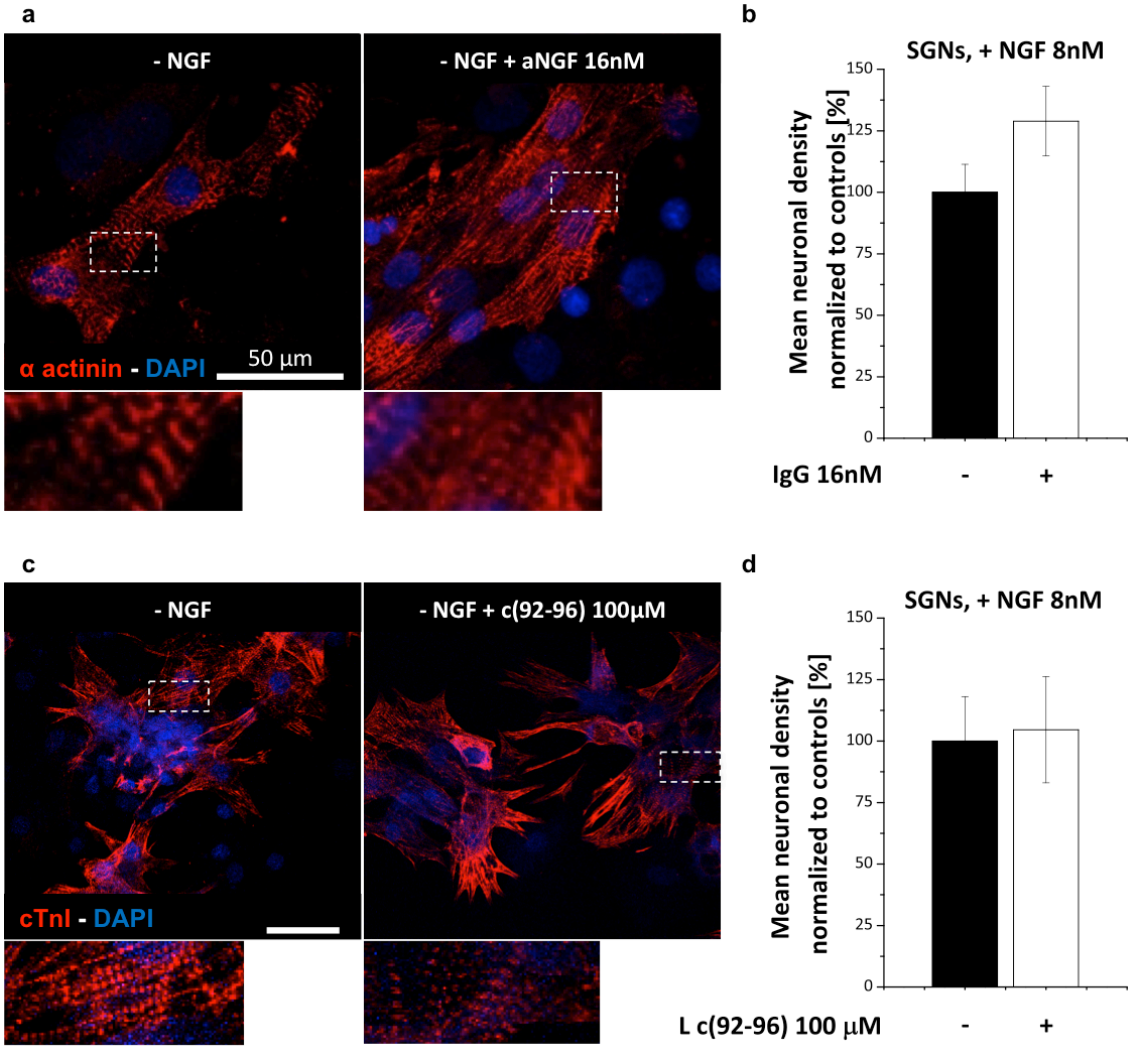

Figure 32 Controls for anti-NGF antibody and c(92-96). (**a, c**) Confocal z-projections on CMs treated with anti-NGF antibody and c(92-96) and stained with DAPI (blue signal) and α actinin (**a**) or cTnI (**c**, red signal). Magnifications of the white boxes are reported. Scale bars: 50µm. (**b, d**) Mean neuronal density of neurons treated with generic IgG (**b**) or linearized c(92-96) in the presence of 8nM NGF (**d**, error bars represent s.e.m., at least n=12 fields per condition).

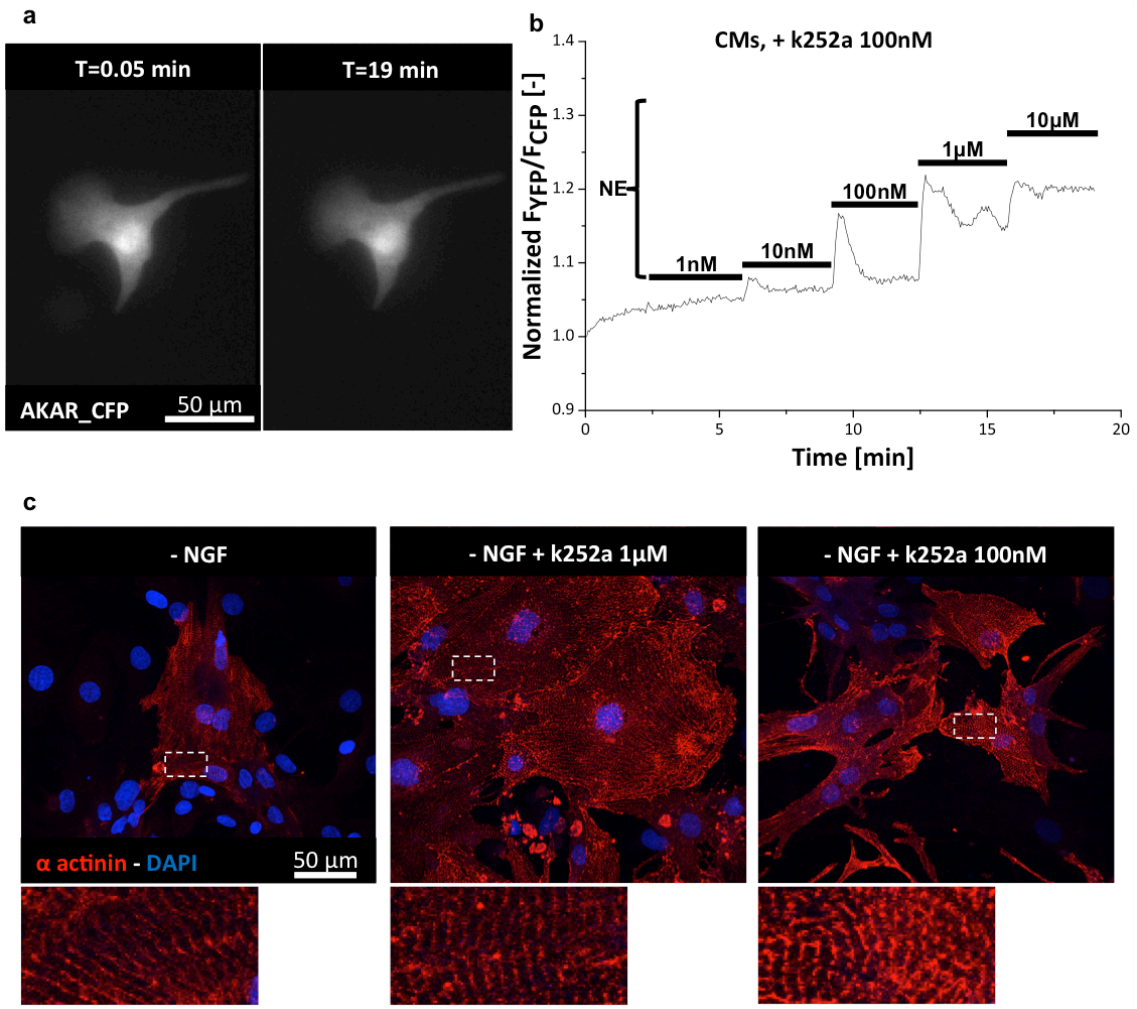

Figure 33 Controls for k252a. (**a**) Fluorescence image on a CM transfected with the AKAR3 construct at the beginning and at the end of the experiment. Scale bar: 50µm. (**b**) Example of NE stimulation of a CM transfected with the AKAR3 construct and incubated with k252a 100nM ON. (**c**) Confocal z-projections of CMs treated with k252a at different concentrations and stained for nuclei (blue signal) and α actinin (red signal). Magnifications of the white boxes are reported. Scale bars: 50µm.

5. Conclusions

In the first part of this PhD thesis, sarcomeric dynamics were analyzed as a result of the interaction between SNs and the heart. In particular, we focused on atrophic remodeling following nutrient/serum deprivation, a common way to induce autophagy and UPS in the muscle. Since starvation shares downstream targets with denervation, a parallelism can be made between the two pro-atrophic stimuli. Starvation was efficient in reducing the sarcomeric area with 20 hours of HBSS treatment, with a much lower effect on the total CM area. We thus concluded that sarcomere degradation is faster than assembly and may precede cytoplasmic remodeling upon nutrient/serum deprivation. Then we analyzed the fate of different sarcomeric proteins and showed that not every protein was equally delocalized and degraded. In particular, α actinin and cTnI resulted delocalized and degraded, whereas actin was only delocalized and cTnT did not change localization or amount. Whether a stronger starvation could affect cTnT levels, will be investigated with prolonged HBSS treatment. In addition, the biological meaning of this differential protein degradation has still to be clarified. One suggestion may come from the observation that starved and partially degraded sarcomeres remain functional. It may be that further protein breakdown that include cTnT, may have negative effects on CM contractility.

After this, we characterized the starvation protocol, detecting activation of both autophagy and UPS. We therefore evaluated the involvement of both protein degradation systems in sarcomeric dismantlement, and provided evidence that autophagy may be involved in the changes described for sarcomeres. Moreover, we provided data of UPS implication in HBSS induced protein breakdown, detecting increased sarcomeric ubiquitination in IF staining. Interestingly, ubiquitin marked sites along sarcomeres were excluded from those marked by phalloidin, suggesting that protein in the M-line were ubiquitinated. The fact that Murf1 is a E3 ubiquitin ligase localized in the M-line and overexpressed upon starvation and denervation, led us to consider its direct involvement in sarcomere dismantle through its overexpression and silencing. CM transfection with Murf1-flag construct caused strong sarcomeric degradation, suggesting that this ubiquitin ligase has a direct role in this process. However, its silencing did not prevent the effects of HBSS treatment, supporting that

protein degradation by Murf1 is not the only path involved in sarcomeric disassembly. A more direct involvement of autophagy will be investigated, as well as a role of other muscle specific ubiquitin ligase, such as Atrogin1/MaFbx. Moreover, recently a new ubiquitin ligase of the muscle has been described, named Musa1 (Sartori R, 2013), and its role is currently being investigated.

In the second part of the PhD thesis, we analyzed the neuro cardiac interaction, with the focus on retrograde signaling between the cardiomyocyte and the neuron, concerning NGF. First we provided evidence that SNs preferentially interact with CMs in heart cryosections, by establishing sites of direct contact that were detected also in TEM analysis. To analyze such interaction, co-cultures were established and characterized. Enrichment of generic cell adhesion molecules at the SN-CM contact site was detected and was time dependent, suggesting that the interaction is subjected to maturation. However, cadherins and β catenin enrichment was not specific for SN in contact with CMs, since it was described also for HN-CM cultures. Since IF and time laps analyses showed that contact site enlargement and stabilization occurs between SNs and CMs, this interaction was considered preferential also *in vitro*.

NGF is a well-characterized neurotrophin that is expressed by the heart, in particular by CMs. Since neurotrophin silencing reduced neuronal density in co-cultures, we concluded that SNs are dependent on CM released NGF. In addition to the preferential SGN/CM interaction and the observation that the speed of retrograde TrkA movements were faster on CMs than other cardiac cells, this evidence supports that NGF signaling is activated between SNs and CMs. We did not consider the other neurotrophins, because TrkC is not expressed by the SGN and neurons are dependent on NT3 for axonal growth only early during development.

Moreover, we hypothesized the involvement of the NCJ in NGF signaling. This idea was supported by TrkA enrichment at SGN/CM contact site in rat heart cryosections. We further tested our hypothesis using *in vitro* co-cultures. Since CM conditioned medium did prevent neuronal death, we concluded that SGN/CM contact is required for appropriate NGF signaling and resulting neuronal survival. This conclusion was further supported by the decrease in contact size along sympathetic processes in contact with NGF silenced CMs and by NGF uptake by SNs interacting with RFP-NGF transfected

CMs. Moreover, these results suggest that a single cell-to-single cell NGF mediated signaling takes place between CMs and SGNs.

In the final part of this work, we interfered with NGF signaling, using 3 different molecules. Whereas every molecule reduced the density of neurons alone, only the membrane permeable k252a had effects on SN density in co-cultures, suggesting that anti-NGF and c(92-96) could not enter the contact site. This led us to conclude that the NCJ is an isolated contact site characterized by high NGF concentration, as estimated by co-culture treatment with 100nM k252a and NGF at different concentrations. Interestingly, estimated concentration was more than the minimal dose required for neuronal survival and sufficient for allowing synaptic potentiation mechanisms.

Altogether, these data led us to define a working model whereby the SGN/CM interaction is characterized by cell adhesion molecules enrichment at the membrane contacts (figure 34), and TrkA receptor is accumulated at the SN membrane close to the CM and accounts for NGF mediated pro-survival signaling. From different measures on TEM and IF confocal images, we obtained a mean cell-to-cell distance of about 70nm and a synaptic bouton size of $1.8\mu m^2$. By approximating the neuronal bouton to a cylinder, we calculated the volume of the intermembrane space in the order of 10^{-15}L, implying that the release of only few NGF molecules in the cleft by the CM would suffice to reach a pro-survival neurotrophin concentration in the nanomolar range. Only in a such isolated microenvironment NGF could reach an appropriate concentration for allowing neuronal survival.

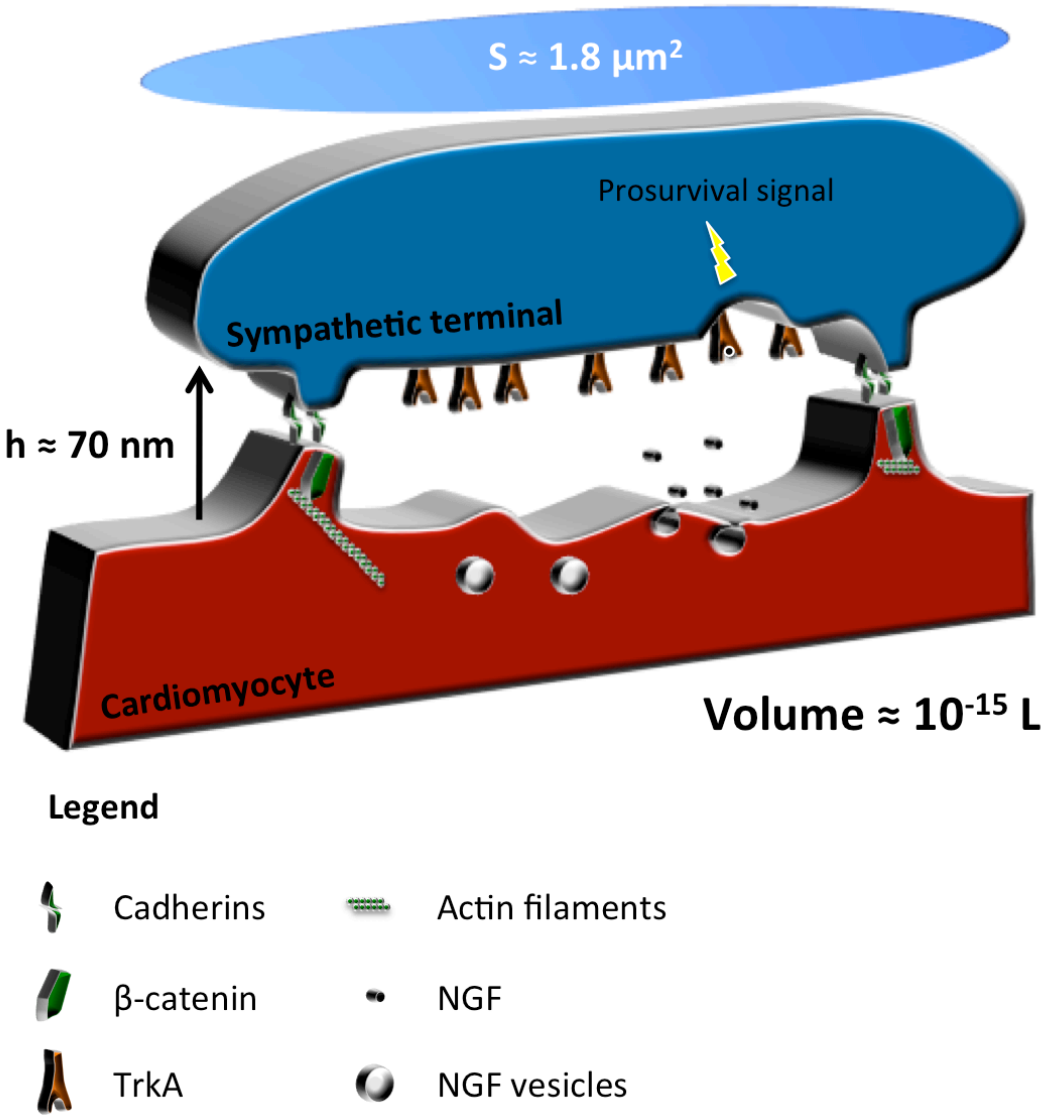

Figure 34 Proposed model of SGN/CM interaction, based on data from NGF signaling.

6. Future perspectives

The future perspectives that arise from showed data, regard the existence of a cross-talk between the NE e NGF signaling and the interaction between SNs and CFs, especially in diseased hearts.

6.1. The NE-NGF link

The first evidence that NE can regulate NGF signaling, was obtained by incubating co-cultures with 25µM propranol in the absence of NGF. Propranolol is a generic β blocker that inhibits adrenergic signaling from the neuron to the CM. As reported in the graph

of figure 35, panel a, we measured a 65.1 ±10.8% decrease in the mean neuronal density upon propranolol treatment, suggesting that interfering with adrenergic signaling may have consequences on neuronal survival. Propranolol did not have side effects on CMs or neurons alone in the presence of NGF (figure 35, panel c). We further investigated the mechanism that led to neuronal death in co-cultures and evaluated whether interference with NE of the serum might have consequences on NGF expression by the CMs. As reported by the RT-qPCR analysis for NGF (figure 35, panel b), we detected a decrease in neurotrophin expression upon 4 hours of treatment with 100μM propranolol (16.94 ±2.23 vs 3.89 ±1.02 fold increase normalized to GAPDH in controls and propranolol treated cells). These results support β blocker administration might have reduced the neuronal density in co-cultures because it lowered NGF expression in CMs. So we can hypothesize that the NE released by SNs modulates NGF expression and synaptic potentiation acting on β adrenergic receptors. Interestingly, CM treatment with high NE concentrations (10μM) lowered NGF expression in the adaptive response to sympathetic hyperactivation (Kaye DM, 2000) and we confirmed these results. This negative regulation seems to act through the stimulation α adrenergic receptors, since prazosin but not propranolol rescued NGF downregulation. These pieces of evidence led us to the hypothesis that low NE levels may upregulate NGF expression, whereas higher levels may downregulate it. Moreover, the two mechanisms of NGF up/down-regulation may act on different adrenergic receptor, since prazosin rescued NGF expression upon high NE treatment and propranolol lowered NGF levels in CM stimulated by the low NE levels of the serum. These two hypotheses will be investigated.

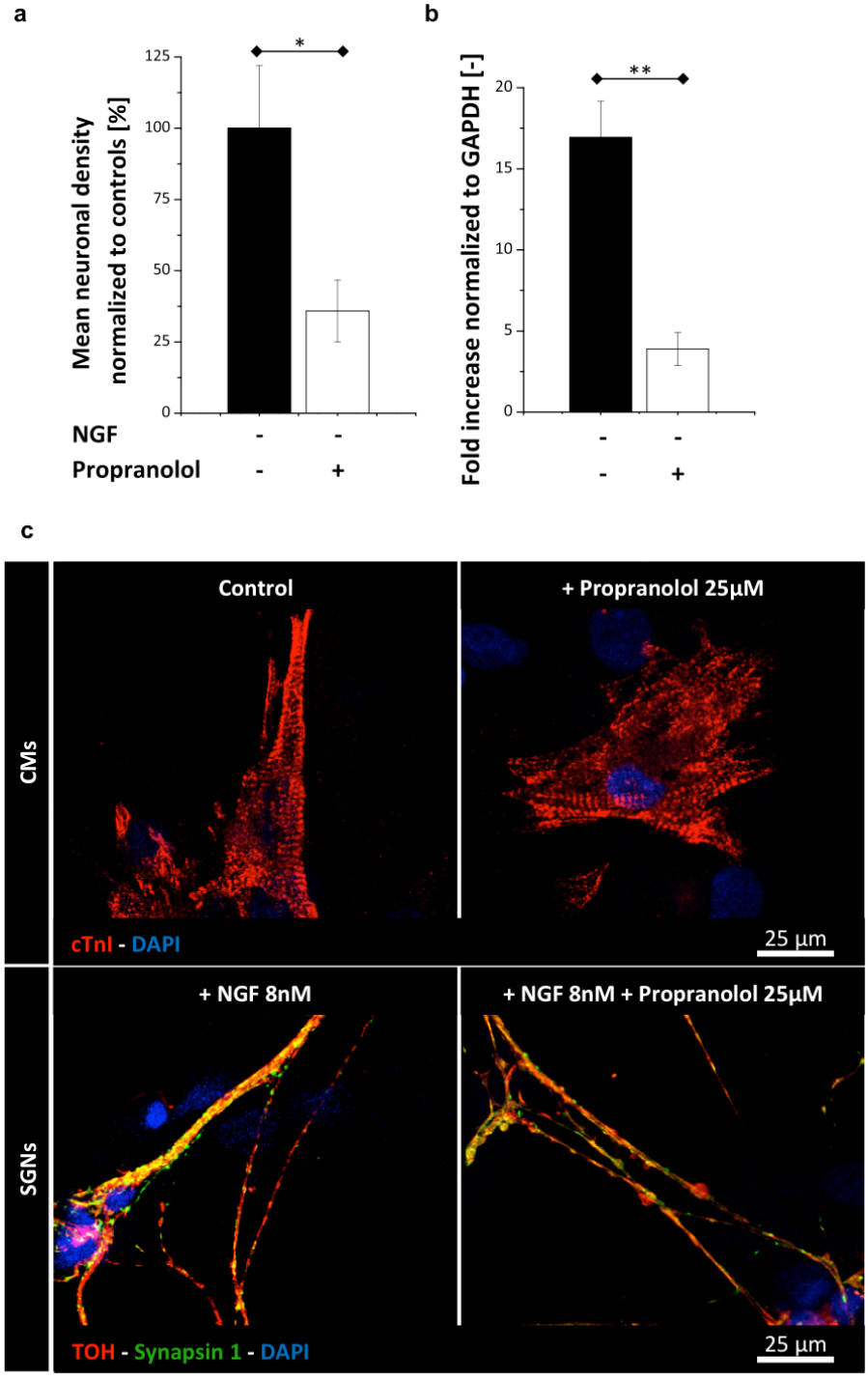

Figure 35 Propranolol treatment reduces neuronal density through NGF downregulation. (**a**) Quantification of the mean neuronal density in co-cultures treated with 25µM propranolol (error bars represent s.e.m., *0.01<p<0.05, at least n=15 fields per condition). (**b**) RT-qPCR analysis on CMs incubated with 100µM propranolol for 4 hours (error bars represent s.e.m., **p<0.01, at least n=3 independent CM cultures). (**c**) Confocal z-projection either on CMs or SGNs treated with 25µM

propranolol and stained for cTnI or TOH (CMs and neurons respectively, red signal), synapsin 1 (neurons, green signal) and nuclei (blue signal). Scale bar: 25μm.

6.2. The interaction between SNs and cardiac fibroblasts

As described before, sympathetic axons interacted for 25.97 ±5.71% of their length with cardiac fibroblasts, which account for the largest cardiac cell population. To further analyze the interaction between CFs and SNs, we performed the IF analysis for synapsin 1 and POH in rat heart cryosections, which showed the presence of some STs in close contact with fibroblasts (figure 36, panel a) supporting that a population of CFs may interact with SNs. Since synapsin 1 is a peripheral membrane protein of synaptic vesicles, these results suggest that the CF-SN interaction may be functional. What is the functional role of SN-to-CF signaling will be investigated, both for NE and NPY. Cultured CFs can express NGF, as detected through the RT-qPCR analysis (figure 36, panel b), further supporting that the observed sites of CF-SN interaction might not be random. The fact that NGF expression levels in CF cultures are higher than those in CM cultures may have consequences on the type of interaction that is established with the SN. For instance, if CFs release higher amounts of NGF, it might be that SNs do not need a close interaction with the CF to survive, as reported for the NCJ. Moreover, fibroblast proliferation in fibrotic hearts might lead to heavy consequences on the innervation pattern. In figure 36, panel d, a normal and fibrotic myocardium of a KO mouse for Atrogin1 and Murf1 is showed[18]. Interestingly, the fibrotic area in the KO myocardium is characterized by the sprouting of sympathetic axons that potentially constitute a pro-arrhythmogenic site.

To further evaluate the effects of sympathetic innervation on cardiac fibrosis, we performed analysis on hearts with acute myocardial infarction (AMI) that were previously denervated. For AMI, ligature of the left descending coronary vessel was performed. Pharmacological sympathectomy was achieved through the administration of 6-OH-DOPA that we reported to reduce sympathetic innervation by a 90%, without

[18] Atrogin1 KO, Murf1 KO hearts were provided by the lab of Prof. Marco Sandri (University of Padova, Padova)

affecting central sympathetic neurons, or cardiac hemodynamics (Zaglia T, 2013), and that does not change much heart rate or blood pressure (Makino M, 1997). Sympathetic denervation was assessed by IF staining for TOH (figure 37, panel a). Moreover, sympathetic nerves were detected in the peri-infarct area with processes extending also in the fibrotic area (figure 37, panel b), further supporting that aberrant innervation may occur in diseased hearts upon fibroblast proliferation. For histological analysis, we performed hematoxylin and eosin staining on infarcted hearts with or without sympathetic innervation (figure 38, panel a). Hearts with AMI showed dilation of the left ventricular chamber and a thinner left ventricular wall when compared to denervated hearts (figure 38, panel b). These effects are probably due to the sympathetic activity and catecholaminergic stimulation after infarction. Interestingly, fibrosis was more diffused among different sections of the innervated heart when compared to the denervated one, including big areas of the apex too (figure 38, panel b). These results support the idea of a SN-to-CF communication may be involved in fibrotic process. Moreover, fibrosis in AMI and KO models is caused by the death of CMs; whether axonal sprouting occurs also in other models of fibrosis will be investigated as well as the pathological implications of such aberrant innervation.

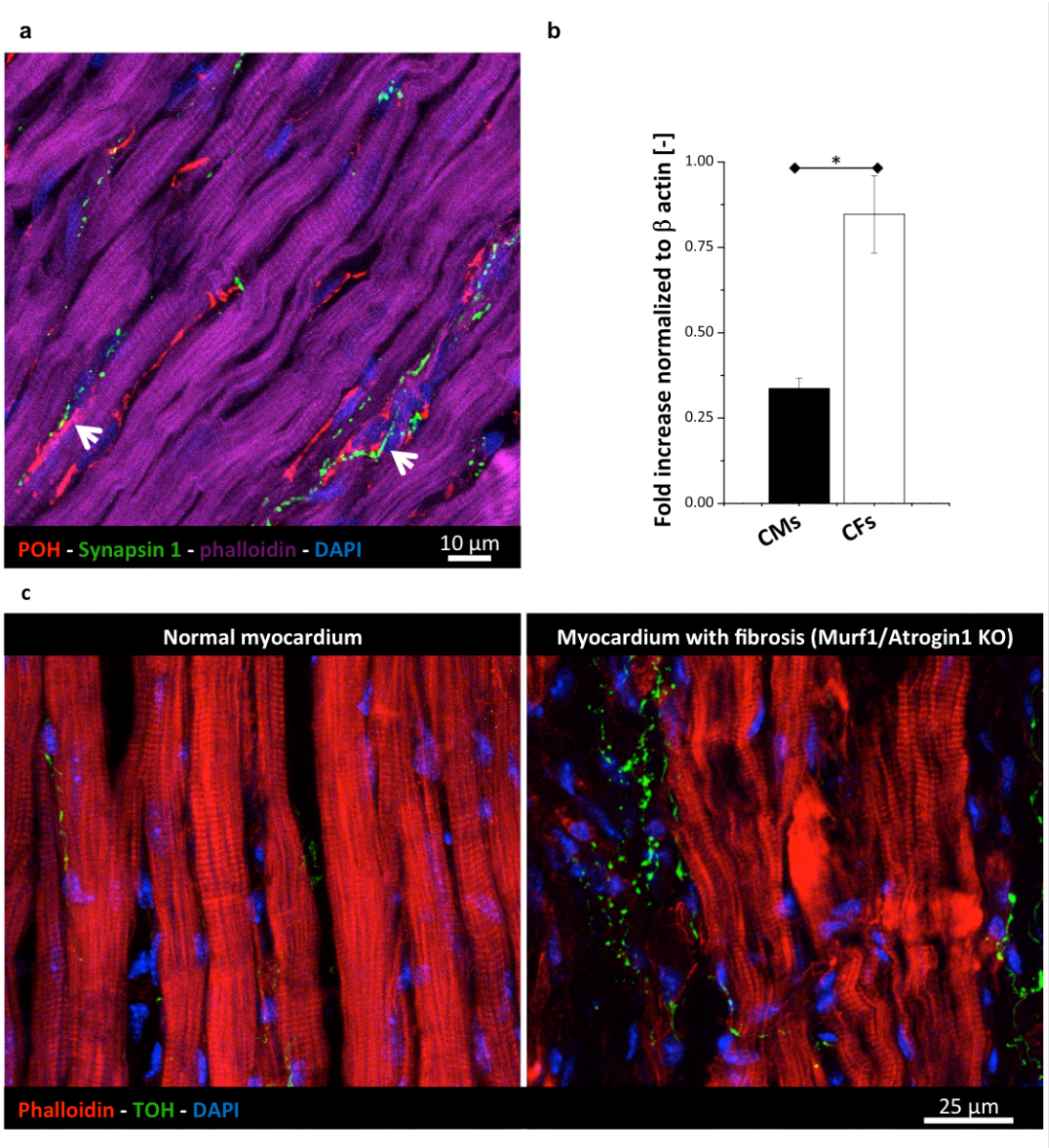

Figure 36 Some SNs interact with CFs. (**a**) Confocal z-projection of the IF staining for POH (red signal), synapsin 1 (green signal), phalloidin (violet signal) and DAPI (blue signale). Arrows indicate STs that are in close proximity to CFs. Scale bar: 10µm. (**b**) RT-qPCR analysis on extracts from 5 days CMs and CFs (error bars represent s.e.m., *0.01<p<0.05, n=3 independent cultures for condition). (**c**) Confocal z-projection of cryosections from normal and fibrotic myocardium stained with DAPI (blue signal), phalloidin (red signal) and for TOH (green signal). Scale bar: 25µm.

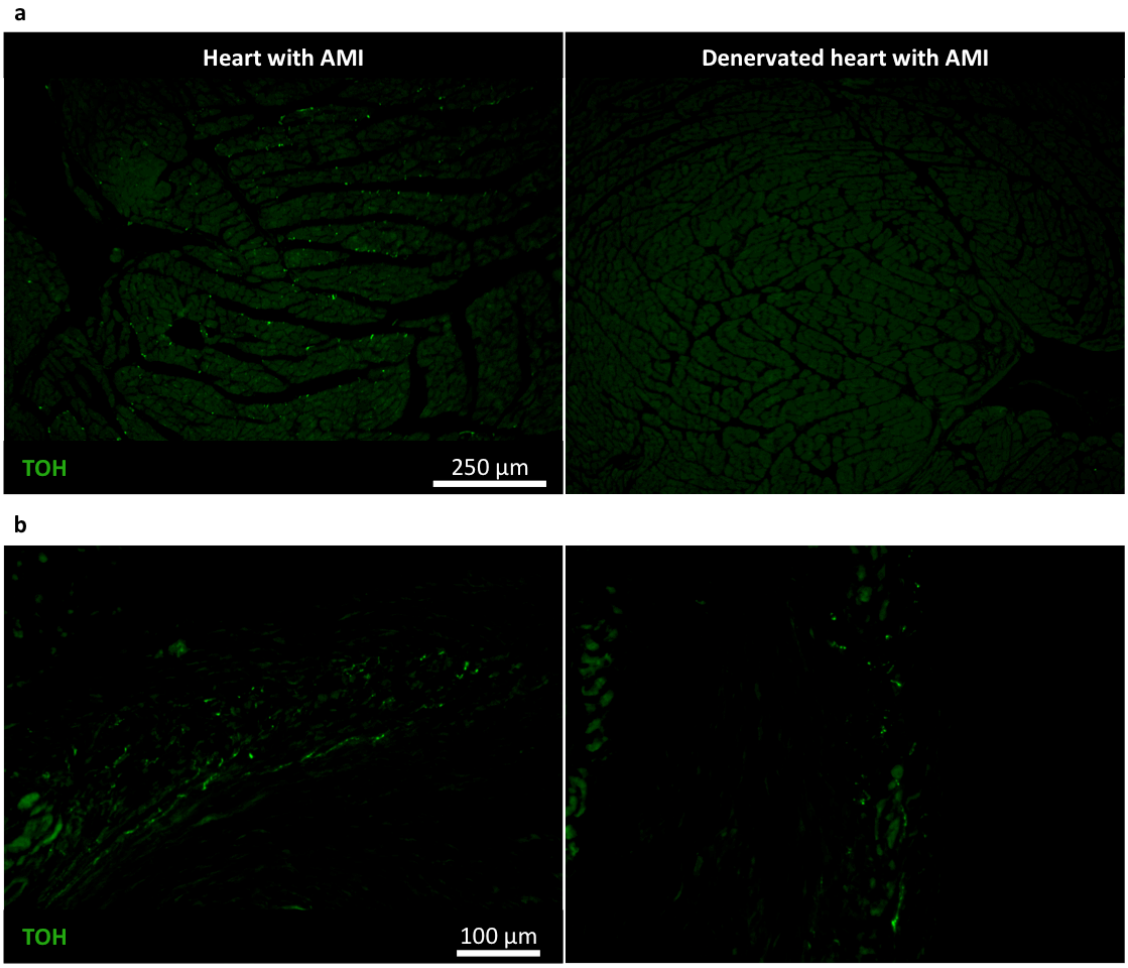

Figure 37 Cardiac sympathetic innervation is extremely reduced upon 6-OH-DOPA administration. (**a**) Fluorescence images of the IF staining for TOH (green signal) on heart cryosections from infarcted mice with (left) or without sympathetic innervation (right). Scale bar: 250µm. (**b**) IF staining for TOH (green signal) of the fibrotic area of the heart with AMI. Scale bar: 100µm.

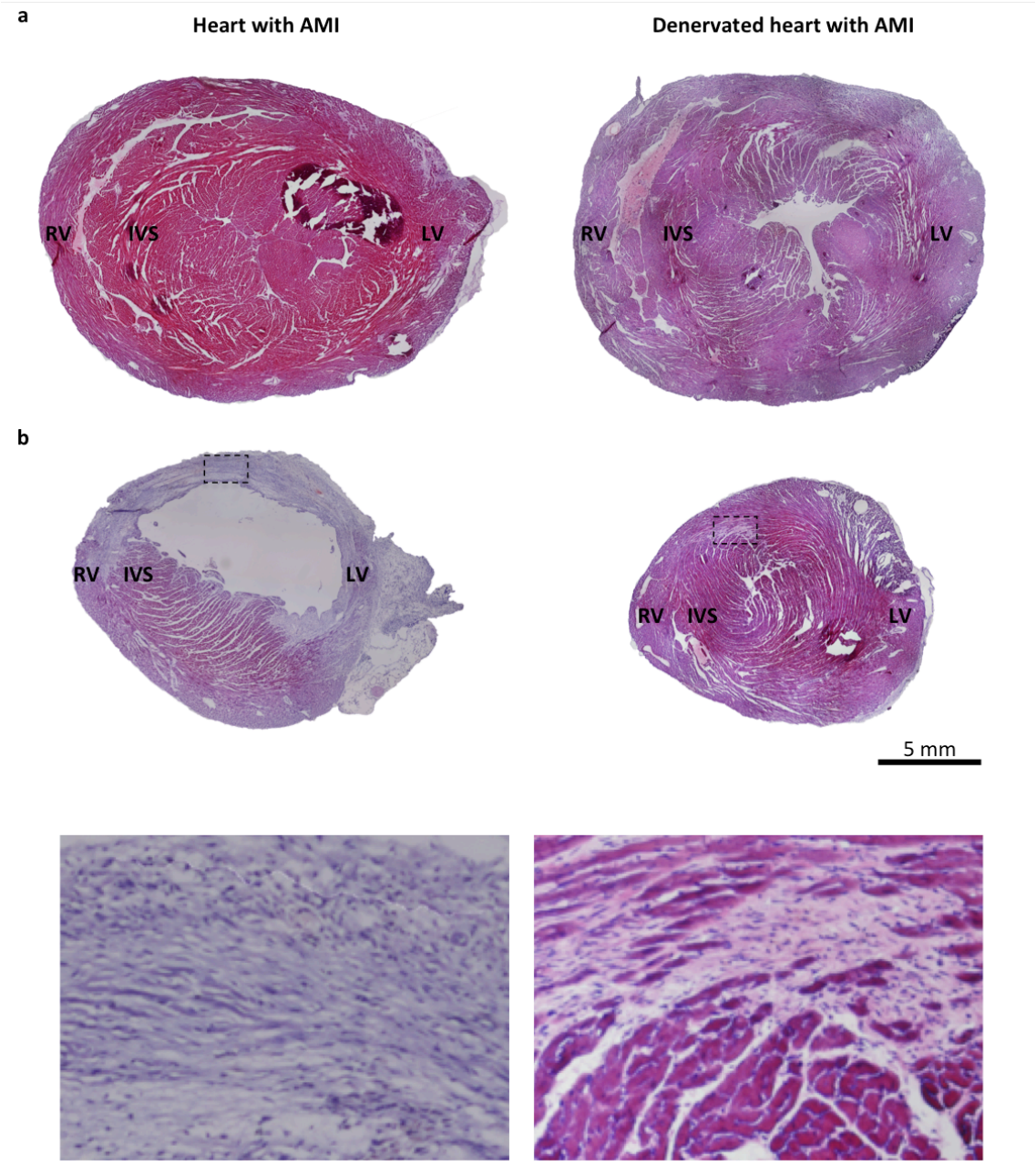

Figure 38 Differences in fibrosis were detected in hearts with AMI with or without denervation. (**a**-**b**) Hematoxylin and eosin staining on infarcted hearts with or without sympathetic innervation (left and right sides of the figure respectively). Images were acquired on cryosections from the upper ventricular area (**a**) and from the apex (**b**) of the hearts. Magnifications of the fibrotic tissues in black boxes are reported. Scale bar: 5mm.

7. Bibliografia

Allen MD, Z. J. (2006). Subcellular dynamics of protein kinase A activity visualized by FRET-based reporters. *Biochem Biophys Res Commun* (348(2):716-21).

Bellinger AM, M. M. (2008). Stressed out: the skeletal muscle ryanodine receptor as a target of stress. *J Clin Invest* (118(2):445-53).

Berg MM, S. D. (1992). K-252a inhibits nerve growth factor-induced trk proto-oncogene tyrosine phosphorylation and kinase activity. *J Biol Chem* (267(1):13-6).

Bers DM. (2000). Calcium fluxes involved in control of cardiac myocyte contraction. *Circ res* (87(4):275-81).

Bers DM. (2002). Cardiac excitation-contraction coupling. *Nature* (415(6868)).

Bers DM. (2001). *Excitation-Contraction Coupling and Cardiac Contractile Force.* Springer.

Bers DM. (2004). Macromolecular complexes regulating cardiac ryanodine receptor function. *J Mol Cell Cardiol* (37(2):417-29).

Bierl MA, J. E. (2005). 'Mature' nerve growth factor is a minor species in most peripheral tissues. *Neurosci Lett* (380(1-2):133-7).

Boateng SY, G. P. (2008). Assembly and maintenance of the sarcomere night and day. *Cardiovasc Res* (77(4):667-75).

Bouaouina M, J. K. (2012). Zasp regulates integrin activation. *J Cell Sci* (125(Pt 23):5647-57).

Brodde OE, O. N. (1984). Human cardiac beta-adrenoceptors: both beta 1- and beta 2-adrenoceptors are functionally coupled to the adenylate cyclase in right atrium. *J Cardiovasc Pharmacol* (6(6):1184-91).

Bru-Mercier G, D. E.-M. (2003). Expression of heart K+ channels in adrenalectomized and catecholamine-depleted reserpine-treated rats. *J Mol Cell Cardiol* (35(2):153-63).

Camelliti P, B. T. (2005). Structural and functional characterisation of cardiac fibroblasts. *Cardiovasc Res* (65(1):40-51).

Cao JM, C. L. (2000). Nerve sprouting and sudden cardiac death. *Circ Res* (86(7):816-21).

Cao JM, F. M. (2000). Relationship between regional cardiac hyperinnervation and ventricular arrhythmia. *Circulation* (101(16):1960-9).

Carpino LA, I. H.-F. (2002). The uronium/guanidinium Peptide coupling reagents: finally the true uronium salts. *Angew Chem Int Ed Engl* (41: 441–445).

Crowley C, S. S.-M. (1994). Mice lacking nerve growth factor display perinatal loss of sensory and sympathetic neurons yet develop basal forebrain cholinergic neurons. *Cell* (76(6):1001-11).

Davies AM. (2009). Extracellular signals regulating sympathetic neuron survival and target innervation during development. *Auton Neurosci* (151(1):39-45).

Deppmann CD, M. S. (2008). A model for neuronal competition during development. *Science* (320(5874):369-73).

Devic E, X. Y. (2001). Beta-adrenergic receptor subtype-specific signaling in cardiac myocytes from beta(1) and beta(2) adrenoceptor knockout mice. *Mol Pharmacol* (60(3):577-83).

Fagan AM, Z. H.-S. (1996). TrkA, but not TrkC, receptors are essential for survival of sympathetic neurons in vivo. *J Neurosci* (16(19):6208-18).

Fan D, T. A. (2012). Cardiac fibroblasts, fibrosis and extracellular matrix remodeling in heart disease. *Fibrogenesis Tissue Repair* (5(1):15).

Fields GB, N. R. (1990). Solid phase peptide synthesis utilizing 9-fluorenylmethoxycarbonyl amino acids. *Int J Pept Prot Res* (35: 161–214).

Frade JM, R.-T. A. (1996). Induction of cell death by endogenous nerve growth factor through its p75 receptor. *Nature* (83(6596):166-8).

Francis N, F. I.-P. (1999). NT-3, like NGF, is required for survival of sympathetic neurons, but not their precursors. *Dev Biol* (210(2):411-27).

Fu YC, C. C. (2004). Norepinephrine induces apoptosis in neonatal rat cardiomyocytes through a reactive oxygen species-TNF alpha-caspase signaling pathway. *Cardiovasc Res* (62(3):558-67).

Glebova NO, G. D. (2004). Heterogeneous requirement of NGF for sympathetic target innervation in vivo. *J Neurosci* (24(3):743-51).

Guo T, Z. T. (2006). Ca2+/Calmodulin-dependent protein kinase II phosphorylation of ryanodine receptor does affect calcium sparks in mouse ventricular myocytes. *Circ Res* (99(4):398-406).

Harrington AW, G. D. (2013). Long-distance retrograde neurotrophic factor signalling in neurons. *Nat Rev Neurosci* (14(3):177-87).

Harrington AW, S. H. (2011). Recruitment of actin modifiers to TrkA endosomes governs retrograde NGF signaling and survival. *Cell* (146(3):421-34).

Howe CL, V. J. (2001). NGF signaling from clathrin-coated vesicles: evidence that signaling endosomes serve as a platform for the Ras-MAPK pathway. *Neuron* (32(5):801-14).

http://eu.idtdna.com/analyzer/applications/oligoanalyzer/. (n.d.).

http://frodo.wi.mit.edu/cgi-bin/primer3/primer3_www.cgi. (n.d.).

http://usefulchem.wikispaces.com. (n.d.).

http://www.e-heart.org. (n.d.).

Ieda M, F. K. (2009). Cardiac innervation and sudden cardiac death. *Curr Cardiol Rev* (5(4):289-95).

Jaggar JH, W. G. (1998). Ca2+ channels, ryanodine receptors and Ca(2+)-activated K+ channels: a functional unit for regulating arterial tone. *Acta Physiol Scand* (164(4):577-87).

Julien C, K. P. (1999). Effects of sympathectomy on blood pressure and its variability in conscious rats. *Am J Physiol* (259(5 Pt 2):H1337-42).

Kanazawa H, I. M.-M.-U. (2010). Heart failure causes cholinergic transdifferentiation of cardiac sympathetic nerves via gp130-signaling cytokines in rodents. *J Clin Invest* (120(2):408-21).

Kase H, I. K. (1987). K-252 compounds, novel and potent inhibitors of protein kinase C and cyclic nucleotide-dependent protein kinases. *Biochem Biophys Res Commun* (142(2):436-40).

Kaye DM, V. G. (2000). Reduced myocardial nerve growth factor expression in human and experimental heart failure. *Circ Res* (86(7):E80-4).

Kimura K, I. M. (2007). Cardiac sympathetic rejuvenation: a link between nerve function and cardiac hypertrophy. *Circ Res* (100(12):1755-64).

Kimura K, I. M. (2012). Development, maturation, and transdifferentiation of cardiac sympathetic nerves. *Circ Res* (110(2):325-36).

Kiriazis H, D. X. (2005). Preserved left ventricular structure and function in mice with cardiac sympathetic hyperinnervation. *Am J Physiol Heart Circ Physiol* (289(4):H1359-65).

Korsching S, T. H. (1983). Nerve growth factor in sympathetic ganglia and corresponding target organs of the rat: correlation with density of sympathetic innervation. *Proc Natl Acad Sci U S A* (80(11):3513-6).

Kuruvilla R, Y. H. (2000). Spatially and functionally distinct roles of the PI3-K effector pathway during NGF signaling in sympathetic neurons. *Neuron* (27(3):499-512).

Lee S, G. S.-E. (2010). Total beta-adrenoceptor deficiency results in cardiac hypotrophy and negative inotropy. *Physiol Res* (59(5):679-89).

LeSauteur L, W. L. (1995). Small peptide mimics of nerve growth factor bind TrkA receptors and affect biological responses. *J Biol Chem* (270(12):6564-9).

Lessmann V, G. K. (2003). Neurotrophin secretion: current facts and future prospects. *Prog Neurobiol* (69(5):341-74).

Levi Montalcini R, H. V. (1953). A diffusible agent of mouse sarcoma, producing hyperplasia of sympathetic-ganglia and hyperneurotization of viscera in the chick embryo. *J Exp Zool* (123:233–287).

Li L, D. J. (2000). Phosphorylation of phospholamban and troponin I in beta-adrenergic-induced acceleration of cardiac relaxation. *Am J Physiol Heart Circ Physiol* (278(3):H769-79).

Libby P, B. R. (2008). *Braunwald's Heart Disease: A Textbook of Cardiovascular Medicine.* Saunders.

Linke WA. (2008). Sense and stretchability: the role of titin and titin-associated proteins in myocardial stress-sensing and mechanical dysfunction. *Cardiovasc Res* (77(4):637-48).

Lipscombe D. (2002). L-type calcium channels: highs and new lows. *Circ Res* (90(9):933-5).

Lockhart ST, T. G. (1997). Nerve growth factor modulates synaptic transmission between sympathetic neurons and cardiac myocytes. *J Neurosci* (17(24):9573-82).

Luther PK. (2009). The vertebrate muscle Z-disc: sarcomere anchor for structure and signalling. *J Muscle Res Cell Motil* (30(5-6):171-85).

Maier LS, B. D. (2007). Role of Ca2+/calmodulin-dependent protein kinase (CaMK) in excitation-contraction coupling in the heart. *Cardiovasc Res* (73(4):631-40).

Maillet M, v. B. (2013). Molecular basis of physiological heart growth: fundamental concepts and new players. *Nat Rev Mol Cell Biol* (14(1):38-48).

Makino M, H. H. (1997). Circadian rhythms of cardiovascular functions are modulated by the baroreflex and the autonomic nervous system in the rat. *Circulation* (96(5):1667-74).

Marx SO, R. S. (2000). PKA phosphorylation dissociates FKBP12.6 from the calcium release channel (ryanodine receptor): defective regulation in failing hearts. *Cell* (101(4):365-76).

Minichiello L, K. R. (1996). TrkB and TrkC neurotrophin receptors cooperate in promoting survival of hippocampal and cerebellar granule neurons. *Genes Dev* (10(22):2849-58).

Mocchetti I, D. B. (1989). Regulation of nerve growth factor biosynthesis by beta-adrenergic receptor activation in astrocytoma cells: a potential role of c-Fos protein. *Proc Natl Acad Sci U S A* (86(10):3891-5).

Mok SA, L. K. (2009). A retrograde apoptotic signal originating in NGF-deprived distal axons of rat sympathetic neurons in compartmented cultures. *Cell Res* (19(5):546-60).

Mowla SJ, P. S. (1999). Differential sorting of nerve growth factor and brain-derived neurotrophic factor in hippocampal neurons. *J Neurosci* (19(6):2069-80).

Nayler WG, S. A. (1980). Effect of prolonged beta-adrenoceptor blockade on heart weight and ultrastructure in young rabbits. *Br J Pharmacol* (68(3):363-71).

Nomura M, N. T. (2011). Facilitated intracellular transport of TrkA by an interaction with nerve growth factor. *Dev Neurobiol* (71(7):634-49).

Ogawa H, A. M. (2012). Nerve growth factor derived from bronchial epithelium after chronic mite antigen exposure contributes to airway hyperresponsiveness by inducing hyperinnervation, and is inhibited by in vivo siRNA. *Clin Exp Allergy* (42(3):460-70).

Pattyn A, M. X. (1999). The homeobox gene Phox2b is essential for the development of autonomic neural crest derivatives. *Nature* (399:366–370).

Paulin D, L. Z. (2004). Desmin: a major intermediate filament protein essential for the structural integrity and function of muscle. *Exp Cell Res* (301(1):1-7).

Pazyra-Murphy MF, H. A. (2009). A retrograde neuronal survival response: target-derived neurotrophins regulate MEF2D and bcl-w. *J Neurosci* (29(20):6700-9).

Pfaffl MW. (2001). A new mathematical model for relative quantification in real-time RT-PCR. *Nucleic Acids Res* (29(9):e45).

Poo MM. (2001). Neurotrophins as synaptic modulators. *Nat Rev Neurosci* (2(1):24-32).

Portbury AL, W. M. (2011). Tearin' up my heart: proteolysis in the cardiac sarcomere. *J Biol Chem* (286(12):9929-34).

Powell SR. (2006, Jul). The ubiquitin-proteasome system in cardiac physiology and pathology. *Am J Physiol Heart Circ Physiol* .

Putcha GV, D. M. (1999). BAX translocation is a critical event in neuronal apoptosis: regulation by neuroprotectants, BCL-2, and caspases. *J Neurosci* (19(17):7476-85).

Qu J, R. R. (2004). Cardiac ion channel expression and regulation: the role of innervation. *J Mol Cell Cardiol* (37(2):439-48).

Qu Y, B. G.-S. (2005). Localization and modulation of {alpha}1D (Cav1.3) L-type Ca channel by protein kinase A. *Am J Physiol Heart Circ Physiol* (288(5):H2123-30).

Riccio A, P. B. (1997). An NGF-TrkA-mediated retrograde signal to transcription factor CREB in sympathetic neurons. *Science* (277(5329):1097-100).

Ryall JG, S. M. (2006). Systemic administration of beta2-adrenoceptor agonists, formoterol and salmeterol, elicit skeletal muscle hypertrophy in rats at micromolar doses. *Br J Pharmacol* (147(6):587-95).

Sartori R, S. E. (2013). BMP signaling controls muscle mass. *Nat Genet* (45(11):1309-18).

Seidah NG, B. S. (1996). Cellular processing of the nerve growth factor precursor by the mammalian pro-protein convertases. *Biochem J* (314:951-60).

Sellers JR. (2000). Myosins: a diverse superfamily. *Biochim Biophys Acta* (1496(1):3-22).

Shao Y, A. W.-A. (2002). Pincher, a pinocytic chaperone for nerve growth factor/TrkA signaling endosomes. *J Cell Biol* (157(4):679-91).

Shcherbakova OG, H. C. (2007). Organization of beta-adrenoceptor signaling compartments by sympathetic innervation of cardiac myocytes. *J Cell Biol* (176(4):521-33).

Shiojima I, S. K. (2005). Disruption of coordinated cardiac hypertrophy and angiogenesis contributes to the transition to heart failure. *J Clin Invest* (115(8):2108-18).

Simpson P. (1983). Norepinephrine-stimulated hypertrophy of cultured rat myocardial cells is an alpha 1 adrenergic response. *J Clin Invest* (72(2):732-8).

Smeyne RJ, K. R. (1994, Mar). Severe sensory and sympathetic neuropathies in mice carrying a disrupted Trk/NGF receptor gene. *Nature* .

Taniguchi M, Y. S. (1997). Disruption of semaphorin III/D gene causes severe abnormality in peripheral nerve projection. *Neuron* (19(3):519-30).

Vincentz JW, R. M. (2012). Ontogeny of cardiac sympathetic innervation and its implications for cardiac disease. *Pediatr Cardiol* (33(6):923-8).

Vliegen HW, v. d. (1991). Myocardial changes in pressure overload-induced left ventricular hypertrophy. A study on tissue composition, polyploidization and multinucleation. *Eur Heart J* (12(4):488-94).

Wang W, Z. W. (2004). Sustained beta1-adrenergic stimulation modulates cardiac contractility by Ca2+/calmodulin kinase signaling pathway. *Circ Res* (95(8):798-806.).

Wang XH, P. M. (1997). Potentiation of developing synapses by postsynaptic release of neurotrophin-4. *Neuron* (19(4):825-35).

White SP, C. C. (1987). Structure of co-crystals of tropomyosin and troponin. *Nature* (325(6107):826-8).

Wiesmann C, d. V. (2001). Nerve growth factor: structure and function. *Cell Mol Life Sci* (58(5-6):748-59).

Wiesmann C, U. M. (1999). Crystal structure of nerve growth factor in complex with the ligand-binding domain of the TrkA receptor. *Nature* (401:184 –188).

Wyatt S, P. L. (1997). Sympathetic neuron survival and TrkA expression in NT3-deficient mouse embryos. *EMBO J* (16(11):3115-23).

Zaglia T, M. G. (2013). Cardiac sympathetic neurons provide trophic signal to the heart via β2-adrenoceptor-dependent regulation of proteolysis. *Cardiovasc Res* (97(2):240-50).

Zhang J, M. Y. (2001). Genetically encoded reporters of protein kinase A activity reveal impact of substrate tethering. *Proc Natl Acad Sci U S A* (98(26):14997-5002).

Zhou Q, R.-L. P. (1999). Cypher, a striated muscle-restricted PDZ and LIM domain-containing protein, binds to alpha-actinin-2 and protein kinase C. *J Biol Chem* (274(28):19807-13).

Zhou S, C. L. (2004). Mechanisms of cardiac nerve sprouting after myocardial infarction in dogs. *Circ Res* (95(1):76-83).

Acknowledgements

For this PhD thesis, I have to thank many people that helped me in different ways. I want to begin from the ones, who did not help me with the experiments but that are the most important people of my life and supported me economically and morally when I needed. These wise people are my mom Adelina, my father Sergio and my sister Laura, and they deserve all my love and my respect. Talking about love, I have to thank my beautiful Andry for her patience during these years of work. In hard moments, her ability to make me think was important to face the adversities.

Thinking to all the people that helped me with this work, first I would like to thank my supervisor Marco and my favorite post doc Tania. When I came in Mongillo's lab 3 years ago, I was just a student. During the PhD, the maturation of a scientific mind requires effort and the presence of big scientific figures that I individuated in Marco and Tania. I am honest when I say this and that I had good fortune to work with them. It is impossible to mention all the reasons for thanksgiving; they helped me not only with experiments, ideas and planning, but also supported me in life adversities. So thank you very much.

Among the people of the lab, I would like to thank Nik for real time pcrs and for cryosections, Silvia, who worked with me a lot at the project of sarcomere degradation, Francesca, who helped me with AKAR3 experiments, Giulia for exchanging ideas on the projects and helping me in the hematoxylin eosin staining, Cimbro for technical support and Valentina, who helped me in the part of cardiac fibrosis.

For molecular biology, I have to thank Giulietta Di Benedetto for NGF-RFP and RFP-zasp constructs, and Raffaele Lo Preiato for NGF constructs that were not used in this work but that will be used in the future. Many thanks also to Andrea Carpi, who dedicated me his free time for planning NGF cloning.

Among the collaborators, many thanks to Prof. Oriano Marin's group, and, in particular, to Michele Sandre, who produced the c(92-96), to Marco Sandri's lab and Roberta Sartori, who produced and gave me part of the plasmids that I used in the work on sarcomere disassembly, and Valerio Gobbo, for the EM. I would like to thank also Prof. Fabio Mammano's group for HeLa cells, Prof. Cesare Montecucco's lab for

PC12 cells and anti-synaptophysin antibody, Dr Claudia Lodovichi's lab for hippocampal neurons and anti-VAMP antibody, Dr Louis Reichardt for anti-TrkA antibody, and Prof. Stefano Schiffino's lab, for anti-TnI and anti-TnT antibodies.
Finally, I would like to thank Prof. Tullio Pozzan and Prof. Stefano Schiaffino for their scientific advices.